# The Philosophical Magazine

UNIVERSITY OF HAWAII
LIBRARY
MAR 20 '62

FIRST PUBLISHED IN 1798

## A Journal of Theoretical Experimental and Applied Physics

Vol. 6 December 1961 No. 72
*Eighth Series*

25s. 0d., plus postage
Annual Subscription £13 10s. 0d., payable in advance

*Printed and Published by*
TAYLOR & FRANCIS LTD
RED LION COURT, FLEET STREET, LONDON, E.C.4

# THE PHILOSOPHICAL MAGAZINE

*Editor*
Professor N. F. Mott, M.A., D.Sc., F.R.S.

*Editorial Board*
Sir Lawrence Bragg, O.B.E., M.C., M.A., D.Sc., F.R.S.
Sir George Thomson, M.A., D.Sc., F.R.S.
W. H. Taylor, M.A., D.Sc.

Authors wishing to submit papers for publication in the Journal should send manuscripts directly to the Publishers.

Manuscripts should be typed in *double* spacing on one side of quarto (8 × 10 in.) paper, and authors are urged to aim at absolute clarity of meaning and an attractive presentation of their texts. Each paper should be preceded by a brief abstract in a form suitable for reproduction in abstracting journals.

References should be listed at the end in alphabetical order of authors and should be cited in the text in terms of author's name and date. Diagrams should normally be in Indian ink on white card, with lettering in soft pencil, the captions being typed on a separate sheet.

A leaflet giving detailed instructions to authors on the preparation of papers is available on request from the Publishers.

Authors are entitled to receive 25 offprints of a paper in the Journal free of charge, and additional offprints can be obtained from the Publishers.

The *Philosophical Magazine* and its companion journal, *Advances in Physics*, will accept papers for publication in experimental and theoretical physics. The *Philosophical Magazine* publishes contributions describing new results, letters to the editor and book reviews. *Advances in Physics* publishes articles surveying the present state of knowledge in any branch of the science in which recent progress has been made. The editors welcome contributions from overseas as well as from the United Kingdom, and papers may be published in English, French and German.

# Thermal Expansion at Low Temperatures
# III. Potassium Chloride

By G. K. White
Division of Physics, Commonwealth Scientific and Industrial Research Organization, Sydney, Australia

[Received May 8, 1961]

## Abstract

Observations of the linear thermal expansion of a potassium chloride crystal have been made between 2° and 30°K, 55° and 90°K, and 273° and 293°K. At the lowest temperatures ($3° < T < 9°$K), the linear coefficient of expansion $\alpha \simeq 5{\cdot}4 \pm 0{\cdot}3 \times 10^{-11}\, T^3$ per °C, which corresponds to a Grüneisen $\gamma$ value of $0{\cdot}39 \pm 0{\cdot}2$. $\gamma$ increases with temperature, particularly in the range 15° to 70°K (cf. $\Theta_D \simeq 235$°K), being about 0·9 at 30°K, 1·25 (60°K) and 1·5 above 200°K. This increase is of the form suggested theoretically by Barron and by Blackman for ionic cubic solids but is greater than they expected. It is not very different from that predicted by Sheard from the pressure variation of the elastic constants.

---

## § 1. Introduction

The property of thermal expansion is generally regarded as arising from the anharmonic terms in the crystal potential energy. The volume coefficient of thermal expansion $\beta$ according to the Mie–Grüneisen theory (e.g. Grüneisen 1926) should be proportional to the specific heat $C_V$: Grüneisen's rule states that

$$\beta = \gamma \chi C_V / V, \qquad \qquad (1)$$

where $\chi$ is the isothermal compressibility, $V$ is the molar volume and $\gamma$ is a dimensionless constant which provides a measure of the 'anharmonicity' of the crystal. On Debye's continuum model, $\gamma$ is related to the characteristic temperature $\Theta_D$ and volume $V$ by the equation $\gamma = -d \ln \Theta_D / d \ln V$. More generally

$$\gamma_i = -d \ln \nu_i / d \ln V,$$

where $\nu_i$ is the frequency of the $i$th normal mode of vibration. Then usually the $\gamma_i$ will not be equal, so that the 'average' $\gamma$ defined by (1) will vary with temperature as does the degree of excitation of the various normal modes $\nu_i$.

Born (1923) has shown theoretically that, even if the $\gamma_i$ are not equal, eqn. (1) should be true at both high temperatures ($T \geqslant \Theta_D$) and at low temperatures ($T \leqslant \Theta_D$), where $\gamma$ would have respective values of $\gamma_\infty$ and $\gamma_0$. Barron (1955) applied Born–von Kármán lattice dynamics to a cubic lattice with central forces between nearest neighbours and, using a Mie–Lennard-Jones potential

$$f(r^2) = -\lambda r^{-m} + \mu r^{-n},$$

he showed that $\gamma_\infty \simeq (m+n)/6$ and $\gamma_\infty - \gamma_0 \leqslant 0{\cdot}3$: for inert gas solids where $m \simeq 6$, $n \simeq 12$ Barron obtained $\gamma_\infty \simeq 3$, $\gamma_\infty - \gamma_0 \simeq 0{\cdot}15$. For ionic crystals of the sodium chloride structure Barron (1957) and Blackman (1957, 1958) have shown that $\gamma$ may change more drastically with temperature and some $\gamma_i$ may assume negative values. For one simplified model Barron obtains $\gamma_\infty \simeq 1{\cdot}6$ and $\gamma_0 \simeq 1$. A more detailed treatment of a two-dimensional ionic lattice has been given by Blackman (1959). Barron and Blackman respectively suggest that the major change in $\gamma$ should occur at temperatures in the vicinity of $0{\cdot}2\ \Theta_D$ and $0{\cdot}14\ \Theta_D$.

Other predictions of the variation of $\gamma$ have been made by Sheard (1958) on the basis of the relation between thermal expansion and elastic anharmonicity. Using a continuum model, Sheard has deduced from Lazarus' (1949) measurements of the pressure variation of elastic moduli that $\gamma_\infty = 1{\cdot}57$ and $\gamma_0 = 0{\cdot}525$ for KCl and $\gamma_\infty = 1{\cdot}60$ and $\gamma_0 = 1{\cdot}23$ for NaCl. Since reported measurements of the expansion coefficient on the alkali halides have not previously extended down to very low temperatures (see, for example, Srinivasan 1955 and Salimäki 1960) and present measurement techniques (White 1961 a) do allow useful data to be obtained down to near 4°K, it seemed interesting to examine potassium chloride as a representative of the ionic crystals.

## § 2. Experimental Details and Results

A potassium chloride crystal of about 5 cm length and 2 cm diameter was grown† by pulling from the melt. The starting material was Merck reagent grade potassium chloride with a divalent cation concentration less than $10^{-5}$ (see Cook and Dryden 1960 for details of crystal growth and purity). The end faces of the crystal were then ground, polished and silvered (by evaporation); the final length was 4·52 cm. A small hole was drilled in one end of the crystal and a few strands of fine copper wire were cemented into the hole with Araldite cold-setting adhesive; this wire was then soldered to a short length of threaded brass rod so that the crystal could be mounted in our differential expansion cell (cell No. 1 of copper as described by White 1961 a). With a spring washer and nut on the threaded rod, the crystal could be held firmly with the drilled end-face sitting on a lapped copper surface. The other end-face formed a parallel plate capacitor with a lapped copper disc 0·02 to 0·03 cm distant.

At room temperature the capacitance of this gap was about 6 pF but at liquid helium temperatures the gap had increased due to much greater overall contraction of KCl compared with the copper cell, so that the capacitance was then near 3 pF. Thus at liquid helium temperatures the detection limit of 1 × $10^{-6}$ pF corresponded to about 1 × $10^{-8}$ cm change in gap.

---

† I am most grateful to Mr. J. S. Cook, of the C.S.I.R.O. Division of Electrotechnology, for producing the crystal.

The linear thermal expansion of the KCl sample was calculated by adding the observed *differential* expansion (KCl versus Cu) to that already found for copper during our calibration procedures for the expansion cell (White 1961 a for details).

Most detailed observations were made in the temperature region between 2° and 31°K but some observations of the average expansion coefficient were also obtained in the temperature intervals 293°–273°K, 90°–80°K, 80°–70°K, 70°–60°K, 61°–55°K. Between 8° and 31°K expansion coefficients were obtained at 0·5° intervals by taking the slope of the expansivity–temperature curve. Below 8° or 9°K this proved rather inaccurate; instead, a graph of $\Delta l/T^3$ versus $T$ was made, this being a straight line through the origin giving a value of $5{\cdot}4 \pm 0{\cdot}3 \times 10^{-11}\, T^3$ per °C for the linear expansion coefficient $\alpha$. Above 8° or 9°K ($T \sim \Theta_D/30$) there appears a gradual departure from the $T^4$ dependence for $\Delta l$ corresponding to a departure from a $T^3$ relation for $\alpha$.

Linear thermal expansion coefficient $\alpha$ and Grüneisen parameter $\gamma$ for KCl crystal

| $T$ (°K) | $10^6\alpha$ (per °C) | $C_V$ (cal/mole deg) | $V$ (cm³/mole) | $10^{12}\chi$ (cm²/dyne) | $\gamma$ |
|---|---|---|---|---|---|
| <8 | $5{\cdot}4 \times 10^{-5}\, T^3$ | $2 \times 465\, (T/234)^3$ | 36·7 | 5·07 | 0·39 |
| 10 | 0·058 | 0·0804 | 36·7 | 5·07 | 0·38 |
| 12 | 0·11 | 0·147 | 36·7 | 5·07 | 0·40 |
| 15 | 0·25 | 0·302 | 36·7 | 5·08 | 0·43 |
| 20 | 0·77 | 0·713 | 36·7 | 5·10 | 0·56 |
| 25 | $1{\cdot}8_2$ | 1·28 | 36·7 | 5·11 | 0·73 |
| 30 | $3{\cdot}3_0$ | 1·99 | 36·7 | 5·12 | 0·85 |
| 65 | 17·2 | 6·85 | $36{\cdot}7_5$ | 5·18 | 1·28 |
| 85 | 23·2 | 8·48 | $36{\cdot}7_5$ | 5·19 | 1·39 |
| 283 | 37·1 | 11·65 | 37·4 | 5·82 | 1·47 |

In the table are shown some values for the linear coefficient $\alpha$, together with values of $\gamma$ taken from eqn. (1) assuming isotropic expansion, i.e. $\beta = 3\alpha$. The data used for $C_V$ (Berg and Morrison 1957), $V$ (Henglein 1925) and $\chi$ (Norwood and Briscoe 1958) are also included in the table. In the figure are included values of $\gamma$ calculated from the expansion coefficient data of Srinivasan (1955) and Salimäki (1960).

## § 3. Discussion and Conclusions

At temperatures less than $\Theta_D/30$ ($\Theta_D \simeq 235$°K for KCl) the thermal expansion measurements indicate that the linear coefficient of thermal expansion varies as $T^3$, as does the specific heat, at least to a first approximation. Present accuracy is insufficient to test whether there is also a $T^5$ term in $\alpha$, comparable with that observed in $C_V$ by Berg and Morrison (1957, see also Barron *et al.* 1957). The value for $\gamma_0$ deduced from this lowest temperature data is 0·39 ($\pm$ 0·02), and indeed $\gamma$ seems to be sensibly constant below 14° or 15°K. $\gamma$ then increases steadily with temperature up to the vicinity of 100°K. Above this temperature $\gamma$ would appear to vary little to judge from our measurements and those of Salimäki (1960), although Srinivasan's values below 150°K do not agree with this. We conclude that $\gamma_\infty$ lies near 1·50.

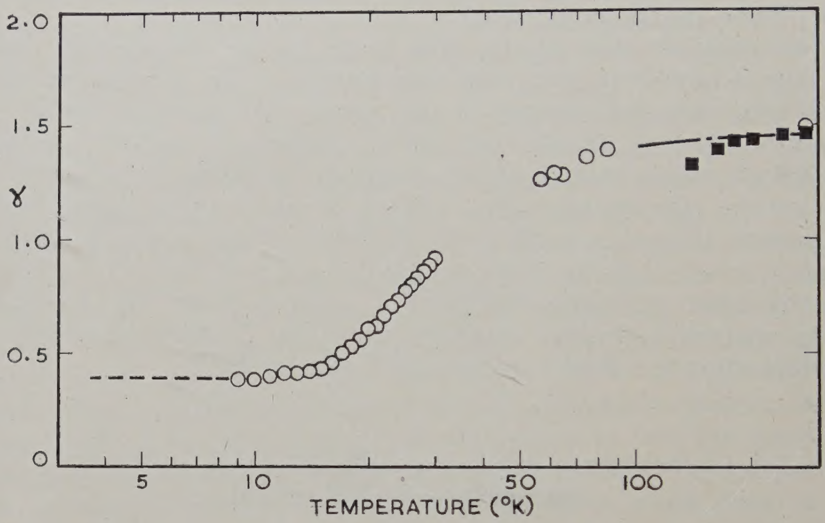

Variation of $\gamma$ with temperature for KCl.
----○○○ Our data.
■ Srinivasan (1955).
——.—— Smoothed curve from Salimäki (1960).

The most rapid change in $\gamma$ with temperature seems to occur between 20° and 40°K, that is in the neighbourhood of $0{\cdot}13\Theta_D$ as predicted theoretically by Blackman. But the total change in $\gamma$ from 1·45 to 0·4 is rather larger than either Barron or Blackman suggested from their theoretical models. However, the change is not very different from that deduced by Sheard (1958) from the third-order elastic constants; Sheard predicted $\gamma_0 \simeq 0{\cdot}52_5$ and $\gamma_\infty \simeq 1{\cdot}57$ for potassium chloride. Shortly it is hoped to extend these observations to sodium chloride, which on the basis of Sheard's calculations should show a much smaller change in $\gamma$.

In conclusion it seems pertinent to remark that this large change in $\gamma$ for KCl is in sharp contrast to observations on cubic metals such as copper, aluminium, iron, palladium, etc. (White 1960, 1961 b), where there is no experimental evidence yet for any marked change in $\gamma$ in so far as the lattice vibrational contribution to expansion is concerned.

## ACKNOWLEDGMENTS

I am most grateful to Mrs. P. C. Zeleny for her frequent assistance with readings and computation and to Mr. J. W. W. Smyth for his help.

*Note added in proof.*—The referee has kindly drawn my attention to recent interferometric measurements by Rubin, Johnston and Altman (*J. phys. Chem.*, **65**, 65, 1961) of the thermal expansion of sodium chloride. Their measurements extend from room temperature down to near 25°K and indicate that $\gamma$ falls from about 1·55 to near 0·98 in this range. We have measured sodium chloride also now down to 4°K and find $\gamma_0 = 0{\cdot}94\ (\pm 0{\cdot}02)$, results above 25°K being in close agreement with those of Rubin *et al.* Measurements have also been repeated on potassium chloride with improved thermometry and although these data agree quite well above 20°K with those given in this paper, there are increasing differences at lower temperature so that below 10°K, $\gamma_0 = 0{\cdot}34 \pm 0{\cdot}02$.

## REFERENCES

BARRON, T. H. K., 1955, *Phil. Mag.*, **46**, 720 ; 1957, *Annals of Physics*, **1**, 77.
BARRON, T. H. K., BERG, W. T., and MORRISON, J. A., 1957, *Proc. roy. Soc.* A, **242**, 478.
BERG, W. T., and MORRISON, J. A., 1957, *Proc. roy. Soc.* A, **242**, 467.
BLACKMAN, M., 1957, *Proc. phys. Soc., Lond.* B, **70**, 827 ; 1958, *Phil. Mag.*, **3**, 831 ; 1959, *Proc. phys. Soc., Lond.*, **74**, 17.
BORN, M., 1923, *Atomtheorie des festen Zustandes* (Leipzig : Teubner).
COOK, J. S., and DRYDEN, J. S., 1960, *Aust. J. Phys.*, **13**, 260.
GRÜNEISEN, E., 1926, *Handb. Phys.*, **10**, 1.
HENGLEIN, F. A., 1925, *Z. phys. Chem.*, **115**, 91.
LAZARUS, S., 1949, *Phys. Rev.*, **76**, 545.
NORWOOD, M. H., and BRISCOE, C. V., 1958, *Phys. Rev.*, **112**, 45.
SALIMÄKI, K. E., 1960, *Ann. Acad. Sci. Fennicae*, VI A, No. 56.
SHEARD, F. W., 1958, *Phil. Mag.*, **3**, 1381.
SRINIVASAN, R., 1955, *J. Indian Inst. Sci.*, **37**, 232.
WHITE, G. K., 1960, *Nature, Lond.*, **187**, 927 ; 1961 a, *Cryogenics*, **1**, 151 ; 1961 b, *Phil. Mag.*, **6**, 815.

# Thermoelectricity of Lithium Alloys at Very Low Temperatures

By D. K. C. MacDonald, W. B. Pearson and I. M. Templeton
Division of Pure Physics, National Research Council, Ottawa, Canada

[Received May 15, 1961]

## Abstract

As lithium is apparently the only alkali metal which will take heterovalent impurities into solid solution, we have prepared alloys with Mg, In and Al and examined their absolute thermoelectric power in the temperature range from about 0·1° to 1·2 °K. We find that the change of diffusion thermoelectric power of Li on alloying is in many ways surprising, and we have discussed whether the observed behaviour may reasonably be attributed to the influence of conduction electron scattering or to a change in the electron density of states of lithium.

## § 1. Introduction

We have been interested for many years in the electron transport properties of the monovalent metals (Groups 1 A and B), particularly because we might expect these metals to offer a first approximation to the ideal free-electron model. In fact it appears that deviations from free-electron behaviour are very appreciable in some of these metals, and probably only Na and K have rather well behaved, nearly spherical Fermi surfaces. Realizing also the importance of electron *scattering*, we have been anxious to examine in detail the effect of homo- and heterovalent impurities on the thermoelectric power of the alkali metals at very low temperatures.

As far as we are aware (see, e.g., Hansen 1958) none of the alkali metals except Li has any solid solubility for heterovalent solutes. Consequently Guénault and MacDonald (1961), in studying the influence of scattering on the thermoelectric power of potassium below 3°K, were limited to the addition of homovalent impurities (Na, Rb and Cs). However, although Li can dissolve certain heterovalent solutes, it is probably the least ideal of the alkali metals; it exhibits a martensitic transformation changing from a b.c. cubic to a c.p. hexagonal structure at about 77°K on cooling (cf. Barrett 1947, 1956, Barrett and Trautz 1948, Bowles 1951, Dugdale 1958) and it appears that the Fermi surface is far from spherical.

Nevertheless, because it is possible to form an extensive solid solution of Mg in Li (cf. Barrett and Trautz 1948) and, as we find also, to dissolve In and Al in small amounts in Li, we have examined the thermoelectricity and electrical resistivity of a number of these alloys at very low temperatures between about 0·1° and 4°K. For measurements in the temperature range obtained by adiabatic demagnetization of a paramagnetic salt, we have used the apparatus and methods described by MacDonald *et al.* (1960). We have already reported some thermoelectric measurements on lithium samples in this temperature range (MacDonald *et al.* 1960) and between 2° and 18°K (MacDonald *et al.* 1958).

## § 2. Experimental Results

We have examined the absolute thermoelectric power, $S$, of Li–Mg alloys containing up to about 10 at. % Mg, and of Li–In alloys with a solute content of up to about 1 at. %. Particular attention has been given to examining very dilute alloys containing these solutes and to examining the 'pure' lithium, melted and prepared in exactly the same manner as the alloys. In addition to these alloys, which were studied in some detail, we also succeeded in making two Li alloys containing a small amount of aluminum in solid solution. Figure 1 shows the residual resistance-ratio, say $\rho$, as a function of nominal solute concentration for alloys containing less than 1 at. % solute, and fig. 2 gives a logarithmic plot of data for the Li–In alloys indicating a reasonable linearity of resistivity with concentration as the latter increases by a factor approaching $10^3$. No resistance minimum was ever observed in the alloys.

Fig. 1

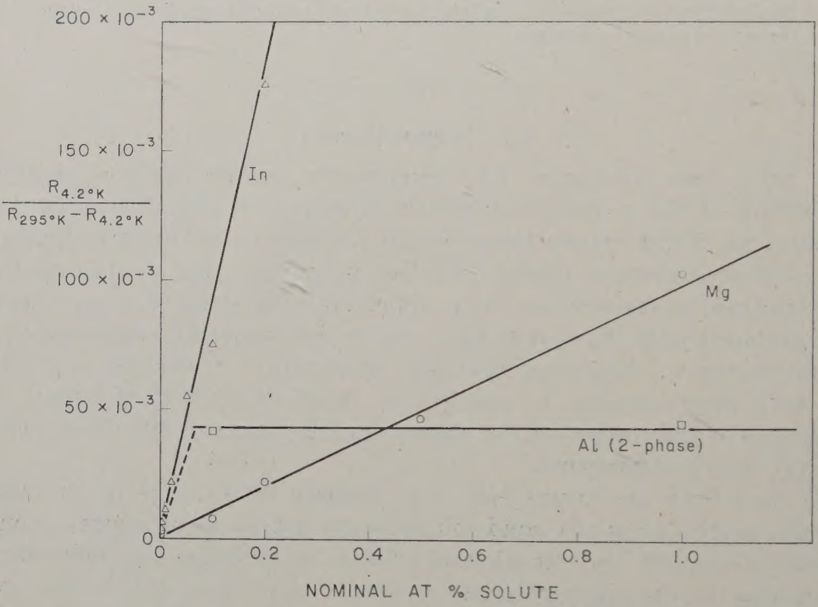

Residual resistance-ratio, $R_{4\cdot2^\circ\mathrm{K}}/(R_{295^\circ\mathrm{K}}-R_{4\cdot2^\circ\mathrm{K}})$, as a function of nominal solute concentration for **Li**–Mg, **Li**–In and **Li**–Al alloys. The two **Li**–Al samples appear not to be single-phase alloys.

We have measured the thermoelectric force, $E$, of the lithium alloys directly as a function of temperature (cf., e.g., fig. 6, MacDonald *et al.* 1960) and from these data we have plotted in fig. 3 the absolute thermoelectric power, $S$, at 1°K against the measured values of $1/\rho$ for each alloy (cf. Nordheim and Gorter 1935, Kohler 1949). It will be seen that down to a value of $1/\rho$ of about 4, $S$ varies in a reasonably linear manner with $1/\rho$. At concentrations greater than about 0·3 at. % In, $S$ abruptly becomes negative with a change of slope in $S$ versus $1/\rho$. $S$ also becomes negative in alloys containing about 10 at. % Mg. These results pose two specific problems that puzzle us: Why does $S$ vary in closely the *same* manner with $1/\rho$ for *both* In and Mg as solute, and moreover why does $S$ decay rather directly towards *zero* for all three solutes in dilute solid solution? Secondly, why does the slope of $S$ versus $1/\rho$ change so sharply, becoming negative, in alloys containing more than about 0·3 at. % In?

Fig. 2

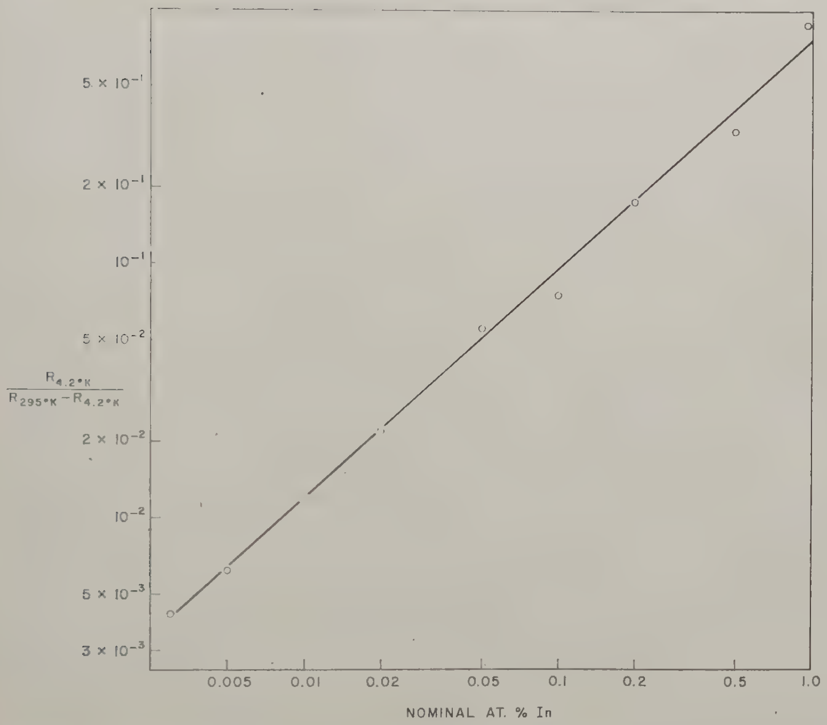

Residual resistance-ratio, $R_{4\cdot2^\circ\mathrm{K}}/(R_{295^\circ\mathrm{K}}-R_{4\cdot2^\circ\mathrm{K}})$, *versus* nominal solute concentration of Li–In alloys plotted on logarithmic scales to cover a wider range of concentration.

We wish to discuss briefly the possible interpretations of this behaviour in terms of the usual theories of thermoelectricity.

Thermoelectric power can arise fundamentally in two different ways when a temperature gradient is applied to a conducting solid: either because of the thermal 'diffusion' or 'migration' of the conduction electrons themselves, or because of direct transfer of momentum from excited lattice waves ('phonons') to the conduction electrons, this being known as 'phonon-drag'. Diffusion thermoelectric power owes its existence to the *electronic* specific heat which varies linearly with $T$. Phonon-drag, however, depends primarily on the heat flow carried by the *lattice* itself, and hence on the magnitude of the lattice specific heat, which decays as $T^3$ at sufficiently low temperatures. The Debye $\theta$ of lithium is relatively high (around 400°K) so that we expect phonon-drag should be negligible below a few degrees Kelvin; moreover the *observed* thermoelectric power is satisfyingly linear with $T$ and, consequently, we shall assume that phonon-drag plays a negligible role in these experiments.

Fig. 3

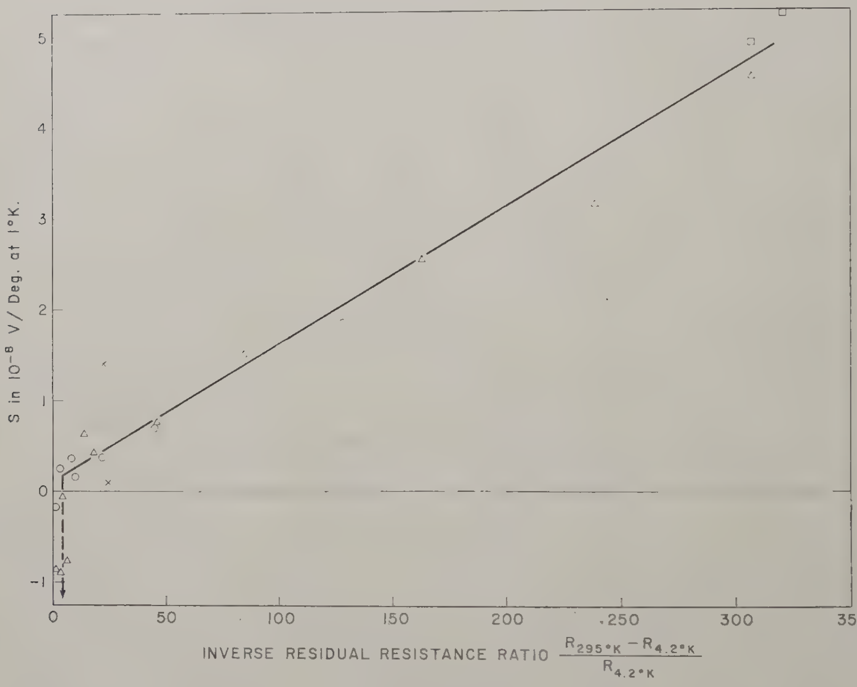

Absolute thermoelectric power, $S$, of Li alloys as a function of their inverse residual resistance-ratio. The arrow close to the ordinate scale indicates that one **Li**–In alloy in that region gave a negative absolute thermoelectric power of as much as $-5\times10^{-8}$ v/deg. ○Li–Mg. △Li–In. △ × Li–Al. □ 'pure' Li melted and prepared in the same manner as the alloys.

When the electron scattering can be adequately represented by a single relaxation time, $\tau(E)$, Mott and Jones (1936) and Wilson (1936, 1953) give for the diffusion thermoelectric power :

$$S=\frac{\pi^2k^2T}{3e}\left(\frac{\partial\log\sigma(E)}{\partial E}\right)_\zeta \quad . \quad . \quad . \qquad (1\,a)$$

$$=\frac{\pi^2k^2T}{3e\zeta}\left(\frac{\partial\log n(E)v^2(E)}{\partial\log E}+\frac{\partial\log\tau(E)}{\partial\log E}\right)_\zeta, \quad . \quad . \qquad (1\,b)$$

where $n(E)$ is the conduction electron density of states, $v(E)$ is an average conduction electron velocity, and $\zeta$ is the electron Fermi energy at which the derivatives are to be evaluated. In eqn. (1 *b*) the first term in the brackets is determined essentially by the properties of the Fermi surface of the conduction electrons, while the second term naturally involves the particular characteristics of the *scattering* processes. Unless there were some particularly unusual scattering mechanism involved, we would strongly expect that the electron scattering by impurity atoms at these very low temperatures should indeed be reducible to a simple relaxation time, and hence that eqn. (1 *b*) should be applicable to our results. Broadly speaking, then, we must argue that the rapid decay in $S$ as we add these solutes to lithium must either be due to a (remarkably rapid) modification of the Fermi surface or to progresssive alteration in the characteristics of the scattering mechanism as the added impurity becomes dominant.

Although it has been suggested (see in particular Cohen and Heine 1958, also Ziman 1959) that the addition of fairly small percentages (say 1 or 2%) of solutes *can* alter appreciably the Fermi surface of a parent metal, it seems very improbable that as little as 0·1 at. % of these solutes would so drastically alter the Fermi surface as to reduce $S$ practically to zero.

If, on the other hand, the initial decay of $S$ towards zero with very small concentrations of solute is in fact simply due to the progressive introduction of a new scattering mechanism, and hence to a progressive change in the second term of eqn. (1 *b*) dependent on the relative concentration of the added solute, then it can readily be shown that a straight line relationship should exist between $S$ and $1/\rho$ where $\rho$ is the resistivity (or resistance-ratio as used here) corresponding to any particular concentration of solute. This ' law ' is due originally to Nordheim and Gorter (1935), and Kohler (1949), and has been discussed and applied again recently by Gold *et al.* (1960), Pearson (1960), and de Vroomen (1959). It assumes specifically that the only function of the added solute is to affect the scattering of the conduction electrons, but *not* to cause any intrinsic change in the electron properties ; hence, if the required straight line relationship is found it offers some confirmation that, over the range of solute concentration involved, the Fermi surface of the parent metal has been unaffected. Although the Nordheim–Gorter–Kohler rule predicts that when a new solute is added to a metal $S$ should alter linearly with $1/\rho$, there seems no particular theoretical reason today why $S$ should not *increase* when one solute is added and *decrease* with another, or for that matter why it should not even change sign in its linear variation with $1/\rho$ as a new solute becomes the dominant scatterer.

One apparently tempting explanation is to suggest that initially the electron scattering in the 'pure' Li samples is always dominated by some very small residual concentration of a solute which gives rise in itself to a large positive thermoelectric power and one is further tempted to suggest that traces of Fe or some other transition metal might be the responsible party (cf., e.g., Gold *et al.* 1960). The second part of the explanation then involves the assumption that most other solutes in Li give rise by themselves to a relatively very much smaller thermoelectric power (practically zero). On the other hand, it is difficult to accept this as a valid explanation because at high temperatures the normal thermal scattering of electrons must completely swamp that due to residual impurity, but the thermoelectric power of 'pure' Li remains stubbornly positive and continues to increase more or less steadily as the temperature rises right up to room temperature. Furthermore, detailed chemical analyses of the various 'pure' Li samples used (for which we are very indebted to Dr. A. T. Prince and Mr. W. R. Inman, Mines and Technical Surveys Department, Ottawa) do *not* indicate that Fe, or any similar element, is present in any significant quantity.

A possible interpretation of the rather sudden change of slope of $S$ versus $1/\rho$ when $S$ at 1°K becomes negative in Li–In alloys containing more than about 0·3 at. % In, is that a modification of the Fermi surface occurs because of the solute. However, we would then expect $S$ for these alloys to be negative also at room temperature, since we attribute the large positive thermoelectric power of *pure* Li at this temperature to the strongly distorted Fermi surface. But, we find experimentally that $S$ for these more concentrated Li–In alloys is *positive* in the room temperature region and consequently this explanation appears untenable, so we can but attribute the change of slope of $S$ versus $1/\rho$ at 1°K to some specific change of scattering mechanism of the solute indium as the concentration is increased. The observed change of $S$ between pure Li and the Li–In alloys at room temperature is consistent with a rather small characteristic thermoelectric power due to In in Li, in accord with the results obtained in the most dilute alloys at low temperatures.

## § 3. CONCLUSION

The change of absolute thermoelectric power of Li at 1°K on alloying with very small amounts of Mg, In or Al, can be attributed to the influence of electron scattering, but if the positive thermoelectric power of the 'pure' Li results from its distorted Fermi surface, then the energy dependence of the scattering due to very small quantities of these impurities is anomalously strong in reducing $S$ rapidly towards zero. Moreover, it is surprising that each of these solutes reduces $S$ to a value *very close to zero*. When more than about 0·3 at. % In is added, $S$ at 1°K becomes negative and the slope of $S$ versus $1/\rho$ changes rather abruptly; an explanation of this based on a change of the electron density of states function of Li does not appear to be tenable, and we presume that some change of electron scattering mechanism must be involved. Although the variable products of the martensitic transformation may possibly influence some of the results, there seems no evidence of this, at least in the very dilute alloys.

## REFERENCES

BARRETT, C. S., 1947, *Phys. Rev.*, **72,** 245; 1956, *Acta cryst.*, **9,** 671.

BARRETT, C. S., and TRAUTZ, O. R., 1948, *Metals Tech.*, April T.P. 2346.

BOWLES, J. S., 1951, *J. Metals*, **3,** 44.

COHEN, M. H., and HEINE, V., 1958, *Advanc. Phys.*, **7,** 345.

DUGDALE, J. S., 1958, Unpublished N.R.C. Report: " The Martensitic Transformation in sodium and lithium ".

GOLD, A. V., MACDONALD, D. K. C., PEARSON, W. B., and TEMPLETON, I.M., 1960, *Phil. Mag.*, **5,** 765.

GUÉNAULT, A. M., and MACDONALD, D. K. C., 1961, *Proc. roy. Soc.* A, **264,** 41.

HANSEN, M., 1958, *Constitution of Binary Alloys*, 2nd ed. (New York: McGraw-Hill Book Company Inc.).

KOHLER, M., 1949, *Z. Phys.*, **126,** 481.

MACDONALD, D. K. C., PEARSON, W. B., and TEMPLETON, I. M., 1958, *Proc. roy. Soc.* A, **248,** 107; 1960, *Ibid.*, **256,** 334.

MOTT, N. F., and JONES, H., 1936, *Theory of Metals and Alloys* (Oxford: Clarendon Press).

NORDHEIM, L., and GORTER, C. J., 1935, *Physica*, **2,** 383.

PEARSON, W. B., 1960, *Phys. Rev.*, **119,** 549.

VROOMEN, A. R. DE, 1959, Thesis, University of Leiden.

WILSON, A. H., 1936, *Theory of Metals*, 2nd ed. 1953 (Cambridge: University Press).

ZIMAN, J. M., 1959, *Proc. roy. Soc.* A, **252,** 63.

# The Kinetics of Precipitation from Solid Solutions by Nucleation and Diffusion Controlled Growth Processes

By J. Burke
Department of Metallurgy, University of Liverpool

[Received in revised form July 14, 1961]

## Abstract

The time-dependence of isothermal precipitation from solid solutions by nucleation and diffusion-controlled growth is derived using the method employed previously (Burke 1960) to discuss the simple growth problem. Numerical solutions are necessary but a short time approximation is developed graphically which is useful for deriving the rate equation for alternative nucleation kinetics.

## § 1. Introduction

The time-dependence of isothermal precipitation from supersaturated solid solutions by the diffusion controlled growth of a fixed number of particles was treated in a previous paper (Burke 1960). The basis of the method was to assume that the average rate of growth of a group of particles where competition for the available solute occurs is given by the rate of growth of an isolated particle multiplied by $x(t)$, the fraction of the available solute remaining in solution at time $t$; the growth rate for an isolated particle was derived using a steady-state approximation to the solution of the diffusion equation.

It has been pointed out (Ham 1961, private communication) that this assumption is equivalent to one used by Wert and Zener (1950) in a modification to their earlier, more well-known works (Wert 1949, Zener 1949). These authors discussed the method in general terms, concluding that it was valid in systems of low initial supersaturation and widely dispersed precipitate particles. Full justification of the method is obtained from Ham's (1958) analysis of the concentration conditions obtaining during diffusion limited growth. Ham's work shows that for an initially uniform solution of low supersaturation where the ultimate precipitate particle size is small compared with their separation, the solute concentration in the solution is virtually identical to the steady-state field for a particle of fixed radius and that the concentration decreases uniformly except within small volumes around the particles. Since these volumes may be neglected the ratio of the instantaneous supersaturation, $\{c_2(t)-c_1\}$, to the initial value, $\{c_2(0)-c_1\}$, is equal to the fraction of solute remaining in solution, $x(t)$. $c_1$ is the equilibrium concentration of solute and $c_2$ is the concentration in the solution. The concentration gradient around a particle is related to $\{c_2(t)-c_1\}$ and thus to $x(t).\{c_2(0)-c_1\}$. This is the assumption used by Burke (1960) and is thus well justified for solutions of low initial supersaturation.

In view of these remarks it is of interest to extend this method of analysis to the more general case in which nucleation of particles occurs concurrently with growth during the reaction. Johnson and Mehl (1939) examined this type of problem but assumed a constant growth rate which is only likely to be found under certain very restricted conditions. In this paper it will be assumed that the growth is limited only by diffusion of solute in the matrix, in which case the radius $r$ is proportional to $t^{1/2}$. It has been shown by Ham (1958) that, provided the shape of the growing particles does not alter during growth, each dimension of three-dimensional particles is also related to $t^{1/2}$ irrespective of shape, correcting the earlier work of Wert (1949) used by Burke (1960) for non-spherical shapes. Thus the present results apply to all shapes provided that they are invariant and that only diffusion of solute is important.

## § 2. NUCLEATION KINETICS

Before the rate equation can be derived it is necessary to know the time-dependence of the nucleation rate. According to classical steady-state theories of nucleation (Hollomon and Turnbull 1953, Turnbull 1956) the rate of formation of stable nuclei of precipitate per unit volume of unreacted material, $\dot{N}$, is given by

$$\dot{N}=N_0 \exp -\frac{\Delta G^*+Q}{RT} \quad . \quad . \quad . \quad . \quad . \quad . \quad . \quad . \quad (1)$$

where $N_0$ is a constant, $\Delta G^*$ is the energy barrier opposing the formation of a stable nucleus and $Q$ is the activation energy for the transfer of an atom across the interface between matrix and nucleus. At constant temperature the time-dependence of $\dot{N}$ arises from ($a$) variations of $\Delta G^*$ as the concentration of solute decreases and ($b$) decrease in the volume available for nucleation. In dilute solutions Ham (1958) showed that the solute concentration in the solution decays uniformly except in negligible volumes near to the precipitate particles. Thus in this case ($b$) may be neglected and only variation of $\Delta G^*$ need be considered.

$\Delta G^*$ is given by

$$\Delta G^*=\text{const.}\frac{\sigma^3}{(\Delta G_V+\epsilon)^2} \quad . \quad . \quad . \quad . \quad . \quad . \quad . \quad (2)$$

where $\sigma$ is the free energy associated with the formation of the nucleus–matrix interface, $\Delta G_v$ is the change in chemical free energy arising from the formation of a nucleus and $\epsilon$ is a measure of the strain energy involved. $\Delta G_v$ and $\sigma$ are dependent upon composition, and thus $x(t)$, in a way which must vary from system to system. It is clearly impossible to set up a generalized expression for $\Delta G^*$ as a function of fractional precipitation even under the idealized circumstances considered by eqns. (1) and (2). Furthermore, transients of unknown duration are to be expected due to a redistribution of embryos and possibly exhaustion of nucleation sites (Turnbull 1948, Avrami 1939). In view of these difficulties it is not feasible to derive the time-dependence of $\dot{N}$ and it is necessary to use an empirical approach considering each system individually. As will be shown in the next section it is quite simple to derive the differential equation for $x(t)$ for any assumed nucleation kinetics but it can be integrated only in certain simple cases. One of these will be used to illustrate the method and also to derive an approximation which facilitates the discussion of other, probably more real, models.

The case considered is that when the instantaneous nucleation rate $\dot{N}(t)$ is proportional to the supersaturation

$$\dot{N}(t)=\dot{N}(0)\,.\,x(t)\,; \qquad (4)$$

i.e. the same concentration dependence is assumed for both nucleation and growth. Equation (4) should apply to non-dilute solutions since, according to Zener (1949), the solute concentration then decreases only in volumes immediately surrounding the precipitate. Thus in this case the time-dependence of $\dot{N}$ occurs mainly through the decrease in available volume. With only slight error the volume available for nucleation is $x(t)$.

## § 3. DERIVATION OF THE RATE EQUATION

The increase in the total volume of precipitate in any time interval from $t$ to $t+dt$ arises both from growth of existing particles (the size of which will vary from the critical nucleus size to a maximum) and the formation of new ones. It will be assumed that the two processes are independent so that the contribution of each to the rate of reaction may be assessed separately and that the size of the critical nucleus is negligibly small.

As pointed out in § 1 the radial rate of growth of a particle growing under diffusion limited conditions is given by a steady-state approximation to the diffusion equation with the concentration in the solution placed equal to the average concentration of solute in solution. Thus

$$R\frac{dR}{dt}=\beta\,.\,x(t), \qquad (5)$$

where $\beta$, a constant for a given system at constant temperature, is given by

$$\beta=D\frac{(c_2-c_1)}{(c_0-c_1)}\,\frac{\sqrt[3]{[(c_0-c_1/c_2)]}}{\sqrt[3]{[(c_0-c_1/c_2)-1]}}\;;$$

$D$ is the diffusion coefficient assumed constant and independent of concentration; $c_0$, $c_1$ and $c_2$ are the solute concentrations in the precipitate, in the solid solution equilibriated with respect to the precipitate and in the initial supersaturated solution respectively. $c_1$ is assumed independent of the size of the precipitate.

For a particle formed at $t=t_1$ $(0<t_1<t)$

$$R^2=2\beta\,.\int_{t_1}^{t} x(t)\,.\,dt, \qquad (6)$$

neglecting the size of the critical nucleus.

Then if $v$ is the volume of this particle

$$\frac{dv}{dt}=4\pi R^2\frac{dR}{dt}=4\pi\sqrt{(2\beta^3)}\,.\,x(t)\left[\int_{t_1}^{t} x(t)\,.\,dt\right]^{1/2} \qquad (7)$$

The number of nuclei formed from $t_1$ to $t_1+dt_1$ is (in view of the assumption defined by eqn. (4))

$$\dot{N}(0)\,.\,x(t_1)\,.\,dt_1.$$

The increment of volume of these particles from $t$ to $t+dt$ is

$$4\pi\sqrt{(2\beta^3)}\,.\,\dot{N}(0)\,.\,x(t)\,.\,x(t_1)\left[\int_{t_1}^{t} x(t)\,.\,dt\right]^{1/2} dt_1$$

and thus the increase in the volume, $V$, of all particles formed up to $t$ is

$$\frac{dV}{dt}=4\pi\sqrt{(2\beta^3)}\,.\,\dot{N}(0)\,.\int_0^t x(t)\,.\,x(t_1)\left[\int_{t_1}^{t} x(t)\,.\,dt\right]^{1/2} dt_1. \qquad (8)$$

To remove $V$ from eqn. (8) it is necessary to multiply by $c_0/c_2-c_1$ the ratio of solute in the precipitate to the initial excess solute in solution.

Then

$$-\frac{dx}{dt}=4\pi\sqrt{(2\beta^3)}\,.\,\dot{N}(0)\left(\frac{c_0}{c_2-c_1}\right)\int_0^t x(t)\,.\,x(t_1)\left[\int_{t_1}^{t} x(t)\,.\,dt\right]^{1/2} dt_1 \qquad (9)$$

$x$ is obtained by integration of eqn. (9) from 0 to $t$ using the boundary condition $x=1$ at $t=0$.

As pointed out in § 2 an equation corresponding to eqn. (9) can be written for any assumed nucleation kinetics. All that is necessary is to replace $x(t_1)$ by the appropriate function in $x$.

Equation (9) has been solved as follows. Let

$$A=4\pi\sqrt{(2\beta^3)}\,.\,\dot{N}(0)\,.\left(\frac{c_0}{c_2-c_1}\right) \qquad (10)$$

$$\int_0^t x(t)\,.\,dt=Z(t) \qquad (11)$$

and

$$\int_0^{t_1} x(t)\,.\,dt=Z(t_1). \qquad (12)$$

Therefore

$$x(t)=\dot{Z} \qquad (13)$$

and

$$x(t_1)=\frac{dZ}{dt_1}. \qquad (14)$$

Substitution of eqns. (10), (13) and (14) into (9) gives:

$$-\ddot{Z}=A\int_0^t \dot{Z}\frac{dZ}{dt_1}\,[Z(t)-Z(t_1)]^{1/2}\,dt_1, \qquad (15)$$

i.e.

$$\ddot{Z}=\tfrac{2}{3}AZ\{Z(t)-Z(t_1)\}^{3/2}\Big|_{t_1=0}^{t_1=t} \qquad (16)$$

and thus

$$=\ddot{Z}-\tfrac{2}{3}A\,.\,\dot{Z}\{Z(t)\}^{3/2}, \qquad (17)$$

since $Z(0)=0$.

By using the relationship $\ddot{Z}=\dot{Z}(d\dot{Z}/dZ)$ eqn. (17) becomes

$$\dot{Z}\frac{d\dot{Z}}{dZ}=-\frac{2A}{3}\,.\,\dot{Z}\{Z(t)\}^{3/2}, \qquad (18)$$

whence

$$\dot{Z}=-\tfrac{4}{15}A\,.\,Z^{5/2}+I, \qquad (19)$$

where $I$ is the constant of integration. At $t=0$, $x=1$, $\dot{Z}(0)=1$ and $Z(0)=0$ and $I=1$. Thus (19) becomes

$$\frac{dZ}{1-(\frac{4}{15})A\,.\,Z^{5/2}}=dt. \qquad (20)$$

Equation (20) was solved numerically for $\dot{Z}=x(t)$ using a DEUCE computer. The result is shown in fig. 1 for three values of $A$ of the order of magnitude likely to be found in actual metal systems. The graphs are in terms of

Fig. 1

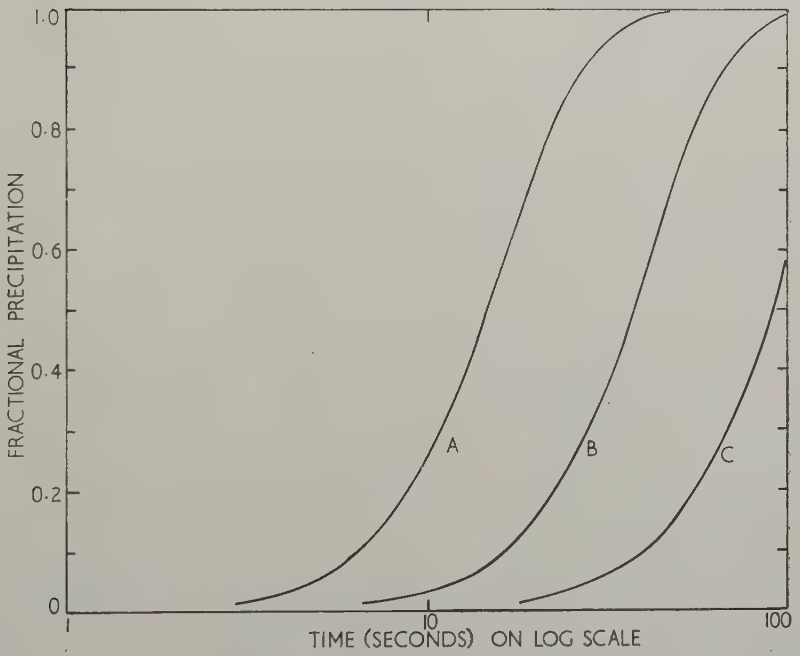

Numerical solutions of eqn. (20). Curves A, B and C are for values of the constant $A$ of $10^{-3}$, $10^{-4}$ and $10^{-5}$ respectively.

the more usual fraction precipitated, $y(t)=1-x(t)$. The curves are of the sigmoidal form and can be brought into coincidence by displacement along the time axis when the latter is on a logarithmic scale. A change in the value of $A$ by a factor of 10 changes the time for half-precipitation by a factor of approximately two-and-half.

## § 4. COMPARISON WITH PREVIOUS TREATMENTS

The earlier Wert–Zener (1949) treatment of reaction rates based upon the Johnson–Mehl method (1939) can be extended to include nucleation and growth processes. The method considers all particles as isolated and the rate of growth is thus given by eqn. (5) without the factor $x(t)$. The increment of volume of precipitate at any given instant is obtained by integrating this equation over all possible sizes. Impingement is allowed for by including the factor $x(t)$ in this integrated growth equation rather than in the growth equation for individual particles, as used in the present method.

The equation corresponding to eqn. (7) is

$$\frac{dv}{dt}=4\pi\sqrt{(2\beta^3)}\,.\,(t-t_1)^{1/2}\,.\,x(t). \qquad (21)$$

If it is assumed that the rate of nucleation per unit volume is constant, the equation corresponding to (9) becomes

$$-\frac{dx}{dt}=\left(\frac{c_0}{c_2-c_1}\right).\,N\,.\,4\pi\,.\sqrt{(2\beta^3)}\,.\,x(t)\,.\int_0^t (t-t_1)^{1/2}\,dt_1 \qquad (22)$$

$$=\frac{8\pi}{3}\sqrt{(2\beta^3)}\,.\left(\frac{c_0}{c_2-c_1}\right)x(t)\,.\,t^{3/2}, \qquad (23)$$

where $N$ is the constant rate of nucleation.

Hence

$$y=1-\exp-\left[\tfrac{16}{15}\pi N\sqrt{(2\beta^3)}\,.\left(\frac{c_0}{c_2-c_1}\right).\,t^{5/2}\right]. \qquad (24)$$

Equation (24) is of the same form as that given by Wert (1949) and Zener (1949) for the growth of precipitates except that the exponent of $t$ is $\frac{5}{2}$ instead of $\frac{3}{2}$. It should be noted that the equation applies to conditions which are slightly different from those postulated for the derivation of eqn. (20). The latter assumes a constant rate of nucleation per unit volume of untransformed phase whereas eqn. (24) expresses nucleation in terms of the volume of sample.

The two results are compared in fig. 2 in which $\log\log 1/1-y$ is plotted as a function of $\log t$. Equation (24) gives a straight line of gradient 2·5 whereas the gradient of eqn. (20) decreases continuously from an initial value of 2·5. However, it is seen that up to $y=0{\cdot}4$ the deviation of eqn. (20) from linearity (the broken line) is small and probably within the experimental uncertainty of many kinetic studies. The gradient of the broken line is 2·47, a value experimentally indistinguishable from 2·5. Thus eqn. (24) is a good short time approximation to the present results.

Fig. 2

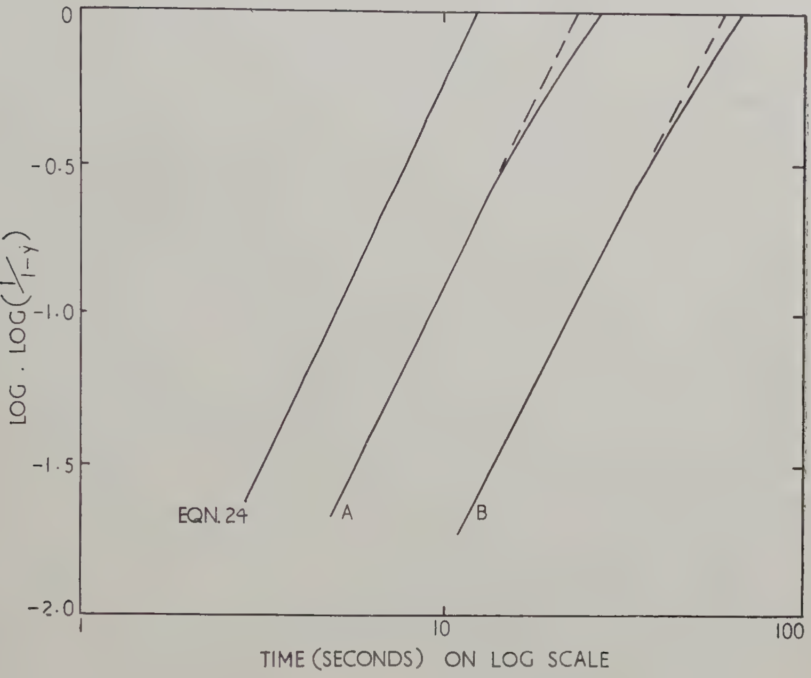

Comparison of the results in fig. 1 (curves A and B) with eqn. (24). A different value of the system parameter has been used for eqn. (24), to displace it along the time axis. The initial stages of A and B are approximately linear with a gradient of 2·47. Broken lines are extensions of linear segments.

## § 5. Discussion

The fractional precipitation as a function of time has been derived for reactions which proceed by nucleation and diffusion controlled growth assuming that the nucleation rate is linearly related to the fractional precipitation. This assumption was selected because (*a*) it is suggested by Zener's (1949) model of precipitation in certain concentrated solutions, (*b*) it is of some empirical interest and (*c*) assuming that growth and nucleation depend on $x(t)$ in the same way, facilitates solution of eqn. (9). As pointed out in § 2 in actual systems $\dot{N}(x)$ may be a very complicated function varying from system to system. Each system requires separate consideration. These empirical rate equations may be derived in two ways. Firstly, by solving eqn. (9) using the appropriate function $\dot{N}(x)$ or $\dot{N}(t)$. This is, in principle, the more satisfactory since the result will apply to all values of $y$. The second is to use the method leading to eqn. (24), which is satisfactory for $y=0$ to $y=0{\cdot}4$. Ham (1958) has shown that eqn. (24), with an exponent of $t$ equal to $1{\cdot}5$, is also a good approximation to the rigorous solution for the growth of precipitates. It is evident that this simple Johnson–Mehl (1939) method is an acceptable substitute for the more fundamentally sound methods in this restricted range of $y$. It has the advantage that eqn. (22) can be readily integrated with various functions for $\dot{N}(t)$ and is thus particularly useful in obtaining approximate rate equations for empirical nucleation and growth laws.

It is appropriate to consider the assumptions made in the derivation of eqn. (9). Growth and nucleation were regarded as independent processes for the purpose of evaluating their respective contributions to the total reaction velocity. This is an over-simplification because nucleation is in fact a growth process of a special kind being influenced by energy factors, such as surface and strain energy, which are of little consequence when the particles attain appreciable dimensions. The attainment of the stable nucleus size is not governed by the diffusion of solute in the parent solution. Furthermore, there must be at least a short time interval immediately after nucleation when the rate of growth is limited by the capture process at the solution–precipitate interface because the diffusion distance is very small and the diffusion flux correspondingly high. Thus, it is reasonable to separate the normal diffusion limited growth from the early growth, including nucleation. An error will arise from assuming that the former growth commences from zero dimensions but it will be negligible in comparison with other errors discussed below.

Other errors at small particle size arise from two sources:

(*a*) The steady-state approximation used for the solution of the diffusion equation becomes inaccurate.

(*b*) The equilibrium concentration, $c_1$, is a function of the size of the precipitate, a factor which is of importance at small sizes.

It follows that the most serious error is likely at values of $y$ between 0 and $0{\cdot}1$. Experimental uncertainty is also greatest in this range due to recalescence, minimum precision in the physical property measurement and anomalous behaviour of physical properties due to coherence. Agreement between experiment and theoretical treatments of reaction kinetics is not to be expected in this range.

The constants in eqn. (20) determine the position of the rate curve on the time axis and not the form of the curve. The latter may be correlated with the time exponent in the approximation, eqn. (24). Within the framework of the present analysis the form is determined simply by the kinetics of the nucleation process. Precipitate geometry has no effect provided that growth is three-dimensional and limited by diffusion, and that the shape is invariant (Ham 1958). Other results arise if growth occurs only in one or two dimensions or if the growth of one or other of the dimensions of discs or cylinders is not diffusion controlled. Conditions under which the latter may occur have been pointed out (Burke, to be published).

## ACKNOWLEDGMENT

The help of Mr. A. Young of the Department of Applied Mathematics with the solution of eqn. (9) is gratefully acknowledged.

## REFERENCES

AVRAMI, M., 1939, *J. chem. Phys.*, **7**, 1103.
BURKE, J., 1960, *Phil. Mag.* **5**, 176.
HAM, F. S., 1958, *J. Phys. Chem. Solids*, **6**, 335.
HOLLOMON, J. H., and TURNBULL, D., 1953, *Progr. metal Phys.*, **4**, 333.
JOHNSON, W. A., and MEHL, R. F., 1939, *Trans. Amer. Inst. min. (metall.) Engrs*, **125**, 416.
TURNBULL, D., 1948, *Trans. Amer. Inst. min. (metall.) Engrs*, **175**, 774; 1956, *Solid State Physics*, **3**, 226.
WERT, C., 1949, *J. appl. Phys.*, **20**, 943.
WERT, C., and ZENER, C., 1950, *J. appl. Phys.*, **21**, 5.
ZENER, C., 1949, *J. appl. Phys.*, **20**, 950.

# Thermal Shock and Fracture in Crystals of Magnesium Oxide

By G. D. Miles and F. J. P. Clarke
Metallurgy Division, Atomic Energy Research Establishment,
Harwell, Berkshire

[Received May 8, 1961]

## Abstract

Crystals of magnesium oxide have been thermally shocked by down-quenching. A single crystal in the as-cleaved condition is shattered by a moderate thermal shock and it is shown that the complex fracture pattern resulting can often be traced back to a single crack nucleus on the crystal surface. If such crack nuclei be removed by chemical polishing the crystal can withstand severe thermal shock without fracturing; the heavy slip produced does not result in crack nucleation by dislocation interaction and reasons for this are discussed. Similar experiments on bi-crystals have shown that the intercrystalline boundary presents a source of weakness which cannot be removed by chemical polishing, and such crystals fracture under moderate thermal shock whatever the state of the surface. Preliminary experiments on repeated low level shocks suggest that crack nucleation may occur under these conditions but the pattern of slip introduced is not the same as that produced by single shocks.

---

## § 1. Introduction

The experiments to be described comprise a study of the flow and fracture behaviour of magnesium oxide crystals under conditions of thermal shock produced by down-quenching into water. The effects of thermal shock at higher rates of heat transfer, such as occur during contact with an arc plasma, are considered in a separate publication (Clarke *et al.* 1961). The nature and magnitude of the heat transfer during quenching, from such perfect surfaces as can be obtained by cleaving or chemical polishing, have not as far as is known been studied before. Such information is important to a discussion of the effects of quenching and so a brief *ad hoc* study was made. Results from this are given in the Appendix.

## § 2. Experimental

The specimens used were cleaved from large crystals (including some bi-crystals) obtained from the Norton Company, Chippawa, Canada. Cleaving was carried out on a pendulum-type machine similar to that described by Gilman *et al.* (1958). Typical extreme specimen sizes were 0·15 cm sq. × 2 cm long and 0·7 cm sq. × 2 cm long. It is usually a consequence of cleaving, that cracks extend on $\{110\}$ planes from the end corners of the block. It is essential that these be removed before quenching, and the ends of the crystals were polished away by allowing each in turn to come into contact with a film of hot orthophosphoric acid carried by a rotating glass wheel. A depth of typically 2–3 mm was removed in this way. When this end-damage had been removed, the whole of the crystal was immersed in boiling orthophosphoric acid, which acts as a chemical polish and removes surface microcracks and defects.

The thermal shock was applied by allowing the crystal to fall from a platinum platform in a furnace into water at room temperature. The prior heating of the specimen was carried out slowly and the crystal was held at maximum temperature for about 15 min to allow equilibrium to be attained. The receptacle containing the water had its bottom and walls protected by tissue papers to prevent any mechanical shock to the crystal, and furnace temperatures up to 1000°c were used. Repeated shocks were applied using an automatic device which raised the crystal (held lightly between ‘ Fluon ’ cups) slowly into the furnace, maintained it for 5 min at the required position in the furnace and then quenched it rapidly before repeating the cycle. In this case temperatures not exceeding 300°c were used.

Dislocations were revealed by etching in a mixture of equal parts saturated ammonium chloride and concentrated sulphuric acid.

## § 3. Characterization of the Thermal Shock

The first consequence of down-quenching is surface strain induced by the temperature change at the surface. The principal variables determining the magnitude of this strain for a given heat transfer rate are temperature change and specimen size. A single parameter will now be derived to enable the thermal shock to be characterized for the differing values of these variables.

The maximum stress, $\sigma_M$, which can be developed assuming a completely linear stress–strain relation has been given by Buessem (1956) for a long cylindrical bar. This case is close enough (Howe 1956) to be used in the present instance and is quoted by Glenny and Royston (1958) as

$$\sigma_M = \frac{\dfrac{E\alpha\Delta T}{1-\mu}}{2\cdot0 + \dfrac{4\cdot3k}{ah} - 0\cdot5 \exp\left(\dfrac{-16k}{ah}\right)}, \quad . \quad . \quad . \quad . \quad (1)$$

where

$E$ = Young's modulus ($3\times10^{12}$ dyn cm$^{-2}$ : Gilman 1959) ;

$\alpha$ = coefficient of linear expansion ($13\cdot5\times10^{-6}$ deg$^{-1}$ c : Kingery 1955) ;

$\Delta T$ = temperature change ;

$\mu$ = Poisson's ratio (0·36 : Kingery 1955) ;

$k$ = Thermal conductivity (taken at $0{\cdot}8 \times$ max. temperature. Values from Kingery 1955);

$a$ = cylinder radius ($=(x+y)/4$ where $x$ and $y$ are width and depth respectively of the crystal: see Howe 1956);

$h$ = heat transfer coefficient ($0{\cdot}1$ cal. sec$^{-1}$ cm$^{-2}$ deg$^{-1}$ C: Appendix).

In practice the onset of plastic flow may prevent this value being attained but the total strain, which is the primary consequence of the shock, will be unaffected by the maximum stress reached. Hence if the yield stress, $\sigma_{\mathrm{y}}$, is known the amount of plastic strain may be deduced. A parameter proportional to the plastic strain would seem to be a meaningful one to use in characterizing the thermal shock, especially in respect of the probability of its resulting in fracture, for the following reasons: firstly because it has been found in conventional tensile and bend tests that microcracks below the critical Griffith size propagate after, and only after, slip has occurred (Clarke and Sambell 1960) and secondly, the probability of crack nucleation in the absence of such microcracks depends, for given surface conditions, on the amount of plastic strain produced (Stokes *et al.* 1961). In previous thermal shock studies the first of these criteria has been found to apply though for experimental reasons the second was not tested (Clarke *et al.* 1961).

Now plastic strain,

$$\epsilon_{\mathrm{p}} = \sigma_{\mathrm{M}}/E - (\text{elastic strain at yield stress})$$

whence a thermal shock parameter, $S$, will be defined by

$$S = \frac{E}{\sigma_{\mathrm{y}}} \, . \, \epsilon_{\mathrm{p}} = \left\{ \frac{\sigma_{\mathrm{M}}}{\sigma_{\mathrm{y}}} - 1 \right\}. \qquad \qquad (2)$$

It is important that the $S$-values should be regarded as only semi-quantitative owing to the possibility of error in the quantities used in their computation.

Taking $\sigma_{\mathrm{y}} = 6 \times 10^8$ dyn cm$^{-2}$ (Clarke and Sambell 1960) and using the values already given, typical values of $S$ are: $S = -0{\cdot}75$ for $\Delta T = 100°$C, $a = 0{\cdot}1$ cm and $S = 21$ for $\Delta T = 1000°$C, $a = 0{\cdot}3$ cm. Negative values of $S$ refer to conditions insufficient to produce *macroscopic* plastic deformation and $S = 0$ should give the minimum temperature difference required for the yield stress to be attained at the surface. However, in practice plastic flow can first be detected, by etching, at half the macroscopic yield stress or even earlier.

## § 4. RESULTS

A summary of the results relating $S$, the crystal condition, and the effects of the quench is given in the table.

### 4.1. *As-cleaved Monocrystals*

Slip commences at $S \simeq -0{\cdot}6$, although at this value it is very sparse (fig. 1 *a*)†. The slip occurs on $\{110\}_{45}$ planes (notation of Stokes *et al.*

---

† Figures 1, 2, 4, 6, 7, 8, 9, 10 and 11 are shown as plates.

1959 a) since the surface tensile stresses can be relieved by shear on these systems but not by shear on $\{110\}_{90}$ planes (Clarke *et al.* 1961). Near the edges of the crystal some slip on these latter planes (which have slip traces in $\langle 110\rangle$ directions) does occur, since the stress distribution is here no longer symmetrical in all directions.

Summary of results relating the thermal shock parameter, $S$, the crystal condition and the effect of the quench

| Thermal shock parameter, $S$ | Type and condition of crystal | Effect |
|---|---|---|
| $<-0\cdot7$ | Any | None |
| $-0\cdot6$ | Any | Slip just detected, e.g. fig. 1 (*a*) |
| 0·15 to 0·75 | Unpolished or ‘ imperfect ’ surface | Cracking produced including shattering in some cases |
| 0·06 to 0·4 | Bi-crystal—‘ perfect ’ surface | Single crack |
| $>0\cdot8$ | Bi-crystal—‘ perfect ’ surface | Shatters |
| $>16$ | Single crystal—‘ perfect ’ surface | No cracking—heavy slip, e.g. fig. 1 (*b*) |

Cracking occurs for $S>$ *ca.* 0·1 and for values rather higher than the minimum (e.g. $S=0\cdot5$) the pattern is complex. A typical example is illustrated in fig. 2 where the crystal is viewed by transmitted light. Cracks appear dark, either as lines, which represent cracks perpendicular to the plane of the photograph, or as dark areas where a crack runs parallel to this plane and below the surface of the crystal. The overall pattern of fine lines is caused by cleavage steps on the crystal surface. The cracking occurs principally on the $\{100\}$ cleavage planes, although cracks on $\{110\}$ planes are not uncommon.

The value of the thermal shock parameter for cracking to occur is quite critical. For example a typical crystal containing crack nuclei showed no cracking at $S=0\cdot2$, but widespread crack branching during a further shock at $S=0\cdot3$.

## 4.2. *Polished Monocrystals*

### 4.2.1. *Incomplete defect removal*

The faces, and in particular the corners produced on crystals by the cleavage process, have been shown to contain microcracks typically $2\cdot5\times10^{-4}$ cm long and it is established that the ductility of the crystals is enhanced if these defects are removed by chemical polishing (Stokes *et al.* 1958, Clarke and Sambell 1960). However, it was found in the initial experiments that although the surface was heavily polished away in this manner until almost all microscopically visible surface defects were removed, a similar pattern of cracking still persisted. For example the crystal represented in fig. 3 (*a*) had been heavily polished by immersion in boiling orthophosphoric acid for 3 min. According to Ghosh and Clarke (1961) this should remove about $10^{-3}$ cm of surface. The pattern of cracking was caused by quenching from 250°c ($S=0{\cdot}15$). By observation of the cleavage steps on the crack surfaces it is possible to ascertain the direction of motion of the crack front in any region (Gilman 1958).

Fig. 3

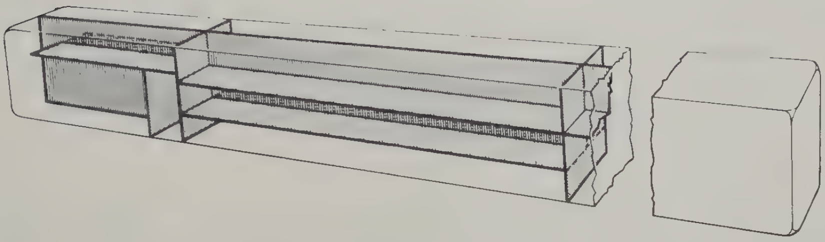

(*a*) Crack pattern in an imperfectly polished and quenched crystal $S=0{\cdot}15$.

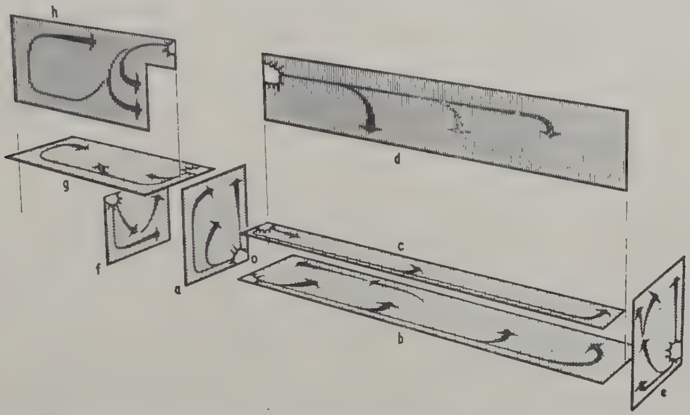

(*b*) Schematic representation of the order of crack propagation. Crack plane *a* starts at surface defect at O. Cracks *b*, *c*, *d*, *g* and *h* branched from *a*. *e* and *f* branched from *b* and *g* respectively.

Thus in the case of fig. 6 the crack has propagated along the directions of the arrows as evidenced by the V formations of the cleavage steps, e.g. at B. A detailed discussion of this phenomenon is given in the aforementioned paper ; in the present work Gilman's observations have been confirmed, and this technique used extensively to ascertain the origin of a particular crack.

By applying this observational method to the present crystal, the internal cracks being observed by focusing the microscope into the crystal, the cracks were found to have spread in the way indicated by the arrows of fig. 3 (*b*). It can be noted that all the cracks with the exception of *a* have their origin where their plane intersects another crack. Similarly the plane *a* with its origin at O was associated with a defect which had been visible at the corner of the crystal before shocking, having been only imperfectly removed by the prior polishing. Thus we can describe the formation of the crack pattern in the specimen as follows : Crack *a* is formed by growth from an existing surface defect ; cracks *b*, *c*, *d*, *g* and *h* all originate in the crack plane *a*, and finally cracks *e* and *f* start from *b* and *g* respectively. The end of the crystal shown separated from it in fig. 3 (*b*) contained several minor cracks which lay within the depth of focus of the microscope objective and thus interfered with one another, so that their origin could not accurately be found. However, they were all interconnected with the larger system, and there is no reason to suppose that they also did not originate from the single nucleus O.

The range of $S$-values given in the table for imperfect crystals reflects the different degrees of perfection produced by varying the preparation conditions rather than the response of crystals similarly prepared. These $S$-values, compared with the results of more careful preparation (§ 4.2.2), do show that the polishing of crystals without *complete* removal of microcracks does not greatly improve the shock resistance of the crystal.

On every occasion in which cracking resulted from a single quench the crack system introduced could be attributed to an origin present beforehand. The effect of complete removal of such crack origins will now be described.

### 4.2.2. *Complete defect removal*

The realization that the cracks could multiply in this way implied that extreme care would be necessary in specimen preparation if the mechanisms of nucleation were to be observed. By a process of careful selection from the cleaved crystals, and prolonged chemical polishing using times as long as 1 hour in boiling acid (removal of $\sim 0{\cdot}03$ cm), a number of crystals were obtained without a single blemish that could be interpreted as a crack when examined microscopically. The surface was very uneven, and the corners rounded following the action of the acid, but there were no sharp steps or grooves that could act as stress concentrators.

One such specimen gave the series of photographs illustrated in fig. 4. It was shocked at various temperatures up to 1000°c, but no cracking was produced. Very dense slip had occurred, however, as evidenced by the presence of slip lines on the surface, and also by the intense birefringence resulting and shown in fig. 4 (*a*). At this stage the specimen had withstood a maximum shock of $S = 15{\cdot}5$ without any evidence of cracking.

A light scratch was now made near one end of one face of the crystal which was then shocked again from 1000°c. On this occasion it fractured into a complex but connected pattern of cracks. The scratch before and after shocking is shown in fig. 4 (*b*) and (*c*) and the appearance of the crack traces on the four faces of the crystal after shocking is drawn out in fig. 5. The original scratch is indicated by the arrow. Although the scratch contained many possible nuclei in fact only two cracks have spread from it (*a* and *b* of fig. 5), at right angles to one another. For example the crack moving directly into the body of the crystal (fig. 4 *c*) started from the nucleus arrowed in fig. 4 (*b*). It is presumed that the remainder of the crack system shown in fig. 5 developed in the same way as in the case described previously.

Fig. 5

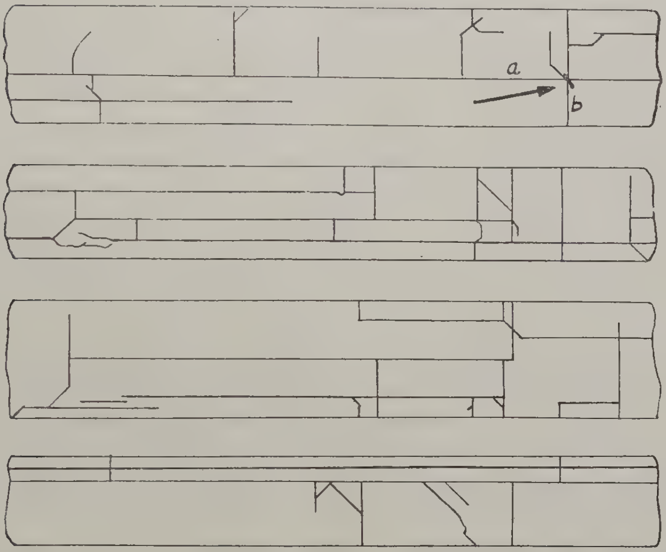

Plan of crack configuration on each face of crystal of fig. 4 (*a–c*). Arrow points to scratch of fig. 4 (*b*).

At such very high $S$-values the density of etch-pits is so great that they can barely be resolved (fig. 1 (*b*) ). Those dislocation systems which can be identified again lie in the $\{110\}_{45}$ planes. It is interesting to note that the distribution of the most dense individual slip systems of fig. 1 (*b*) (marked by added lines) is very similar to fig. 1 (*a*), a very lightly shocked crystal.

Successful quenches from temperatures *ca.* 1000°c are experimentally extremely difficult, due to the sensitivity of the polished crystal surface to contact with other surfaces. As evidenced in fig. 4, cracking in this high temperature range can be catastrophic, from a small scratch such as is easily produced by contact with any hard surface. However, a number of quenches from 1000°c of carefully polished crystals showed that for a single quench either the distribution or the amount of slip produced was unsuitable to produce microscopically observable crack nuclei by, for example, dislocation interactions.

### 4.3. *The Effect of Intercrystalline Boundaries*

A number of tests have been made using bi-crystals in order to ascertain the effects of an intercrystalline boundary. The boundary was roughly in the centre of the crystals and would typically make angles of up to 20° with a plane normal to the specimen's longer axis. The orientation change of the lattice across the boundary would be of the order 10°. A study of the effect of boundary angles was not made.

It was found that the presence of the boundary was a weakening influence on the crystal. Thus although the remainder of the surface appeared free from defects after prolonged polishing, and a high shock-resistance was expected by analogy with the single-crystal observations, the bi-crystals shattered at comparatively low values of $S$. For example, with $S=0{\cdot}9$, widespread cracking was observed, and on another crystal there was limited cracking in the region of the boundary at as low a value as $S=0{\cdot}05$.

By observation of the cleavage steps on the crack surfaces as described earlier, it was possible to isolate the origin of cracking, and in all cases (a total of six) the cracking occurred from the region of the boundary at a position where it intersected a corner of the crystal. An illustration of this point is given in fig. 6 which shows the corner of a crack plane from which the crack has spread. The boundary is indicated (arrowed A) crossing the top right-hand corner of the photograph, and remembering that the V formation of the cleavage steps (e.g. at B) indicates the direction of motion of the crack, it can be seen that the cracking has spread from the point E on the boundary. The initial spreading of the crack into a long area (arrowed C in the photograph) is characteristic not only of crack growth from intercrystalline boundaries but of microcrack growth in general. This feature will be dealt with in a future paper on the mechanisms of microcrack growth. Figure 7 (*a*) shows at lower magnification the whole of the crack plane which separated the crystal into two pieces, and the region of fig. 6 is indicated in the right hand corner (arrowed A). This photograph illustrates features common to all cases of fracture and so will be referred to again in § 4.4.

Cracks associated with the boundary, but not spreading into a major system, have occasionally been observed and an example of several such cracks is given in fig. 8. The long crack AB nearest the lower right of the picture is part of the main crack pattern, but the others appear to be isolated from it.

### 4.4. *General Features of Crack Propagation*

The evidence of the cleavage steps in fig. 7 (*a*) is typical of all crystals tested in that it shows how the crack propagated initially round the outside of the crystal before spreading inwards towards the centre. Often the crack spreads in both directions around the crystal from the origin, and a large step is left where these oppositely moving cracks (by now not on identical cleavage planes) meet. Such a step is visible (arrowed B) in fig. 7 (*a*).

The cleavage steps form traces parallel to the local direction of motion of the crack front. The actual shape of the front can also be observed under certain circumstances. When a crack moves sufficiently slowly plastic flow occurs at its tip, and the crack nucleates many small loops of dislocations ahead of itself (Gilman 1957, 1958). The loss of energy from the crack by this plastic flow can cause it to stop. If now the crack is started again, as it moves through the region of the dislocations its front becomes heavily jogged by the screw components and the density of cleavage steps is suddenly increased. By inspection of fig. 7 (*b*), which is the same view as 7 (*a*) but etched, we see that this has occurred repeatedly as the crack moved inwards. The etching reveals the dislocations nucleated by the crack, and the crack front can be seen to have moved inwards fairly uniformly round three sides of the crystal, with some ten discontinuities in its motion.

Another feature of interest can be seen in fig. 6 (arrowed D). This type of pattern, shown in greater detail in fig. 9, occurs where a crack front makes an approximately perpendicular approach to a crystal edge. The side face, also in fig. 9, shows that this structure takes the form of a departure from the normal cleavage plane of the crack.

### 4.5. *The Effects of Repeated Shocking*

Owing to the extreme sensitivity of the thermal shock behaviour to surface condition in the crystals, it is difficult to be certain that a failure after repeated shocking is not a consequence of some damage to the surface at a late stage in the life. In an attempt to eliminate this possibility and to provide reproducible shocking conditions crystals were repeatedly quenched while held loosely at each end in ‘Fluon’ cups. The $S$-values for each quench were $\simeq 0{\cdot}8$. Several crystals shattered after a few hundred cycles at this level, although their surface was initially perfect. The origin of cracking could not be discovered since the crystals broke typically into 30–40 pieces. However, one crystal withstood 1250 shocks at $S = 0{\cdot}95$ cycle$^{-1}$ without any evidence of cracking, although when etched the separate pits could not be distinguished over most of the surface (fig. 10). The cumulative $S$-value for this crystal would be equivalent to a surface strain of about 25%.

Although the evidence conflicts as to whether the strain produced by repeated shocks can induce crack nucleation, it does appear that the slip distribution differs in some respects from that caused by a single heavier shock. Thus, as we increase the number of shocks, the sparsely populated initial bands similar to those of fig. 1 (*a*) gradually become wider and spread towards one another. Figure 11 (*a*) shows a crystal which has been shocked repeatedly at $S = 1{\cdot}0$, and etched at three stages of its life (after 1, 10 and $\simeq 50$ shocks). The configuration of the slip bands at these times is clearly revealed by the three depths of etching.

The rectangular unslipped blocks between the bands remain sharply delineated after more shocks although they gradually reduce in size and are eventually eliminated. Blocks still visible in a very heavily slipped crystal can be seen in fig. 10. A further feature of the etched surface is the curved ‘ traces ’ extending from the corners of the unslipped blocks in fig. 10. These traces appear as the boundary between regions in which the dislocations differ in Burgers vector. An example of the complex patterns so produced is given in fig. 11 (*b*).

Neither the blocks nor the traces are observed in crystals singly shocked at a higher stress level. Possibly the greater ease of cross slip at higher temperatures makes the edge of bands more diffuse, and although unslipped regions can still exist they do not have the sharp boundaries characteristic of these phenomena.

## § 5. Discussion

### 5.1. *General Behaviour*

The microcracks left in the crystal after cleaving are generally too small to propagate as Griffith cracks but the finding that they do propagate after plastic flow has occurred (table) is consistent with previous studies (Clarke and Sambell 1960, Clarke *et al.* 1961). The mechanism of microcrack growth will not receive further discussion here but it will be noted that once started the crack propagation is controlled by the stress distribution introduced by the thermal shock. During cooling the outer layers of the crystal are subject to tensile stresses, which are balanced by compressive stresses in the interior. The ‘ crack front ’ grows only through tensile regions, which explains its initial movement from the nucleus around the periphery of the crystal. As the cooling front moves inwards it carries the tensile region with it and so the crack front also moves into the body of the crystal. However, its movement is discontinuous because the crack moves much faster than the cooling front. Thus even for the case of a square bar cooled under conditions of infinite heat transfer it can be shown, following McAdams (1954), that the centre temperature of a bar of magnesium oxide 4 mm square takes 0·3 sec to complete 90% of the temperature change ; and in the present case the time will be increased by the finite heat transfer rate. Now Gilman *et al.* (1958) have shown that for the case of lithium fluoride a crack moving at less than $6\times10^3$ cm sec$^{-1}$ nucleates dislocations. If we assume a similar value for magnesium oxide the crack in fig. 7 (*b*) would have crossed all the dislocation-free regions in between the bands in less than $2\times10^{-5}$ sec. Hence it is believed that the crack front moves discontinuously and that the dislocation bands of fig. 7 (*b*) represent its successive positions.

The branching of the cracks into the observed pattern can readily be understood. Since the stresses are entirely the result of constraint of surface deformation, then if the surface is allowed to expand in a given region by the opening of a crack, the stresses which would have been present across the line of the crack are relieved. This does not however apply to the stresses which would have been present parallel to the crack ; these are unaffected. If these stresses are to be relieved the crack must branch and it does so along the energetically favoured cleavage planes. That there should be nuclei enabling the cracks to branch is an immediate prediction of the experimental data obtained in tensile and other tests on magnesium oxide. Once a single crack is present, the crystal changes from being a ' polished ' crystal to one containing an ' as-cleaved ' surface which has repeatedly been shown to contain flaws which initiate fracture. Microcracks would be expected to occur at the corner made by the cleavage and polished faces and indeed (see fig. 3 (*b*)) it is observed that many branch cracks originate near this type of corner. However, not all branch cracks originate exactly in a corner and cleavage steps may also act as nuclei. These have been shown to be sources of stress concentration and have been observed to produce cracking under thermal shock conditions (Marsh 1960, Clarke *et al.* 1961).

### 5.2. *Possibility of Crack Nucleation by Dislocation Interaction*

It has been established by other forms of stressing, that the interaction of dislocations in slip-bands can give rise to crack nuclei from which the crystal can fail (Stokes *et al.* 1959 *b*, Keh *et al.* 1959, Whapham and Makin 1960, Clarke 1960). The evidence from the present work is that under the heavy slip conditions produced by down-quenching no crack nuclei are produced by dislocation interaction. In the next two paragraphs suggestions to explain this will be made.

Recent work of Stokes *et al.* (1961) has indicated that the flow and fracture behaviour is strongly influenced by the density and distribution of slip at the onset of plastic flow. Very fine slip either stabilizes cracks at a size below the limit of microscopic resolution or upsets the usual crack nucleation process altogether. As a result they found that a crystal with very fine slip was capable of deformation typically 10% before crack nucleation led to immediate fracture; there was no formation of microscopically visible cracks during the deformation, in contrast to crystals with a coarser slip configuration. The explanation appears to be that in the case of a small number of intrinsic sources most of the plastic flow at any instant is confined to the edge of a few slip bands, where the local high stress concentration is conducive to the dislocation avalanches which often precede crack nucleation. A high number of intrinsic sources however tends to homogenize the stress throughout the crystal and inhibit these avalanches.

Now the slip systems introduced by quenching are evenly distributed and dense ; stable cracks are never observed. This is similar to the fine slip case of Stokes *et al.* (1961), and if the criteria they enunciate are applicable, quenched crystals should be capable of considerable deformation before crack nucleation or growth could take place. But under theoretically ideal conditions the plastic deformation cannot exceed $\alpha \,.\, \Delta T/1-\mu$ which with $\Delta T = 900°\text{C}$ is only 1·8%; and this figure will be considerably reduced in practical conditions. For example with $S = 16$ which represents the most severe single shock of the present experiments the strain is only *ca.* 0·3%. If this explanation is valid it should be unlikely for any size of carefully polished crystal to fracture as the result of a single quench. Neither the thermal shock conditions of the present experiments nor those previously reported (Clarke *et al.* 1961) led to stabilized cracks. In fact the evidence is that microcracks very readily propagate in spite of fine slip and this suggests that the effect of such slip is to inhibit the *formation* of microcracks rather than to stabilize them at a very small size.

### 5.3. *Bi-crystals*

In the present work bi-crystals fractured at stress factors similar to those for unpolished or imperfectly polished single crystals. As was mentioned in § 4.3, a striking feature of the failures from intercrystalline boundaries is that they occurred in all cases from a region of the boundary where it intersects a corner of the crystal. Now the corner is favoured as a nucleation point for a crack, on either of two counts. Both of these arise from the possibility of heat transfer out of this region from two faces of the crystal, and not from one face as elsewhere. Firstly, there is the possibility that this additional heat transfer will give rise to higher strains in this region, and secondly a given strain may be reached more quickly. The latter alternative seems the more important since even at high $S$-values when the overall strain is more than sufficient to cause widespread cracking, the fracture still occurs from a corner.

Westwood (1961) has proposed a mechanism for crack nucleation at intercrystalline boundaries, from the cooperative action of bands of edge dislocations approaching the boundary from opposite sides. And as pointed out in § 4.1 such a slip configuration will, in the absence of cracks, be found principally in the corners. However, in the present work, although a single band of edge dislocations was observed in one instance in the region of the crack origin, it is not felt that the same mechanism is in operation and results to date suggest, though do not confirm, that the dislocations found near cracks may be caused by, rather than causing, the cracking. Similarly it is not considered that the cracks in fig. 8 necessarily arise from the associated edge dislocations. It could well be that the $\{110\}_{90}$ systems have propagated after the crack AB had spread and are due to the disturbance of the stress distribution by the presence of cracks. As discussed in § 5.1, this would leave stress components parallel to the cracks which could cause slip on $\{110\}_{90}$. In any case, edge components are not always present on both sides of the boundary (fig. 8, cracks *a* and *b*) as required for Westwood's mechanism. Westwood's work was done under compression conditions and it may be that the tensile conditions of the present work do not favour the occurrence of the same mechanism.

## ACKNOWLEDGMENTS

We should like to acknowledge helpful discussions with several of our colleagues in the Ceramics Group, with Mr. E. Glenny of N.G.T.E., Pyestock, and with Mr. J. B. Huffadine of the Plessey Co., Towcester ; we are indebted to Messrs. K. D. Cooper and B. E. Pinchin of the Photographic Group for taking the high-speed films referred to in the Appendix. We are particularly grateful to Mr. J. Williams for helpful criticisms during the research, and to both him and Dr. P. Murray for their encouragement and support of the work.

## APPENDIX

When the heat transfer coefficient between a surface and a boiling liquid is measured it is usually found to depend critically on the temperature difference between the surface and the liquid. For small temperature differences (typically up to 50°c in the literature) boiling occurs by discrete bubbles, usually from favoured ‘ nuclei ’ on the surface. The bubbling action stirs the surrounding liquid and consequently the transfer rate is high. For larger temperature differences a new mode of boiling occurs : the surface becomes completely blanketed by a sheath of vapour, and the heat transfer, which can now occur only by radiation or gaseous conduction across the film, drops to a very low value (see, for example, McAdams 1954).

These different modes are clearly important in the present work since if ‘ film boiling ’ occurs during high temperature quenches, and ‘ bubble boiling ’ during lower ones, the heat transfer rates in the two cases would be by no means comparable.

Hence a series of high-speed cinematograph films of crystals during quenching was made, using a framing-rate of about 2000–3000 frames/sec. The evidence of these films was that bubble boiling occurred in quenches both from as low as 180°c and as high as 1000°c. However, a crystal which had been fingered (thus transferring grease) before quenching, and so not having the high degree of surface perfection usual in the polished crystals in this work, was found to cool by ‘ film boiling ’ on quenching from 1000°c. The time of cooling in this case was some 6–7 times longer than usual, and although the crystal contained many microcracks and other imperfections which would normally have caused it to shatter, it remained intact. These results provided fairly clear evidence that ‘ film boiling ’ is not an important occurrence in the present work. It is suggested that the bubble anchoring-sites provided by surface imperfections are not present in polished and unhandled crystals, and the bubbles are able to break away before they coalesce to form a film.

The value of the heat transfer coefficient to be used in our calculation of $S$-values can be found approximately from these cine-films. Thus by measuring the time taken for boiling to cease after the crystal enters the water, and writing : $\theta_0$ = bath temperature (20°C), $\theta_1$ = initial temperature, $\theta_2$ = 'average' temperature of crystal when boiling stops, we can derive an equation

$$h = 2\cdot 3\,\frac{mC}{A}\,\frac{1}{t}\,\log_{10}\left(\frac{\theta_1-\theta_0}{\theta_2-\theta_0}\right)$$

where $h$ = heat transfer coefficient assumed constant, $m$ = mass of crystal, $c$ = specific heat of crystal, $A$ = surface area of crystal, $t$ = time of cooling as defined earlier. The equation is derived assuming Newton's law of cooling to apply, and that a change of surface temperature of $\Delta\theta$ produces a similar change in the 'average' temperature of the block. This is clearly not strictly true but the calculation serves as a guide to the order of magnitude of $h$, which is important when the wide range of values quoted in the literature (e.g., Kingery 1955) is considered. The results so obtained are in good agreement with those derived using data for the variation of mean temperature with time and heat transfer coefficient from Glenny and Royston (1958).

Using the observed values $t = 1\cdot 0$ sec for 1000°C quench, $t = 0\cdot 2$ sec for 160°C quench ; then if we take $\theta_2 = 120$°C, $h_{1000} = 0\cdot 08$ c.g.s. units, $h_{160} = 0\cdot 08$ c.g.s. units. The quantity $\theta_2$ is however ill-defined, and by altering the value assumed for this it is possible to vary the value of $h$. For example, if $\theta_2 = 105$°C, $h_{1000} = 0\cdot 08$ c.g.s. units, $h_{160} = 0\cdot 11$ c.g.s. units.

However, even by changing both $\theta_2$ and $\theta_0$ to extreme values, $h$ is not altered by more than a factor of two. We will hence take for $h$ in the present calculations the typical value $h = 0\cdot 1$ cal cm$^{-2}$ sec$^{-1}$ deg$^{-1}$ C excess.

## REFERENCES

BUESSEM, W. R., 1956, *High Temperature Technology*, edited by I. E. Campbell (New York : John Wiley), p. 460.

CLARKE, F. J. P., 1960, *Special Ceramics : Symposium, July* 1959, *Proceedings*, edited by P. Popper (London : Heywood & Co.).

CLARKE, F. J. P., and SAMBELL, R. A. J., 1960, *Phil. Mag.*, **5,** 697.

CLARKE, F. J. P., SAMBELL, R. A. J., and MILES, G. D., 1961, *Trans. Brit. ceram. Soc.*, **60,** 5, 299.

GHOSH, T. K., and CLARKE, F. J. P., 1961, *Brit. J. appl. Phys.*, **12,** 44.

GILMAN, J. J., 1957, *Trans. Met. Soc. A.I.M.E.*, **209,** 449 ; 1958, *Ibid.*, **212,** 310 ; 1959, Conference on Fracture, Swampscott, April.

GILMAN, J. J., KNUDSEN, C., and WALSH, W. P., 1958, *J. appl. Phys.*, **29,** 601.

GLENNY, E., and ROYSTON, M. G., 1958, *Trans. Brit. ceram. Soc.*, **57,** 645.

HOWE, P. W. H., 1956, N.G.T.E. (Pyestock) Memorandum M263.

KEH, A. S., LI, J. C. M., and CHOU, Y. T., 1959, *Acta Met.*, **7,** 694.

KINGERY, W. D., 1955, *J. Amer. ceram. Soc.*, **38,** 3.

MARSH, D. M., 1960, *Phil. Mag.*, **5,** 1197.

MCADAMS, W. H., 1954, *Heat Transmission* (New York : McGraw-Hill).

STOKES, R. J., JOHNSTON, T. L., and LI, C. H., 1958, *Phil. Mag.*, **3,** 718 ; 1959 a, *Trans. Met. Soc. A.I.M.E.*, **215,** 437 ; 1959 b, *Phil. Mag.*, **4,** 137 ; 1961, *Ibid.*, **6,** 9.

WESTWOOD, A. R. C., 1961, *Phil. Mag.*, **6,** 195.

WHAPHAM, A. D., and MAKIN, M. J., 1960, *Phil. Mag.*, **5,** 237.

# The Pressure Dependence of the Thermoelectric Power of the Alkali Metals at Room Temperature

By J. S. Dugdale and J. N. Mundy†
Division of Pure Physics, National Research Council, Ottawa, Canada

[Received May 16, 1961]

## Abstract

The thermoelectric power $S$ of the alkali metals has been measured under pressures up to 3000 atmospheres at room temperature. A pressure of about 400 atmospheres causes $S$ to change sign in caesium. The results are discussed in terms of the distortion of the Fermi surface under pressure. A relationship between $S$ and the pressure coefficient of electrical resistivity is noted.

## § 1. Introduction

We report here the results of some experiments to determine the effect of pressure on the thermoelectric power of the alkali metals at room temperature. First, we shall describe the experimental methods; then, after presenting the results, we shall give a short discussion of their significance in the last section.

## § 2. Experimental

The specimens were extruded bare wires about 50 cm long and about 0·5 mm in diameter. They were extruded under oil which had been thoroughly dried so as to reduce oxidation and contamination of the specimens.

Since the effects to be measured were in general small (except in caesium) the thermoelectric power of the compressed metal was measured in relation to that of the same metal uncompressed. Thus, in general, two specimen wires were made for each experiment. Because of the difficulties of making caesium wires and because the changes of thermoelectric power in caesium were large, its thermoelectric power was determined as a function of pressure directly against that of an uncompressed wire of lead.

Both the specimen wires (i.e. the uncompressed wire and the wire to be compressed) were mounted in Teflon tubing with a copper cup at each end. A copper wire was embedded in the alkali metal in the cup and this ensured a good electrical contact with the specimen. The mounted specimens were then placed, one into the high pressure tubing, the other into a German-silver tube. The high pressure tubing was closed with plugs having copper electrodes sealed into them with 'Araldite', an electrically insulating material with strong bonding power.

---

† National Research Council, Postdoctorate Fellow. Now at the Institute for Molecular Physics, University of Maryland, U.S.A.

The two thermocouple tubes were mounted vertically parallel to each other with their ends immersed in two oil baths at different temperatures (fig. 1). The temperature of both baths was controlled to better than 1/50°c. The tubing extended well into both baths so that, where a pressure gradient existed (in the electrodes leading out of the pressure tube) or where the specimens were joined to the electrodes, there was no temperature gradient. The temperature of the lower bath was measured using a platinum resistance thermometer and the temperature difference between the baths using a copper–constantan thermocouple.

Fig. 1

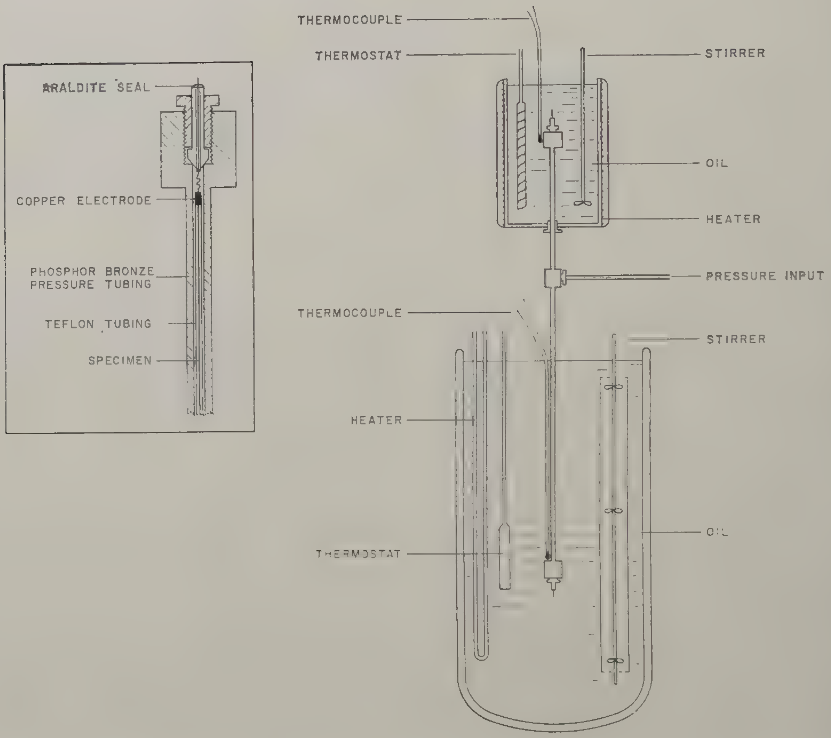

Diagram of the apparatus. The inset shows a closer view of the electrode assembly.

The lower electrodes of the specimens were joined together with a copper wire and the upper pair, across which the potential was to be measured, went via a switch (having negligible thermal e.m.f.'s) to a galvanometer amplifier circuit. The galvanometer amplifier, with a sensitivity of 0·05 $\mu$v, was used as a null detector in a potentiometer circuit. At a pressure of three thousand atmospheres and a temperature difference of 10 °c, a typical thermoelectric force was of the order of 10 $\mu$v which could thus be measured with an accuracy of about 1%.

The measurements of thermoelectric e.m.f. were usually made with three different temperature intervals for each specimen. The full pressure range was 3000 atmospheres and readings were made at intervals of about 500 atmospheres. Measurements were made with both increasing and decreasing pressure but there was never any significant difference between the corresponding values so obtained.

The absolute thermoelectric power of each metal in this temperature region was determined by measuring the thermoelectric force of the uncompressed metals against lead using the same temperature baths and measuring circuit. The values for the absolute thermoelectric power of lead were taken from the work of Christian *et al.* (1958).

## § 3. Experimental Results

Details of the specimens used are given in table 1 which gives the residual resistance ratio as an indication of the purity of the material. In table 2 we give values of the absolute thermoelectric power, $S$, at 0 °c as determined in these experiments. The values of $S$ for sodium, potassium and rubidium agree well with previous determinations (MacDonald 1954). Those for lithium and caesium differ somewhat from Bidwell's values (Bidwell 1924) but his results were not very accurate. As we shall see, the thermoelectric

Table 1

| Metal | Source | Residual resistance ratio: $R_{4\cdot2^\circ\mathrm{K}}/R_{0^\circ\mathrm{C}}$ | Bath temperatures (in °c) used in pressure measurements |
|---|---|---|---|
| Li | Lithium Corporation of America | $2\cdot6\times10^{-3}$ | 33 and 54<br>33 and 71<br>33 and 85 |
| Na | Unknown (reagent grade metal) | $6\cdot3\times10^{-4}$ | Same as lithium |
| K | Mines Safety Appliances Ltd., Toronto | $8\cdot0\times10^{-4}$ | 0 and 36<br>0 and 48<br>19 and 49 |
| Rb | Messrs. A. D. Mackay and Co., New York | $3\cdot3\times10^{-2}$ | 0 and 10<br>0 and 20<br>0 and 30 |
| Cs | Messrs. A. D. Mackay and Co., New York | $6\cdot5\times10^{-3}$ | 0 and 10<br>0 and 16·5<br>0 and 20·4 |

power of caesium is extremely sensitive to compression and this is probably sufficient to account for the discrepancy here since previous measurements have been made on specimens in capillary tubes. Our measurements on lithium have been repeated using quite different apparatuses and all our determinations agree within the experimental error. We shall therefore adopt our value.

In general, the raw data from the experiments consist of values of the thermoelectric e.m.f. of the thermocouple (comprising the compressed and uncompressed metals) as a function of pressure for a given difference of temperature between the two junctions. From such results obtained with different temperature intervals it is then possible to deduce $\Delta S$, the difference in thermoelectric power between the compressed and uncompressed metals, as a function of pressure and hence of volume. The actual temperature intervals used for the different metals are indicated in table 1.

Table 2

| Metal | $S_0$ ($\mu$v/°K) | $d \ln S/d \ln V$ | Source of data |
|---|---|---|---|
| Li | 10·6 | 0·43 | These experiments |
| Na | − 5·8 | 2·1 | ,, |
| K | −12·9 | −0·36 | ,, |
| Rb | − 9·5 | 0·39 | ,, |
| Cs | − 0·9 | 50 | ,, |
| Cu | | 2·6 | Bridgman (1949) |
| Ag | | 6·3 | ,, |
| Au | | 4·4 | ,, |

$S_0$ is the value of the absolute thermoelectric power of the metal at 0°C. $d \ln S/d \ln V$ is the volume derivative of $S$ at this temperature.

In fig. 2 we show the full results of $S$ versus pressure; this figure makes use of the absolute values of $S$ at zero pressure shown in table 2. The figure illustrates that in all the metals except potassium the initial effect of pressure on $S$ is to make its magnitude diminish. In potassium the magnitude of $S$ first increases and then under further pressure begins to decrease. The behaviour of caesium is very striking: at about 400 atmospheres the thermoelectric power is zero and at higher pressures becomes positive. $S$ is remarkably linear with pressure and, at the highest pressures we were able to achieve on a caesium specimen, $S$ was over four times its initial magnitude and opposite in sign.

Since caesium is such a soft and reactive metal we had considerable difficulties in making and mounting the wires. Moreover, they were then rather liable to break under pressure: one specimen was measured up to 800 atmospheres before breaking, another to only 170 atmospheres and a third to 2000 atmospheres. All three gave the same values for the change in $S$ with pressure where the readings overlapped.

Fig. 2

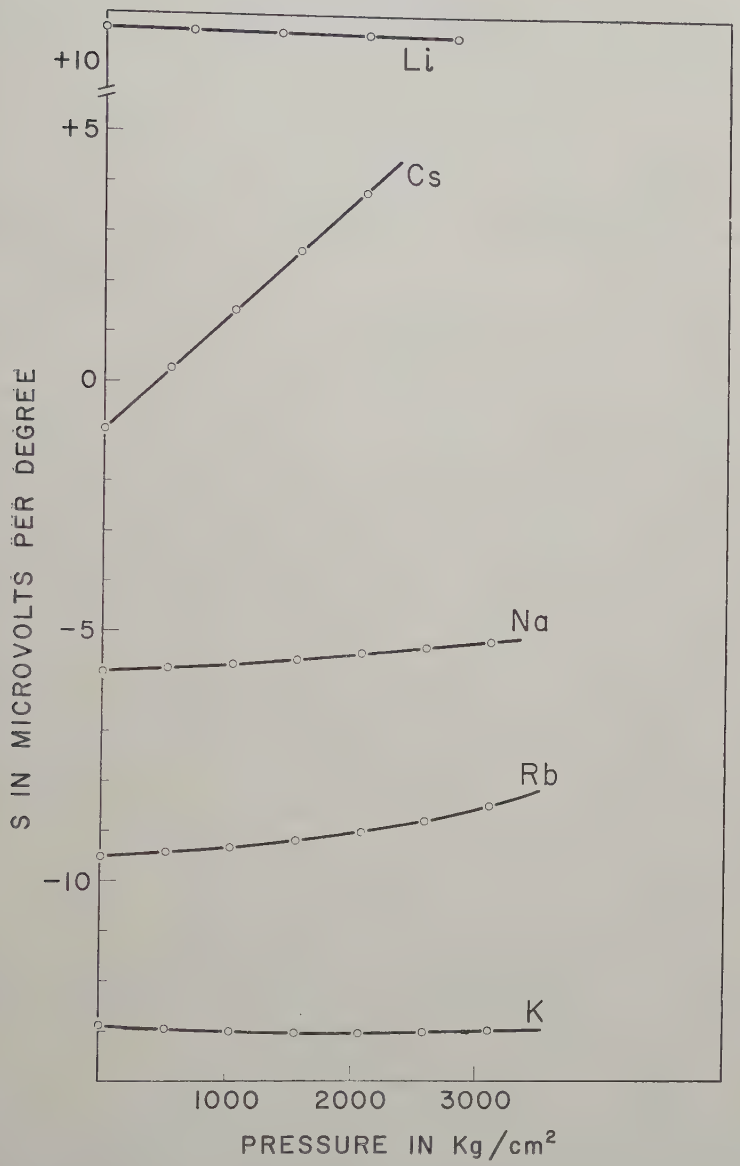

The thermoelectric power of the alkali metals as a function of pressure at 0°c.

To bring out more details of the changes in $S$ and to eliminate the effects of the different compressibilities of the various metals we show in fig. 3 a graph of $\Delta S/S_0$ versus the relative volume change, $\Delta V/V_0$. In table 2 the initial values of $d \ln S/d \ln V$ for the alkali metals are tabulated; as might be expected caesium is clearly outstanding.

Fig. 3

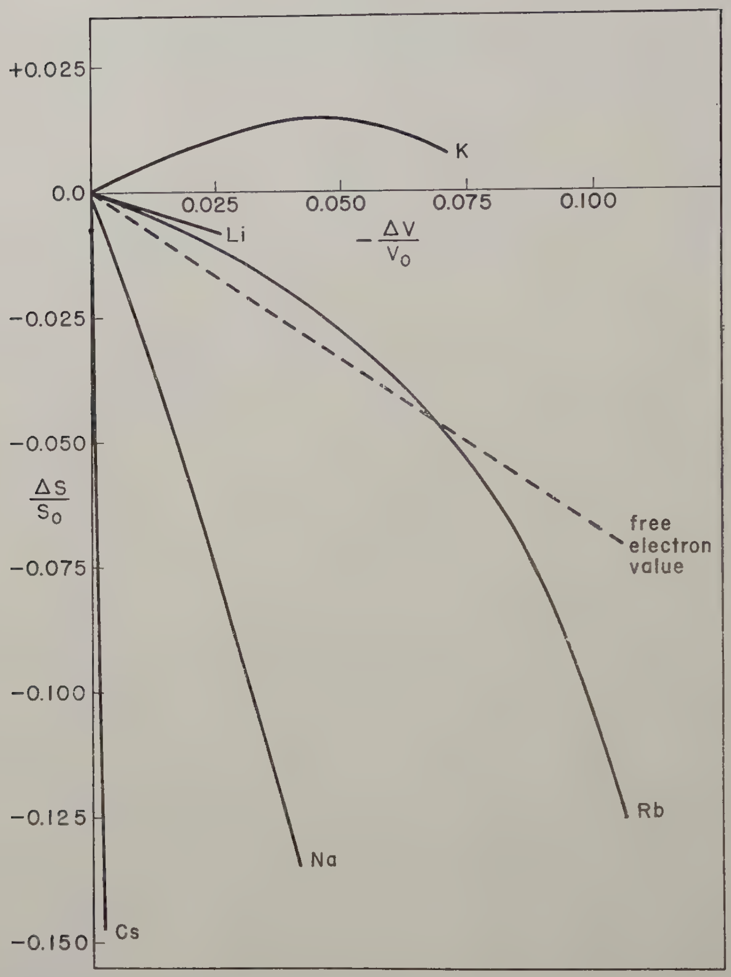

The fractional change in thermoelectric power of the alkali metals versus the fractional volume change at 0°c.

## § 4. Discussion

At high temperatures the thermoelectric power, $S$, of a monovalent metal is related to its resistivity, $\rho$, by the following expression (Mott and Jones 1936, p. 310):

$$S = -\frac{\pi^2 k^2 T}{3e}\left\{\frac{\partial \log \rho(E)}{\partial E}\right\}_{E=E_F}, \quad . \quad . \quad . \quad . \quad (1)$$

where the derivative measures the change in resistivity as the electron energy, $E$, varies in the neighbourhood of the Fermi energy $E_F$. This expression which applies at temperatures greater than $\theta$, the characteristic lattice temperature, is valid for any shape of Fermi surface but takes no account of phonon drag effects. In the following discussion, we shall assume that phonon drag effects are negligible in the thermoelectric power of the monovalent metals at room temperature. Although theoretically such a contribution is not impossible, it does appear from the experimental curves of $S$ versus temperature that the effect has died out by 0°c.

It is convenient to rewrite eqn. (1) in the form:

$$S=-\frac{\pi^2k^2T}{3eE_{\mathrm{F}}}\left\{\frac{\partial\ln\rho(E)}{\partial\ln E}\right\}_{E=E_{\mathrm{F}}}, \quad . \quad . \quad . \quad . \quad . \quad . \quad (1\,a)$$

in which we shall assume that $E_{\mathrm{F}}$ is given by its free electron value. The dimensionless quantity

$$\left\{\frac{\partial\log\rho(E)}{\partial\log E}\right\}_{E=E_{\mathrm{F}}}$$

(which for convenience we shall call $x$) has been evaluated for free electrons by various authors (see for example Wilson 1953). Whatever its precise value, one would not expect it to depend on volume so that since $E_{\mathrm{F}}$ is proportional to $V^{-2/3}$ for free electrons, $d\ln S/d\ln V=\frac{2}{3}$ in this case. The line corresponding to this volume dependence is indicated in fig. 3.

Even when we are dealing with electrons in an actual metal, it is probably still a reasonable approximation to assume that $E_{\mathrm{F}}\propto V^{-2/3}$ so that if the volume dependence of $S$ departs greatly from the free electron line this must be ascribed mainly to variations of $x$ with volume. Such a variation of $x$ would occur if the shape of the Fermi surface were changing markedly with pressure. We may write for the conductivity of a pure metal at high temperatures $\sigma\propto\tau A\langle v\rangle$, where $A$ is the area of the Fermi surface, $\langle v\rangle$ the mean Fermi velocity and $\tau$ the electron–phonon relaxation time (see for example Ziman 1960, p. 262). Consequently, one term which contributes to the thermoelectric power is the rate of change of $\tau$ with energy at the Fermi level. When the Fermi surface is in the neighbourhood of the Brillouin zone boundary there are at least two mechanisms whereby this derivative can become large and negative. Jones (1955) showed that $\tau(E)$† is essentially inversely proportional to the density of states at the Fermi level and because the slope of the density of states versus energy curve becomes very large as the Fermi level approaches the zone boundary this could make $S$ positive. As Ziman (1961) notes, however, this condition does not persist beyond the point of contact. Another mechanism which could make $\tau(E)$ decrease with $E$ when the Fermi surface is near the zone boundary is the increase in the number of possible Umklapp processes as $E$ increases and brings the Fermi surface closer to the zone boundary (cf. the discussion of the positive value of $S$ in lithium by Cohen and Heine (1958)).

Another term contributing to $S$ which one would expect to be important when the Fermi surface is about to touch the zone boundary is the change of $A$ with energy. In a monovalent metal this derivative will be positive if the Fermi surface does not touch the first Brillouin zone boundary, since then the area of the surface will increase with energy. When, however, the surface touches the zone boundary, then in general the surface will *decrease* (cf. Ziman 1960, p. 397). This change should be quite sudden. On the other hand, the calculations of Ziman (1961) on the high temperature thermoelectric power of the noble metals indicate that it is not possible to account for the positive value of $S$ in these metals from the energy dependence of $A$ and $\langle v \rangle$ alone. From what we have said, however, it does seem clear that when in a monovalent metal the Fermi surface is close to the zone boundary the thermoelectric power will be very sensitive to further distortion of the Fermi surface. It is in this manner that we interpret the behaviour of caesium (see below).

---

† In general when the Fermi surface is distorted $\tau$ will be anisotropic and a suitable average must be taken.

Although we have, as yet, no very direct evidence about the shapes of the Fermi surfaces of the alkali metals, general considerations of their properties and a calculation of their band structure suggest that the Fermi surfaces of sodium and potassium are nearly spherical, that of rubidium somewhat distorted and those of caesium and lithium so much so that, in lithium at least, the Fermi surface may touch the zone boundary (Cohen and Heine 1958, Ham 1960). The calculations of Ham (1960) also show that except in sodium the effect of pressure on all the alkali metals is to increase the energy gap at the centre of the Brillouin zone faces, i.e. to increase the distortion of the Fermi surface; in sodium the surface appears to remain nearly spherical. In the light of these conclusions, let us briefly consider the results for each metal.

*Caesium:* It seems reasonable to suppose that at room temperature and zero pressure the Fermi surface of caesium is nearly touching the zone boundary. Since an increase in pressure increases the distortion of the Fermi surface this, as indicated above, could explain the extreme sensitivity of the thermoelectric power of caesium to pressure. This explanation is also consistent with the behaviour of the electrical resistivity of caesium under pressure (see below and also Dugdale and Gugan (1962)).

It is, perhaps, worth noting that because the thermoelectric power of caesium is so sensitive to volume, the thermal contraction on cooling to 4°K (equivalent to that produced by a pressure of about 1600 atmospheres at 0°C) would be sufficient to alter drastically the value of $S$. The large thermal expansion coefficient of caesium around room temperature also means that a large part of the apparent temperature variation of $S$ at these temperatures (when measured at constant pressure) is due rather to changes in volume than to the intrinsic dependence of $S$ on temperature.

*Rubidium:* From the dependence of the electrical resistivity of rubidium on pressure it seems that at pressures of rather less than 10 000 atmospheres its thermoelectric power should show behaviour similar to that found in caesium (cf. Dugdale and Gugan 1962). The fairly rapid change in slope of the rubidium curve in fig. 3 is perhaps a foreshadowing of this behaviour.

*Potassium and sodium:* Surprisingly enough, the thermoelectric power of sodium and that of potassium behave quite differently from one another under pressure. Even in sodium, which we believe should present the simplest example, the change of $S$ with pressure does not conform to that expected on the simple free electron theory.

*Lithium:* As already discussed, it seems probable that when the Fermi surface of a monovalent metal is very close to the Brillouin zone boundary, the thermoelectric power becomes highly sensitive to a further distortion of the surface. If this is accepted we can make some deductions from the present experiments about the Fermi surface of lithium. From the calculations of Ham (*loc. cit.*) the distortion of the Fermi surface with volume change should be qualitatively similar in lithium to that in the three heavier alkali metals†. As we mentioned above, the band structure calculations and properties of lithium suggest that the Fermi surface must be highly distorted and either close to or actually in contact with the zone boundary. If the former were true we should then expect $S$ to vary very rapidly with volume but experimentally $d \ln S/d \ln V$ is found to be quite small (see table 2). In fact the thermoelectric power of lithium is even less sensitive to compression than that of copper, silver or gold (see table 2) all of which have Fermi surfaces which touch the zone boundary. On this basis we would conclude that in lithium the Fermi surface is already in contact with the Brillouin zone boundary. This conclusion would also seem to be supported by the behaviour of the electrical resistivity under pressure as measured by Bridgman (1952) at room temperature. The resistivity continues to increase steadily with decreasing volume unlike that of all the other alkali metals which show minima in the resistance versus volume curves.

### 4.1. *Relationship between S and the Pressure Coefficient of Electrical Resistivity*

At temperatures greater than $\theta$, the characteristic temperature of the lattice, the ideal electrical resistivity of a metal may be written as follows:

$$\rho_i = \frac{KT}{M\theta^2}$$

where $M$ is the mass of the metallic ions and $K$ is a measure of the electron–lattice interaction. Thus the isothermal volume coefficient of resistivity may be written as:

$$\frac{d \ln \rho_i}{d \ln V} = \frac{d \ln K}{d \ln V} - 2\frac{d \ln \theta}{d \ln V}.$$

If we take $-d \ln \theta/d \ln V = \gamma$, the Grüneisen parameter, we can evaluate $d \ln K/d \ln V$ from the high temperature pressure coefficient of electrical resistivity. The quantity $d \ln K/d \ln V$ may be thought of as a measure of the change in resistivity with volume that would occur in a metal if the amplitude of its lattice vibrations did not change. The parameter, $x$, on the other hand, measures the change in resistivity of the metal when its Fermi energy is altered. It might be expected that these two quantities should be related and indeed there is a close connection between their values for the monovalent metals (cf. Dugdale and Gugan 1962). This is illustrated in fig. 4 in which we plot $d \ln K/d \ln V$ against $x$ evaluated at 0°c for these metals. If all the change in resistivity with volume were due to the change in Fermi energy (except that due to the change in $\theta$) we might expect that for free electrons $(d \ln K/d \ln V)/x$ would equal $d \ln E_F/d \ln V$, i.e. $-\frac{2}{3}$. This ratio is shown as the dashed line in fig. 4; for many of the metals it appears to fit the relationship surprisingly well.

---

† In lithium, however, the lowest energy state at the mid point of the zone face is p-like whereas in the other three metals it is s-like.

Fig. 4

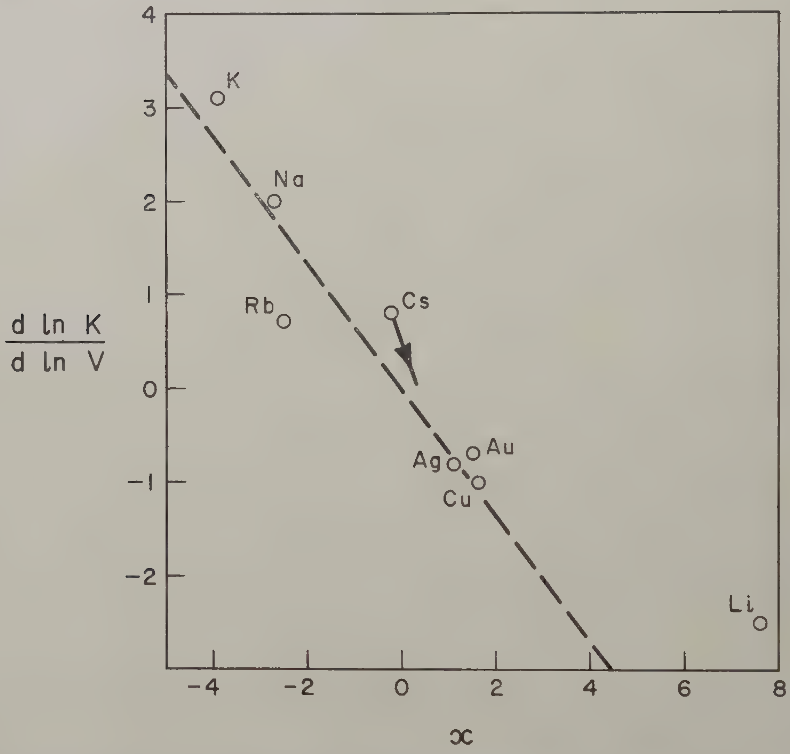

$d \ln K/d \ln V$ derived from the pressure coefficient of electrical resistivity versus $(d \ln \rho/d \ln E)_{E=E_F}$ derived from the thermoelectric power at 0°c for the monovalent metals.

We have estimated approximately how $d \ln K/d \ln V$ and $x$ change with pressure in caesium and this change is indicated in the figure by the line with the arrow. There is still considerable uncertainty in the data on the pressure dependence of the electrical resistivity of caesium and rubidium at low pressures so that the points in fig. 4 for these metals are rather uncertain; there is also some uncertainty about the precise values of the parameters for the noble metals (cf. Ziman 1961). Nevertheless it seems clear that there is a close relationship between $d\ln K/d\ln V$ and the thermoelectric power at high temperatures and that this relationship persists in caesium when it is compressed.

It would, of course, be of great interest to follow the behaviour of the thermoelectric power of the alkali metals (in particular caesium and rubidium) to higher pressures; experiments for this purpose are being prepared.

## ACKNOWLEDGMENTS

We would like to thank Dr. D. K. C. MacDonald for his interest and encouragement and for many stimulating discussions. We are also very grateful to Dr. J. M. Ziman for his helpful criticisms of the manuscript. Finally we thank Mr. A. A. M. Croxon for his valuable help with the experiments.

## REFERENCES

BIDWELL, C. C., 1924, *Phys. Rev.*, **23,** 357.
BRIDGMAN, P. W., 1949, *The Physics of High Pressure* (London: Bell and Sons Ltd.); 1952, *Proc. Amer. Acad. Arts Sci.*, **81,** 165.
CHRISTIAN, J. W., JAN, J.-P., PEARSON, W. B., and TEMPLETON, I. M., 1958, *Proc. roy. Soc.* A, **245,** 213.
COHEN, M. H., and HEINE, V., 1958, *Advanc. Phys.*, **7,** 395.
DUGDALE, J. S., and GUGAN, D., 1962 (to be published).
HAM, F. S., 1960, *The Fermi Surface.* Proceedings of Cooperstown Conference (New York: John Wiley and Sons Inc.).
JONES, H., 1955, *Proc. phys. Soc., Lond.*, A, **68,** 1191.
MACDONALD, D. K. C., 1954, *Report of Bristol Conference on Defects in Crystalline Solids* (London: The Physical Society), p. 383.
MOTT, N. F., and JONES, H., 1936, *The Theory of the Properties of Metals and Alloys* (Oxford: Clarendon Press).
WILSON, A. H., 1953, *The Theory of Metals*, 2nd edition (Cambridge).
ZIMAN, J. M., 1960, *Electrons and Phonons* (Oxford: Clarendon Press); 1961, *Advanc. Phys.*, **10,** 1.

# Etchants for Revealing Dislocations in Lithium Fluoride and Other Crystals

By A. R. C. Westwood, H. Opperhauser, Jr., and D. L. Goldheim
Research Institute for Advanced Studies, Baltimore 12, Maryland, U.S.A.

[Received June 5, 1961]

## Abstract

Aqueous solutions of long chain fatty and perfluoro-acids can be used to reveal the points of emergence of dislocations in lithium fluoride. Of particular interest are the $C_{14}$–$C_{18}$ acids, for dilute aqueous solutions ($10^{-5}$ N–$10^{-6}$ N) of these acids reveal clearly the ' tracks ' of slowly moving dislocations. It is suggested that the many available surface-active agents may provide a ready source of potential inhibitors for a variety of crystal-etchant systems.

The revelation of 'fresh' dislocations by means of etch pits requires first, the provision of a suitably undersaturated corrosive environment, and second, some means of inhibiting or retarding the motion of kinks away from the nucleating dislocations (Cabrera 1960, Gilman 1960).

Gilman *et al.* (1958) have demonstrated that one way of satisfying the latter requirement is to chemisorb a complexing ion at the kink. In their etchant for LiF, ferric ions complex with neighbouring fluorine ions at the kink site and this results in a decrease in the rate of dissolution parallel to the surface and the production of a pyramidal pit. However, these studies also demonstrated that to be an effective inhibitor for LiF, an adsorbing cation must be within 25% of the size of the $Li^+$ ion, must form a stable fluoride complex and must have a stable fluoride salt with low solubility in water. Such requirements would appear to limit the number of potentially useful cationic inhibitors for a given crystal–solvent system.

During an investigation of the effects of adsorbed polar molecules on the mechanical properties of crystals, the possibility of these molecules acting as inhibitors became apparent. Subsequent experiments demonstrated that aqueous solutions of long chain fatty and perfluoro-acids can indeed reveal the points of emergence of dislocations and other surface features of interest.

Etch pits produced by aqueous solutions of caprylic acid ($C_7H_{15}COOH$) and pentadecafluoro-octanoic acid ($C_7F_{15}COOH$) at dislocation sites in LiF are shown in figs. 1 and 2†.

---

† Figures 1, 2 and 3 are shown as plates.

Etch pits produced in myristic ($C_{13}H_{27}COOH$) and stearic ($C_{17}H_{35}COOH$) acid solutions can be an order of magnitude smaller than etch pits produced in the standard $FeCl_3$ etchant during the same etching period—say 0·5–1·0 μ in size. It appears that these polar molecules are strongly adsorbed and thus are relatively powerful inhibitors. This enables such etchants to reveal clearly the tracks of slowly moving dislocations. Figures 3 (*a*), (*c*), (*d*), (*e*) and 4 (E–F) illustrate the extensive and serrated cross-gliding of $(110)\langle 1\bar{1}0\rangle$ screw dislocations discussed by Johnston and Gilman (1960). The etchant was stearic acid ($\sim 5 \times 10^{-6}$ N). Figure 3 (*b*) is an example of tracks associated with the movement of unstable screw-edge–screw half-loops introduced during cleaving and revealed by a myristic acid etchant ($\sim 8 \times 10^{-5}$ N). Such half-loops are quite shallow and are mainly in the edge orientation—fig. 4 at G—but the line tension is sufficient to cause the screw components to cross-glide a micron or so producing a bowed track—e.g. at A in fig. 3 (*b*).

Fig. 4

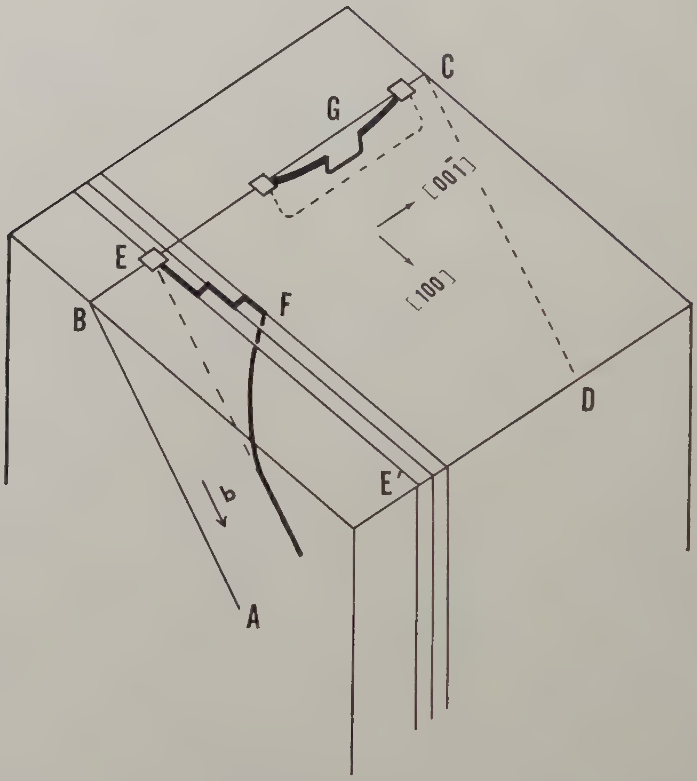

Interpretation of fig. 3.

Initially, etch pits produced on dislocations in myristic and stearic acid solutions are flat bottomed. After a certain etching time, which appears to depend on the concentration and chain length of the adsorbing molecule, the pits become pyramidal. It is believed that this behaviour results from chemisorption and complex formation with the ions surrounding the core of the dislocation itself. Such a process is likely to affect the core energy available for the nucleation of kinks.

The significance of adsorption at dislocations with regard to Rebinder phenomena and a possible mechanism for the etching process will be discussed elsewhere (Westwood 1962).

The present observations lead one to suggest that the many available surface active agents, particularly the fatty acids, may provide a ready source of potential inhibitors for a variety of crystal-etchant systems. Recent observations by Wernick and Thomas (1960) and Gatos and Lavine (1960) appear to substantiate this view.

## ACKNOWLEDGMENTS

We are grateful for the financial support received from Watertown Arsenal Laboratories and in particular the continued interest of Mr. Murray Jacobson and Mr. John Alexander.

## REFERENCES

CABRERA, N., 1960, *Surface Chemistry of Metals and Semiconductors* (New York: John Wiley), p. 71.
GATOS, H. C., and LAVINE, M. C., 1960, *J. appl. Phys.*, **31,** 743.
GILMAN, J. J., 1960, *Surface Chemistry of Metals and Semiconductors* (New York: John Wiley), p. 136.
GILMAN, J. J., JOHNSTON, W. G., and SEARS, G. W., 1958, *J. appl. Phys.*, **29,** 747.
JOHNSTON, W. G., and GILMAN, J. J., 1960. *J. appl. Phys.*, **31,** 632.
WERNICK, J. H., and THOMAS, E. E., 1960, *Trans. Amer. Inst. min.* (*metall.*) *Engrs*, **218,** 763.
WESTWOOD, A. R. C., 1962, *Phil. Mag.* (to be published).

# Cross-slip and Fatigue in Metals at Low Temperatures

By P. Feltham
Department of Metallurgy, The University, Leeds

[Received February 4, 1961]

## Abstract

The mutual annihilation of jogged screw dislocations approaching one another on non-parallel slip planes is shown to give rise to a type of recovery which accounts satisfactorily for the pronounced decline in the rate of work-hardening observed in f.c.c. metal crystals above a certain shear stress, frequently denoted by $\tau_{\mathrm{III}}(T)$. The relation $\tau_{\mathrm{III}}=(\tau_{\mathrm{III}})_0[1-(mkT/Q)]$, deduced from the model, where $(\tau_{\mathrm{III}})_0=\tau_{\mathrm{III}}(0)$, $m=30$ and $Q$ the energy of vacancy formation, agrees well with the experimental data for aluminium, copper, gold and nickel up to about $0{\cdot}15\ T_{\mathrm{m}}$, where $T_{\mathrm{m}}$ (°K) is the temperature of melting. It is suggested that the heat evolved during such dislocation annihilations facilitates the clustering of slip into bands observed at stresses above $\tau_{\mathrm{III}}$ by catalyzing further destructive interactions, and that condensation of vacancies formed in the process of cross-slip provides the crack nuclei in slip clusters from which fatigue fractures spread. The temperature dependence of the fatigue limit appears to be the same as that of $\tau_{\mathrm{III}}$.

## § 1. Introduction

Electron-micrographic studies of slip markings developing on the surfaces of single crystals of face-centred cubic metals in the process of deformation led Diehl *et al.* (1955) to the conclusion that thermally activated cross-slip was responsible for the comparatively sharp decline in the work-hardening rate when the applied shear stress exceeded a certain critical value, generally denoted by $\tau_{\mathrm{III}}(T)$. This view was restated in later work reviewed by Seeger *et al.* (1959), as well as in the more recent paper on the development of slip in f.c.c. metals, by Mader and Seeger (1960). As a prerequisite of the process two partial dislocations must approach one another to within about one lattice spacing, when they can recombine to give an undissociated screw dislocation according to eqn. (1):

$$(a/6)\,[1\ \bar{2}\ 1]+(a/6)\,[2\ \bar{1}\ \bar{1}]=(a/2)\,[1\ \bar{1}\ 0]. \qquad (1)$$

In this reaction one of the partial dislocations is assumed to be held fixed by some barrier, such as a Cottrell–Lomer lock, while a force per unit length (Cottrell 1953)

$$F\simeq(Ga^2/24\pi r)-\gamma \qquad (2)$$

is tending to displace the mobile partial towards its partner. In eqn. (2) $G$ is the shear modulus, $a$ the length of the cube edge of the lattice, $r$

the distance separating the partials, and $\gamma$ the stacking-fault energy. On writing $F=\tau\mathbf{b}_1\simeq\frac{1}{2}\tau\mathbf{b}$, where $\mathbf{b}_1$ and $\mathbf{b}$ are the Burgers vectors of the mobile partial and the complete screw dislocation respectively, also putting $r=b$ and $a^2=2b^2$, one obtains for this critical shear stress

$$\tau_c=(G/6\pi)-(2\gamma/b). \qquad (3)$$

For copper, with $G=5\times10^5$ kg/cm², $\gamma=50$ erg/cm² and $b=2{\cdot}5$ Å, one finds $Gb/6\pi=664$ erg/cm², so that $\tau_c=2{\cdot}3\times10^4$ kg/cm², which is by a factor of about 20 greater† than the value obtained by slight extrapolation for the stress at the end of the stage of linear hardening of copper crystals deformed at 4·2°K (Blewitt *et al.* 1955).

Attempts to account for this discrepancy have relied on the assumption that high stress peaks existed at the heads of arrays of dislocations piled up against Cottrell–Lomer barriers. However, on the basis of extensive experimental studies of dislocation structures, carried out in recent years by electron microscopy and etch-pit methods, it is now reasonably certain that neither unrelaxed groups containing many dislocations nor Cottrell–Lomer locks long enough to anchor piled-up groups are present in deformed pure metals (Mott 1960)‡.

Reconsideration of the mechanism of cross-slip, and of its role in the transition from the second (' linear ') to the third stage of hardening, therefore becomes desirable, and is attempted in the present work on the basis of a model which accounts quite well for the experimental observations, but in which neither Cottrell–Lomer barriers nor piled-up groups of dislocations play a part.

## § 2. THE MODEL OF CROSS-SLIP

The main characteristics of the cross-slip mechanism we propose to examine will be assumed to be as follows:

(*a*) The transition to a low work-hardening rate at $\tau_{\mathrm{III}}(T)$ is initiated by recovery due to the mutual annihilation of screw dislocations of opposite signs, occurring after their migration and approach.

(*b*) The stress $\tau_{\mathrm{III}}$ is attained when, as a consequence of the preceding increase in dislocation density due to straining, the creep rate due to the migration and loss of screw dislocations becomes comparable to that imposed on the crystal by the tensile testing machine.

(*c*) Movement of the dislocations is impeded by the frictional drag of jogs, which generate vacancies in ' ploughing ' through the crystal.

---

† The much lower value derived for this factor by Feltham and Copley (1960) arises from a numerical error in their calculation.

‡ It is in any case questionable whether Cottrell–Lomer locks could be effective barriers for piled-up screw dislocations (Hosford *et al.* 1960), and whether even large pile-ups, if they existed, would suffice to force the partials together (Ball 1959).

(*d*) At the low temperatures considered the vacancies formed by moving jogs are assumed to remain ' frozen in ' at the points of formation, but, as the resultant force on the jog will in general not lie entirely at right angles to its Burgers vector, the jog can escape from the vacancy. The trail of vacancies left by a jog in a migrating screw dislocation need not therefore be continuous and colinear. The energy barrier to jog migration in this ' athermal ' process is then equal to that of vacancy formation, and is linearly dependent upon the shear stress acting on the dislocation containing the jog (Seeger 1955)†.

A schematic representation of one possible variant of screw/screw annihilation is shown in fig. 1. Here the screw dislocations $S_1$ and $S_2$ approach one another on their respective slip planes until, having reached positions such as $S_1'$ and $S_2'$, they annihilate‡. Cottrell–Lomer barriers are not essential; sufficiently high stresses to recombine the partials are automatically attained when the dislocations are only a few lattice spacings apart, and ' stabilization ' of the dislocations is assured by the drag of jogs. However, the creep rate will not, in the main, be determined by the comparatively high rate of approach of the dislocations in such ' sink ' configurations, but by the lower velocity of migration between sources and the sinks.

Fig. 1

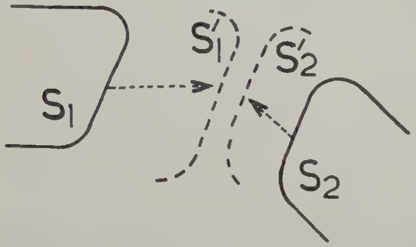

Approach of two screw dislocations moving on intersecting slip planes, resulting in mutual annihilation. Jogs are not shown.

Now, if $\tau$ is the effective shear stress acting on an element of dislocation containing a jog, the latter will migrate with velocity

$$v=\nu b \exp\{-(Q/kT)[1-(\tau/\tau_0)]\}-\nu b \exp\{-(Q/kT)[1+(\tau/\tau_0)]\},$$

where $\nu$ is an atomic frequency of order $10^{11}$ sec$^{-1}$, $b$ the interatomic spacing, $Q$ the energy of vacancy formation, and $\tau_0$ the shear stress at which the jog would move adiabatically. As, at low temperatures $Q \gg kT$, and $\tau$ is equal to an appreciable fraction of $\tau_0$, the second exponential term, which allows for the possibility of the movement of the jog against the shear stress, may be neglected. Then taking account of (*b*), assuming that $\tau/\tau_0$ may be replaced by $\tau_{\rm III}/(\tau_{\rm III})_0$ as the strain rate $\dot{\epsilon}$ arising from creep facilitated by screw/screw annihilation becomes comparable with that imposed by the tensile testing machine, we have

---

† Seeger (1955) considers a similar ' athermal ' model in which the vacancies formed remain aligned like beads on a string. The energy barrier is then determined by the work required to form a vacancy next to an existing one.

‡ The energy liberated as ' thermal spikes ' by the annihilation must be at least equal to the sum of the core energies of the dislocations lost, i.e. of the order of $0{\cdot}1Gb^3$ per length $b$ of coalesced dislocation. In copper this equals about $\frac{1}{2}$ ev. By assisting further screw/screw interactions such thermal spikes may thus initiate an autocatalytic process of clustering of slip into bands, such as is known to become pronounced on deformation at stresses exceeding $\tau_{III}$.

$$\dot{\epsilon} = \nu N A \mathbf{b} \exp\{-(Q/kT)[1-\tau_{\rm III}/(\tau_{\rm III})_0]\}. \quad . \quad . \quad . \quad (4)$$

In eqn. (4) $N$ is the number of dislocation elements per unit volume contributing to creep, and $A$ the area swept out by one such element in one jump forward. The shear stress $(\tau_{\rm III})_0$ necessary to deform the crystal adiabatically may vary somewhat with temperature, as will be shown below. The linear stress dependence of the activation energy arises as in Seeger's (1955) model mentioned under (*d*) above. If we take $\dot{\epsilon}$ to be of order $10^{-5}$ sec$^{-1}$, i.e. rather less than strain rates generally used in tensile tests, then with the usual estimates of the parameters outside the bracket in eqn. (4) one obtains†

$$Q\{1-[\tau_{\rm III}/(\tau_{\rm III})_0]\} = mkT, \quad . \quad . \quad . \quad . \quad (5)$$

with

$$m = \ln(\nu N A \mathbf{b}/\dot{\epsilon}) \simeq 30. \quad . \quad . \quad . \quad . \quad (6)$$

The bracketed term in eqn. (5) may be written in the form

$$[(\tau_{\rm III})_0 - \tau_{\rm III}]/(\tau_{\rm III})_0 = \Delta\tau_{\rm III}/(\tau_{\rm III})_0, \quad . \quad . \quad . \quad . \quad (7)$$

and as, at sufficiently low temperatures, we must have

$$\Delta\tau_{\rm III} \ll (\tau_{\rm III})_0, \quad . \quad . \quad . \quad . \quad . \quad . \quad . \quad (8)$$

it is then permissible to regard $(\tau_{\rm III})_0$ as temperature independent, so that eqn. (5) yields

$$\tau_{\rm III} = (\tau_{\rm III})_0[1-(mkT/Q)] \quad . \quad . \quad . \quad . \quad (9)$$

and

$$(d\tau_{\rm III}/dT)/(\tau_{\rm III})_0 = -mk/Q. \quad . \quad . \quad . \quad . \quad (10)$$

Thus $\tau_{\rm III}$ should decrease linearly with increasing temperature at a rate given by eqn. (10). Before discussing these results we revert to a more detailed examination of $(\tau_{\rm III})_0$.

Now, if for a strain rate $\dot{\epsilon}_1$ at a temperature $T_1$ the mean spacing between screw dislocations beginning to approach one another as in fig. 1 is $d_1$, then on raising the temperature rapidly to $T_2$, keeping the stress constant, we shall have $\dot{\epsilon}_2 > \dot{\epsilon}_1$, and when, after some transient creep, the strain rate has diminished to $\dot{\epsilon}_1$ a new mean spacing will have been attained with $d_2 > d_1$. The mean internal stress in the flow region will therefore be slightly smaller at $T_2$ than at $T_1$, and the crystal will also deform more readily adiabatically at the higher temperature, i.e.

---

† Provided pronounced thermal recovery is absent the variation of $m$ with $T$ is probably negligible. If, for example, $N$ should decrease slightly as the temperature is raised, a concurrent increase in $A$ may be expected to take place, leaving $m$ virtually unaltered.

$$(\tau_{\mathrm{III}})_0\,|_{T_2} < (\tau_{\mathrm{III}})_0\,|_{T_1}, \quad T_2 > T_1. \qquad . \quad . \quad . \quad (11)$$

One may allow for this in eqn. (4) by utilizing the fact that $\tau_{\mathrm{III}}$ diminishes with increasing temperature, and write

$$(\tau_{\mathrm{III}})_0 = \tau_{\mathrm{III}}(\alpha - \beta T), \quad \beta T \ll \alpha, \quad \beta > 0, \qquad . \quad . \quad . \quad (12)$$

where $\alpha$ and $\beta$ are constants. As $\tau_{\mathrm{III}} \to (\tau_{\mathrm{III}})_0$ when $T \to 0$ (eqn. (4)), we must have $\alpha = 1$, and then, on neglecting $\beta T$, eqns. (10) and (12) yield

$$d \ln \tau_{\mathrm{III}}/dT = -mk/Q \qquad . \quad . \quad . \quad . \quad . \quad . \quad . \quad (13)$$

instead of the linear relation given by eqn. (10).

## § 3. Comparison with Experiment

A survey of the experimentally determined temperature dependence of $\tau_{\mathrm{III}}$ shows that it is quite well represented by a logarithmic relation (eqn. (13)) over larger temperature intervals than by eqn. (10), e.g. in crystals of copper (78–573°K) and gold (78–700°K) (Seeger *et al.* 1959), in nickel (4·2–300°K) (Haasen 1958) and dilute Cu–Ga alloys (Haasen and King 1960).

Fig. 2

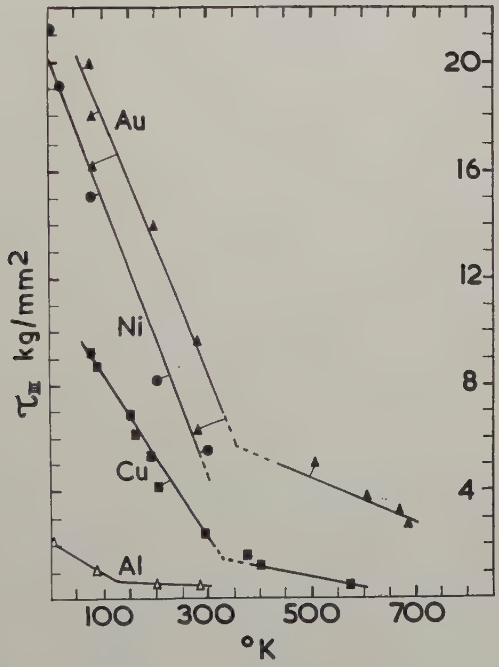

Temperature dependence of $\tau_{\mathrm{III}}$ in f.c.c. metal crystals. Data from Hosford *et al.* (1960), (Al), Seeger *et al.* (1959), (Au, Cu), and Haasen (1958), (Ni). In the case of gold only the ordinate represents $10 \times \tau_{\mathrm{III}}$.

Representation of the $\tau_{III}/T$ relation on a linear stress scale indicates that eqn. (10) is also well obeyed up to comparatively high temperatures (fig. 2). In aluminium crystals the transition from the second to the third stage of hardening is indistinct, and the determination of $\tau_{III}$ is liable to appreciable subjective error. Nevertheless for crystals of [123] orientation the transition is discernible (Hosford *et al.* 1960), and the approximate values of $\tau_{III}$ are also shown in fig. 2.

However, in view of the suggestion (Feltham 1958) that the temperature dependence of the fatigue limit should be the same as that of $\tau_{III}$ the former was plotted as function of $T$ in fig. 3, in which $\sigma_f$ represents the peak value of the alternating stress leading to failure of polycrystalline specimens of 99·99% purity aluminium after $10^6$ cycles (McCammon and Rosenberg 1957). The shape of the curve is clearly similar to that of the curves in fig. 2.

Fig. 3

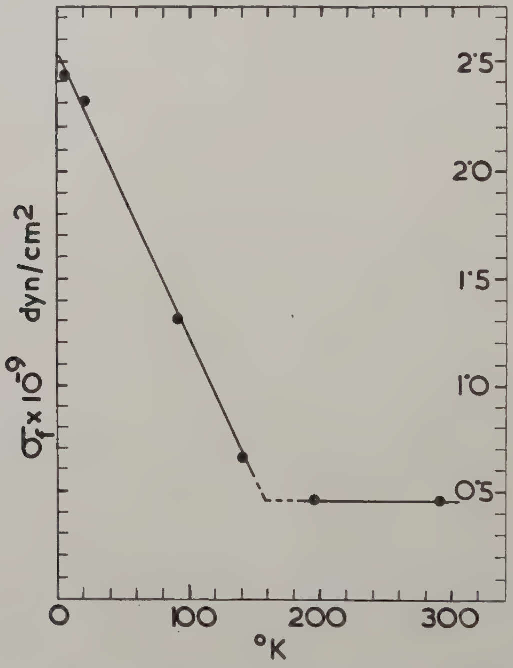

Temperature dependence of the tensile peak stress leading to fatigue failure of 99·99% aluminium polycrystals after $10^6$ stress reversals. (McCammon and Rosenberg 1957). The activation energy derived from the steep part of the curve by means of eqn. (10) is 0·51 ev.

Finally, the table shows values of $Q$ obtained from figs. 2 and 3 by means of eqns. (10) and (13) with $m=30$, as well as the activation energies for low-temperature transient creep obtained with polycrystalline specimens in stage III by Thornton and Hirsch (1958). Activation energies for vacancy formation are also given. It can be seen that values of $Q$ deduced by means of eqn. (10) are in fair agreement with the corresponding values for vacancy formation, but that activation energies deduced from eqn. (13) are too low; presumably the breaks in the curves in figs. 2 and 3 are indications of the occurrence of significant structural changes at higher temperatures (Clarebrough *et al.* 1955), which do not come to light in the semi-logarithmic representation. 'Best' straight lines drawn through all the points, and used in conjunction with eqn. (13), may then give misleading, low values of $Q$.

Activation energies $Q$ (ev)

| | Eqn. (10) | Eqn. (13) | Logarithmic creep (80°K) | Vacancy formation |
|---|---|---|---|---|
| Al | 0·42†<br>0·51‡ | — | $0{\cdot}5 \pm 0{\cdot}35$(a) | 0·50(b) |
| Au | 1·2 | 0·9 | $0{\cdot}8 \pm 0{\cdot}35$(a) | $0{\cdot}95 \pm 0{\cdot}1$(c)<br>$1{\cdot}02 \pm 0{\cdot}06$(d) |
| Cu | 1·1 | 0·5 | $0{\cdot}7 \pm 0{\cdot}35$(a) | 1·1(e)<br>0·7(b) |
| Ni | 1·0 | 0·6 | $1{\cdot}6 \pm 0{\cdot}6$(a) | 1·4(f) |

† From fig. 2. ‡ From fig. 3.

(a) Thornton and Hirsch (1958); (b) Gertsriken and Slyusar (1960); (c) Bradshaw and Pearson (1957); (d) Bauerle *et al.* (1956); (e) Granato *et al.* (1958); (f) Takamura (1956).

## § 4. CONCLUSIONS

The model of cross-slip proposed in the present paper accounts satisfactorily for the observed temperature dependence of $\tau_{\mathrm{III}}$, eqn. (10) representing the relation well at temperatures below about $0{\cdot}15\ T_{\mathrm{m}}$ in crystals of f.c.c. metals for which data are available. Deviations from the linear temperature dependence at higher temperatures may be a consequence of the occurrence of significant structural changes, possibly facilitated by the migration of point defects.

The similarity of the effect of changes of temperature on $\tau_{\mathrm{III}}$ and on the fatigue limit suggests that coalescence of vacancies formed in the process of slip-band formation provides crack nuclei for the spread of fatigue damage. As the ratio of fatigue strength to ultimate tensile strength is virtually constant in f.c.c. and in hexagonal metals at low temperatures (McCammon and Rosenberg 1957), cracks leading to ductile fracture probably nucleate in a similar manner.

## REFERENCES

BALL, C. J., 1959, *Phil. Mag.*, **4,** 1377.

BAUERLE, J. A., KLABUNDE, C. E., and KOEHLER, J. S., 1956, *Phys. Rev.*, **102,** 1182.

BLEWITT, T. H., COLTMAN, R. R., and REDMAN, J. K., 1955, *Rep. Conf. Defects in Solids* (London : The Physical Society), p. 369.

BRADSHAW, F. J., and PEARSON, J., 1957, *Phil. Mag.*, **2,** 379.

CLAREBROUGH, L. M., HARGREAVES, M. E., and WEST, G. W., 1955, *Proc. roy. Soc.* A, **232,** 252.

COTTRELL, A. H., 1953, *Dislocations and Plastic Flow in Crystals* (Oxford : Clarendon Press), p. 74.

DIEHL, J., MADER, S., and SEEGER, A., 1955, *Z. Metallkde.*, **46,** 650.

FELTHAM, P., 1958, *Phil. Mag.*, **3,** 806.

FELTHAM, P., and COPLEY, G. J., 1960, *Acta Met.*, **8,** 542.

GERTSRIKEN, S. D., and SLYUSAR, B. F., 1960, *Fiz. Met. i Metalloved.*, **6,** 1061.

GRANATO, A., HIKATA, A., and LUCKE, K., 1958, *Acta Met.*, **6,** 470.

HAASEN, P., 1958, *Phil. Mag.*, **3,** 384.

HAASEN, P., and KING, A., 1960, *Z. Metallkde.*, **51,** 722.

HOSFORD, W. F., FLEISCHER, R. L., and BACKOFEN, W. A., 1960, *Acta Met.*, **8,** 187.

MADER, S., and SEEGER, A., 1960, *Acta Met.*, **8,** 513.

MCCAMMON, R. D., and ROSENBERG, H. M., 1957, *Proc. roy. Soc.* A, **242,** 203.

MOTT, N. F., 1960, *Trans. Met. Soc., A.I.M.E.*, **218,** 962.

SEEGER, A., 1955, *Phil. Mag.*, **46,** 1194.

SEEGER, A., BERNER, R., and WOLF, H., 1959, *Z. Phys.*, **155,** 247.

TAKAMURA, J., 1956, *Metal Physics*, **2,** 112.

THORNTON, P. R., and HIRSCH, P. B., 1958, *Phil. Mag.*, **3,** 738.

# The Behaviour of Point Defect Clusters in Irradiated Metals

By R. S. Barnes
Metallurgy Division, Atomic Energy Research Establishment, Harwell

[Received June 29, 1961]

## Abstract

A simple model, where clusters of interstitial atoms compete with the equivalent number of vacancies left in the crystal for subsequent interstitial atoms, is used to discuss the rate of accumulation of the vacancies and the conditions governing the size of the interstitial atom clusters. Recombination becomes important at an interstitial cluster size which is dependent upon the relative interaction distances of interstitial atoms with vacancies and dislocation lines.

## § 1. Introduction

The thin-film technique has made it possible to observe clusters of point defects in irradiated metals and already many observations have been reported (Barnes 1961, Barnes and Mazey 1960, Makin *et al.* 1961, Silcox and Hirsch 1959). At temperatures where clusters form, their nature and distribution will determine the level at which vacancy–interstitial atom annihilation becomes important and the point defect accumulation rate diminishes. This paper attempts, with a simple model, to discuss the rate of accumulation of the point defects and the rate of growth of the clusters in specific cases.

## § 2. The Model

Various arguments have been advanced which suggest that the larger dislocation loops (fig. 1†) which form in an irradiated metal are produced from plate-like clusters of interstitial atoms (Barnes and Mazey 1960, Makin *et al.* 1961). The following dislocation reaction has been proposed to explain how they form the glissile loops observed in f.c.c. crystals (Barnes 1961):

$$\frac{a}{3}(\bar{1}\bar{1}\bar{1})+\frac{a}{6}(1\bar{2}1)+\frac{a}{6}(\bar{2}11)\rightarrow\frac{a}{2}(\bar{1}\bar{1}0).$$

The much smaller dots, often seen in addition, have been attributed to vacancies clustered on a much finer scale. Upon heating to the self-diffusion temperature the dislocation loops begin to disappear near the grain boundaries but many of the small vacancies clusters remain up to much higher temperatures[†]. This suggests that the vacancy clusters are not of the same form as the interstitial atom clusters, i.e. dislocation loops with Burgers vectors of opposite sign,

---

† The figures are shown as plates.

$$\frac{a}{3}(111)+\frac{a}{6}(11\bar{2})\rightarrow\frac{a}{2}(110),$$

for then climb of both would occur at the same temperature: the vacancies from one cancelling the interstitials from the other. This independence in behaviour can be explained if the vacancies form a stable configuration, and high resolution electron micrographs of annealed copper and silver have shown that the dots are tetrahedral in shape (Barnes 1961), and are presumably tetrahedra of stacking faults such as those seen in some quenched metals (Silcox and Hirsch 1959). Such a structure, having $(a/6)(110)$ dislocations along its edges, should be very stable and have little strain field around it to attract interstitial atoms.

A simple model can be constructed from these deductions and used to discuss the conditions when direct annihilation of vacancies and interstitial atoms becomes important.

## § 3. Annihilation Effects

The interstitial atoms, which are generated at a rate $\dot{c}$, migrate at the temperatures considered with a jump frequency $\nu$ and are either captured at a sink (present in atomic concentration $c_S$) or are annihilated on meeting a vacancy (present in atomic concentration $c_V$)[‡]. The probability per atomic jump of an interstitial atom being captured at a sink is $c_S$ and at a vacancy is $xc_V$, where $x$ measures the effectiveness of a vacancy to capture a near-by interstitial atom.

Thus the atomic concentration of interstitial atoms migrating at one time is

$$c_1=\frac{\dot{c}}{\nu(xc_V+c_S)},$$

when the rate of loss of interstitial atoms is balanced by the rate of replacement. (This state is normally attained in much less than one second.) The rate of deposition of interstitial atoms at the sinks is equal to the rate of accumulation of vacancies in the lattice, i.e.

$$\frac{dc_V}{dt}=\frac{\dot{c}c_S}{xc_V+c_S}.$$

---

[†] The denuded zone containing no dislocation loops but containing the normal number of the vacancy clusters can be seen near the grain boundary in fig. 1.

[‡] The model neglects the trapping of interstitial atoms and so only applies to metals at temperatures sufficiently high that trapping is not significant.

Initially the grain boundaries and dislocation lines are the only sinks ($c_S \gg xc_V$) and $c_i$ rapidly attains a steady value

$$c_i = \frac{\dot{c}}{\nu c_S}$$

and all the vacancies produced are retained

$$\frac{dc_V}{dt} = \dot{c}.$$

However, the steadily accumulating vacancies eventually capture as many of the interstitial atoms as do the sinks and fewer reach the sinks. This happens when

$$xc_V = c_S,$$

i.e. when

$$c_i = \frac{\dot{c}}{2\nu c_S} \quad \text{and} \quad \frac{dc_V}{dt} = \frac{\dot{c}}{2}.$$

Thereafter the rate of arrival of interstitial atoms at the sinks is diminished as also is the rate of vacancy accumulation in the lattice until

$$xc_V \gg c_S \quad \text{when} \quad c_i = \frac{\dot{c}}{\nu xc_V} \quad \text{and} \quad \frac{dc_V}{dt} = \frac{\dot{c}c_S}{xc_V}.$$

## § 4. DISLOCATION LOOPS

If the interstitial atoms precipitate to form dislocation loops, small at first but growing steadily as they (and not the permanent dislocations) capture further interstitial atoms, then either

$$c_S = \frac{4\pi r_c^2}{a^2} c_1 \quad (r < r_c) \qquad \text{or} \qquad c_S \doteq \frac{(2\pi)^2 r_c r}{a^2} c_1 \quad (r > r_c),$$

where $c_1$ is the atomic concentration of the loops of radius $r$ which can attract and capture interstitial atoms from a distance $r_c$. As the number of clustered interstitial atoms must equal the number of vacancies in the lattice ($c_i$ is very small at temperatures where $\nu$ is appreciable)

$$c_V = \frac{\pi r^2}{a^2} c_1.$$

The rate of accumulation is halved when $xc_V = c_S$, i.e. when either

$$r = (4/x)^{1/2} r_c \quad (r < r_c) \qquad \text{or} \qquad r = (4\pi r_c)/x \quad (r > r_c).$$

If

$$\frac{\dot{c}_V}{\dot{c}_1} < \frac{4\pi r^2}{xa^2}$$

there will be little recombination of point defects and the rate of accumulation will be the maximum ($\dot{c}$) until the clusters begin to overlap at very high doses. This will occur when the nucleation of interstitial atom clusters is frequent, and then the radius of these clusters will never reach the value $(4/x)^{1/2} r_c$.

The table gives some values for the radius at which the accumulation rate halves for various values of $x$ and two values of $r_c$. In each case two values of $r$ are given, one for $r < r_c$ and the other $r > r_c$ and the one in brackets is that which does not apply.

| $x$ | $r_c = 10a$ | | $r_c = 20a$ | |
|---|---|---|---|---|
| 100 | $2a$<br>$(1{\cdot}2a)$ | 6 Å | $4a$<br>$(2{\cdot}4a)$ | 12 Å |
| 10 | $6{\cdot}3a$<br>$12a$ | ~30 Å | $12{\cdot}6a$<br>$24a$ | ~60 Å |
| 1 | $(20a)$<br>$120a$ | 360 Å | $(40a)$<br>$240a$ | 720 Å |
| 0·1 | $(63a)$<br>$1200a$ | 3600 Å | $(126a)$<br>$2400a$ | 7200 Å |

## § 5. DISCUSSION

At temperatures where the mobility of the interstitial atom is appreciable but that of the vacancies is limited, the initial rate of point defect accumulation ($\dot{c}$) will be halved when the probability of the interstitial atoms being captured at sinks is equal to that at vacancies. In reality the sinks are not distributed uniformly throughout the material but occur only at the dislocations or grain boundaries themselves. The effective sink concentration is much greater near the sink and the rate of increase in $c_V$ decreases first at positions most remote from the sinks and last near the sinks. Thus eventually vacancies will cease accumulating in the remote regions and the vacancy concentration will increase towards the sink. An inhomogeneous vacancy concentration will result, with the sinks becoming protected from further interstitial atoms with a sheath of vacancies. Eventually in the case of a grain boundary, this sheath prevents further loss of interstitial atoms there. However, the interstitial atoms captured by the sinks cause a deposition of material there and if the sink is a dislocation line it climbs. Helical dislocations have been observed in copper irradiated at about 200°C presumably due to this (fig. 2). The dislocation could climb through this sheath and improve its ability to collect interstitial atoms, saturation only occurring at very high doses.

If the number of sinks is small then recombination will become important with a low concentration of vacancies. For example with the assumptions that $r_c = 10a$, $a = 3$ Å, $x = 1$ and the dislocation concentration is $10^8$ cm$^{-2}$ recombination will halve the accumulation rate when $c_V = 6 \times 10^{-6}$. If however the interstitial atoms are able to form into clusters, then $c_S$ will become greater than it was initially and higher concentrations of vacancies will accumulate before annihilation becomes important. For example if the above values are assumed but in addition the interstitial atoms precipitate as dislocation loops, they grow to a radius of 360 Å (table) before the accumulation rate is halved. If say $10^{15}$ loops $\mathrm{cm}^{-3}$ had formed this would correspond to a vacancy concentration ($c_V$) of $5 \times 10^{-4}$; much higher than without the loops. However, if fewer loops nucleate then annihilation becomes important earlier but the individual loops grow more quickly.

If the attractive distance between an interstitial atom and a vacancy is large (i.e. $x$ is large) the rate of accumulation will begin to fall off when the interstitial atom clusters are small, and if there are many clusters nucleated their rate of growth will be very small. In such cases their size may be so small that they cannot be seen. The value of $x$ will be largest when the vacancies are single in a metal with a long-range attraction between vacancies and interstitial atoms. This might be the case in a b.c.c. lattice and account for the apparent difficulty in observing loops in the b.c.c. metals. For a given metal, the value of $x$ will be smallest when the vacancies are clustered, e.g. as a void $r = 30$ Å when $x$ would be reduced by factor $\sim 10$ from that when the vacancies were single.

Many materials have been examined in the electron microscope after irradiation and no point defect clusters observed. Either the interstitial atom clusters are not nucleated or they are too small to be resolved. The former would happen if the initial dislocation density was very high but the vacancies left behind would probably form clusters and might be seen†.

At low temperatures or in very high fluxes the nucleation rate of interstitial loops is likely to be high and although vacancies will accumulate to a high concentration before annihilation becomes important, the loops will be limited in size and in the extreme case where nucleation is frequent the loops will not exceed a radius $r = (4/x)^{1/2} r_c$. Higher temperature or lower fluxes should be more advantageous for observing loops directly (particularly when $x$ is larger and $r_c$ is small). The loops will then climb more quickly through their protective sheaths becoming large and forming a dislocation network.

## § 6. CONCLUSIONS

Only when the concentration of vacancies reaches a value $c_V \sim c_S/x$ (where $c_S$ is the sink concentration and $x$ depends upon the attraction distance between the vacancies and the interstitial atoms) is recombination of the point defects important. This value of $c_V$ (which is normally large) will be increased if dislocation loops form and in the proposed model will be attained when the loops are of a radius

$$r = (4/x)^{1/2} r_c \quad (r < r_c) \qquad \text{or} \quad r = (4\pi r_c)/x \quad (r > r_c).$$

---

† However, in the case of electron irradiation possibly neither interstitial atom clusters nor vacancy clusters form because of the absence of a ‘ spike ’,

This size will be reached later the more numerous are the loops. Thus it is necessary to reduce the number of loops if large loops are to be seen in a reasonably short time and this is more necessary when $r_c/x$ is small, i.e. when the efficiency of vacancies to capture interstitial atoms is greatest. However, in general the loops will climb through the surrounding sheath of vacancies which form and eventually grow until they interact with other loops and form a network.

## ACKNOWLEDGMENTS

I am grateful to Mr. D. J. Mazey who supplied the photographs, and to Messrs. M. W. Thompson, A. C. Roberts and Dr. M. J. Makin for useful discussion.

## REFERENCES

BARNES, R. S., 1961, *Disc. Faraday Soc.* No. 31, 38.
BARNES, R. S., and MAZEY, D. J., 1960, *Phil. Mag.*, **5**, 1247.
MAKIN, M. J., WHAPHAM, A. D., and MINTER, F., 1961, *Phil. Mag.*, **6**, 465.
SILCOX, J., and HIRSCH, P. B., 1959, *Phil. Mag.*, **4**, 72, 1356.

# The Dislocation Distribution in Face-centred Cubic Metals after Fatigue

By R. L. Segall†, P. G. Partridge‡ and P. B. Hirsch
Crystallographic Laboratory, Cavendish Laboratory, Cambridge

[Received February 20, 1961]

## Abstract

Transmission electron microscope observations of fatigued Cu, Ni and Au show that these metals contain a high density of dislocation loops. Similar results have been obtained for stainless steel fatigued at high stress. Some of these loops are elongated in a direction normal to the Burgers vector, which suggests strongly that they are formed from sessile jogs in screw dislocations. No correlation between surface slip striations and dislocation distribution has been found.

The observed distribution of loops explains the absence of asterism on x-ray photographs reported previously. Furthermore, the loops are observed to anneal out in a temperature range in which the stored energy is released, and the fatigue hardening disappears. Fatigue hardening is discussed in terms of loops; the annealing of the loops is also considered in detail.

## § 1. Introduction

Previous electron microscope observations of the dislocation distribution in fatigued metals have been confined to face-centred cubic aluminium (Segall and Partridge 1959, Wilson and Forsyth 1959) and stainless steel (Hirsch *et al.* 1959). Fatigued aluminium was found to contain many small dislocation loops, and, if the mean stress during fatigue is zero, other dislocations arranged in a random manner, polygonization being absent. In these two respects the dislocation distribution differs from that in unidirectionally deformed specimens where the dislocations are arranged in a cell structure (Segall and Partridge 1959). In the case of stainless steel fatigued at low stress the dislocations are arranged in broad bands coinciding with the fatigue striations observed optically on the specimen surface, but it was not possible to resolve clearly the dislocation distribution within the striations (Hirsch *et al.* 1959).

The work on Cu, Ni, Au and stainless steel described in the present paper was done with the aim of studying the effect of variation of stacking-fault energy on the nature of the dislocation distribution in face-centred cubic metals.

---

† Now at C.S.I.R.O., Division of Tribophysics, Melbourne, Australia.
‡ Now at C.E.G.B., Berkeley Nuclear Research Laboratories, Glos.

## § 2. EXPERIMENTAL TECHNIQUE

All polycrystalline specimens were in the form of 1 mm sheet and were fatigued with zero mean stress. The copper specimens were fatigued in push–pull in an Amsler Vibrophore at a frequency of approximately 200 c.p.s. at stresses to give lives between $3 \times 10^5$ and $2 \times 10^6$ cycles. These specimens have been examined at an estimated 10%, 50% of the life and also after failure. The nickel, gold and stainless steel specimens were fatigued in plane bending, with zero mean stress, in an Avery machine at a frequency of 1400 c.p.m. The gold was examined after $1{\cdot}8 \times 10^6$ cycles, an estimated 50% of the life. The nickel was examined after 50%, 80% of the life and after failure; the fatigue life of the nickel at the chosen stress was of the order of $2 \times 10^6$ cycles. The plane bending specimens were taken from within about 100 μ of the surface of the test pieces so that they were from the region of maximum stress.

The purities, grain sizes and annealing treatments of the specimens are given in table 1.

Table 1

| Metal | Purity | Grain size | Annealing treatment (*in vacuo*) |
|---|---|---|---|
| Cu | Spec. pure<br>O.F.H.C. | 0·5 mm<br>0·1 mm | 1 hr at 800°c<br>1 hr at 600°c |
| Ni | Carbonyl nickel† 99·96% | 0·1 mm | 24 hrs at 880°c |
| Au | 99·99% | 0·5 mm | ½ hr at 800°c |

† H.P.M. grade, kindly supplied by Mond Nickel Co. Ltd.

Four copper crystals of different orientation, shown in fig. 1‡, were studied. The crystals, grown from spectroscopically pure copper in the form of $8 \times 1{\cdot}3 \times 0{\cdot}05$ cm sheet specimens, were kindly supplied by Mr. A. Howie. They were grown from the melt in a gradient furnace. The crystals were fatigued in plane bending for $5 \times 10^4$ cycles, an estimated 10% of their life.

The thin films for electron microscopy were prepared by electropolishing as described by Tomlinson (1958). To obtain specimens from the region of maximum stress, after fatigue in plane bending, the specimens were first polished from one side to a thickness of about 200 μ. They were then polished from both sides. The films were examined in a Siemens and Halske Elmiskop I operating at 100 kv.

The heating stage designed by Whelan (1960) was used in these experiments. With this stage thin films can be studied in the electron microscope at any temperature between 20°c and 1000°c. In later experiments a combined heating and stereo stage designed by Lally (to be published) was used. Bulk annealing of the fatigued metals was performed in a conventional furnace with a vacuum better than $10^{-4}$ mm Hg.

---

‡ Figures 2–5, 7, 9 and 10, and 12 are shown as plates.

Fig. 1

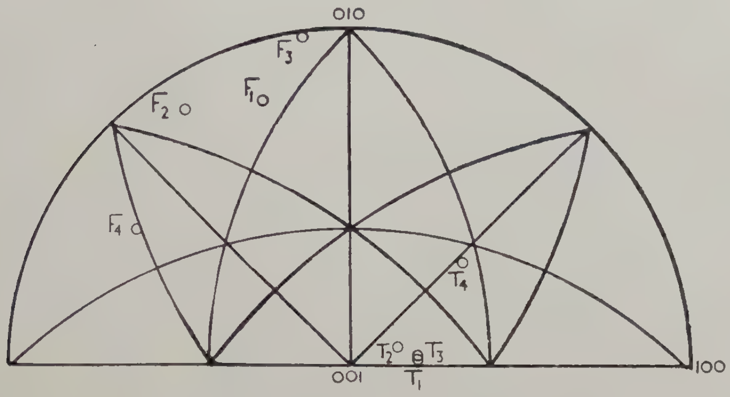

Orientation of copper single crystals; $T_1$, $T_2$, $T_3$, $T_4$ and $F_1$, $F_2$, $F_3$, $F_4$ are the orientations of the tensile axis and foil normal of crystals 1, 2, 3, 4 respectively.

## § 3. EXPERIMENTAL RESULTS ON DISLOCATION DISTRIBUTIONS

### 3.1. *Experiments on Cu Single Crystals*

In all the crystals examined, the dislocations were found to be concentrated in local regions a few microns in extent (with densities of the order of $10^{10}$–$10^{11}$ cm$^{-2}$) separated by regions of similar width but with a lower dislocation density (of the order of $10^8$ cm$^{-2}$). Figures 2 (*a*), (*b*) show typical areas in crystals 3 and 4 (see fig. 1) after $5 \times 10^4$ cycles at room temperature (10% of the estimated life). These dislocation distributions are different from those in unidirectionally deformed crystals (Howie 1960) in which a cell structure is formed in stage II and stage III of the stress-strain curve.

Surface observations of the distribution of slip lines in copper single crystals (Thompson *et al.* 1956, Broom and Ham 1959) show that at this stage in the fatigue test, slip is concentrated in broad bands 10–50 $\mu$ wide, called striations. These may run across the whole specimen and are separated by regions (called matrix) of the order of 0·1 mm wide. There is no direct correlation between these surface striations and the dislocation distribution inside. The dislocation arrangement is homogeneous on a scale of microns, and no superimposed inhomogeneity on a larger scale, corresponding to striations, has been detected. Although no observations were made of the dislocation distribution just below the surface, such observations were carried out for polycrystals (see below) and these showed that the distributions below the surface and in the interior are similar. It is clear therefore that the regions corresponding to the striations contain both areas in which the dislocations are densely clustered, and other relatively dislocation free areas. Furthermore, any possible differences between dislocation distributions in the striations and matrix (Broom and Ham 1957, 1959) are not observable by the techniques used in the present work.

At higher magnifications most of the dislocations in the dense regions are found to be in the form of loops. For crystals 1, 2, 3 orientated for single slip (fig. 1) the loops are elongated. Orientation determinations show that the direction of elongation is generally parallel to the $\langle 211 \rangle$ direction in the active slip plane and normal to the Burgers vector. A representative example is shown in fig. 3 (*a*). In crystal 4, orientated for double slip, the loops are everywhere more nearly equiaxed, as shown in fig. 3 (*b*). It should be emphasized that in each type of crystal the dislocation distribution is similar in all areas examined. There is a wide range of sizes of loops, from the smallest diameter resolvable (about 50 Å) to several 100 Å. Some of the elongated loops are several 1000 Å long.

### 3.2. *Experiments on Polycrystals*

The arrangement of dislocations in fatigued polycrystalline specimens of Cu, Ni, and Au was found to be similar to that in Cu single crystals, i.e. the dislocations are again concentrated in local regions a few microns in extent (with densities of the order of $10^{10}$–$10^{11}$ cm$^{-2}$) separated by regions of similar width containing few dislocations (density of the order of $10^8$ cm$^{-2}$). Figure 4 shows a typical example for Ni after $10^6$ cycles at room temperature, estimated to correspond to 50% of the life. As in the case of Cu single crystals, no correlation could be found between the scale of the surface striations and that of the dislocation distribution inside; although in this case the lack of correlation is more difficult to establish since the striations occur on a finer scale than in single crystals and possibly on several slip systems in a single grain. It should also be noted that polygonization, or cell structure formation, as found in unidirectionally deformed specimens (e.g. Hirsch 1958), is not observed.

Copper specimens were examined after various numbers of cycles at a given stress and no significant difference in dislocation distribution was detected after 10% and 50% of the fatigue life, or after failure. No difference was detected between the specimens failed in $3 \times 10^5$ and $2 \times 10^6$ cycles. The dislocation distributions were also found to be similar in two types of Cu specimen differing in purity and grain size.

A few specimens of fatigued Cu and Ni were also thinned by electropolishing from one side (for technique see Hirsch *et al.* 1959, Thomas and Hale 1959); in this way the dislocation distribution just below the surface was investigated and observed to be similar to that in the interior of the specimens.

At high magnification many of the dislocations were clearly resolved as loops; the range of sizes is similar to that in Cu single crystals (see

§ 3.1). In some areas the dislocation loops are elongated, and the direction of elongation is along ⟨211⟩ directions. A particularly clear example for Ni (after $10^6$ cycles) is shown in fig. 5 (*a*); in the case of Cu the loops are on the whole rather narrower than in Ni and appear as rather irregular elongated 'thick' dislocations (fig. 5 (*b*)). Other areas contain a high density of very small, more or less equiaxed loops (diameter of the order of 100 Å or less) (fig. 5 (*c*)). The density of the small loops appears to be higher in Cu than in Ni. The nature of the distribution of loops is similar to that observed for single crystals of Cu, and it is likely therefore that the loops elongated along ⟨211⟩ occur in regions where slip is mainly confined to one system, while the more equiaxed loops are formed in areas where multiple slip takes place.

It is interesting to note that fatigued Au contain a large concentration of dislocation loops (fig. 5 (*d*)); tetrahedra of stacking faults, such as those formed after quenching and ageing (Silcox and Hirsch 1959 a), are not observed even after ageing the fatigued specimens at 250°C.

Apart from the dislocation loops, long but very joggy dislocation lines can also be seen on the micrographs (for example figs. 5 (*a*), (*b*), (*c*)).

In the experiments on an 18/8 austenitic stainless steel reported previously (Hirsch *et al.* 1959) low stresses were used, giving fatigue lives of the order of $10^7$ cycles. An identical specimen of stainless steel fatigued at a high stress, giving a life of $5 \times 10^4$ cycles, contained elongated dislocation loops similar to those in Cu, Ni and Au. A typical area is shown in fig. 5 (*e*). No distinction could be made between matrix and striations in this high stress specimen. At high stresses therefore stainless steel behaves in a similar manner to Cu, Ni or Au.

## § 4. ANNEALING OF DISLOCATION DISTRIBUTIONS

### 4.1. *Experimental Results*

A polycrystalline specimen of Ni was fatigued for $1 \cdot 6 \times 10^6$ cycles (estimated 80% of fatigue life) and subsequently annealed in bulk, *in vacuo*, successively at temperatures from 300°C to 600°C in steps of 50°C, with the specimen 15 min at each temperature. Up to and including 350°C no change in dislocation density or distribution could be detected. At 400°C a slight reduction of dislocation density occurs, and this becomes more marked at 450°C. At 500°C over 50% of the dislocations are estimated to have annealed out, at 550°C about 90% and at 600°C very few loops remain. The dislocation loops therefore anneal out rapidly in the temperature range 450°C–550°C; the observed decrease of dislocation density is presented graphically in fig. 6. Micrographs of dislocation distributions are shown in figs. 7 (*a*), (*b*), (*c*) for 350°C, 450°C and 500°C. These confirm that the majority of the dislocations are in the form of loops. Examination of numerous micrographs indicates that the smaller loops anneal out first, i.e. that the loops which remain tend to be the larger ones, and that the round and elongated loops anneal out in a similar temperature range. However, there is some evidence that the long loops may take rather longer to anneal out, since after annealing at 500°c or 550°c there are still many narrow elongated loops visible. Some of these long loops appear to anneal out in two stages; in the first of these the loop changes shape and tends to break up into a series of smaller round loops; in the second stage the loops anneal out by climb according to the usual process. The first of these processes, called ' pinching ' is illustrated in fig. 8, and fig. 9 shows a clear example in Ni. The effect can also be seen at A in fig. 7(*c*). The ' pinching ' process has been observed more clearly in Zn (Price 1960), where it takes place considerably more rapidly than the shrinkage of loops by climb. The same process has also been observed independently in MgO by Washburn *et al.* (1960). It should be emphasized that in fatigued Ni this process has been observed in relatively few cases.

Fig. 6

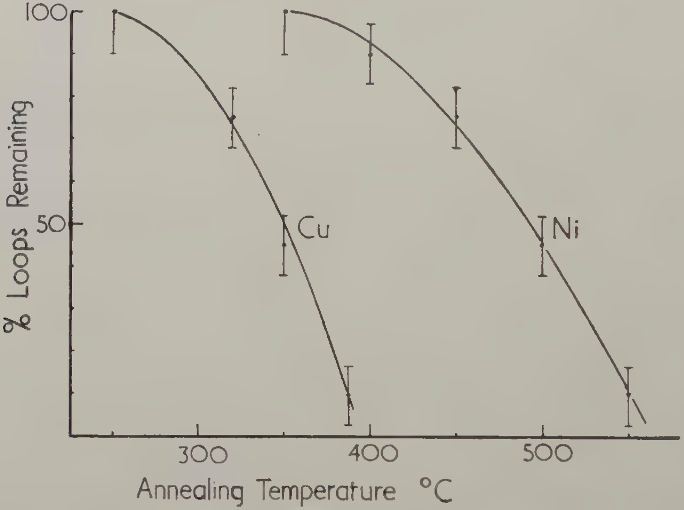

Decrease in dislocation loop density after 15 min anneals at increasing temperature, for fatigued copper and nickel polycrystals.

Very similar observations have been made for Cu, but in this case the loops annealed rapidly in the temperature range 320°c–390°c, as shown in fig. 6. Rather fewer examples of ' pinching ' were found than for Ni.

A few Cu specimens were also examined on the heating stage in the electron microscope. In this case some of the loops could be seen to shrink and joggy dislocations became straight by climb at about 350°c.

The details of the annealing process could be observed more clearly in a specimen pre-annealed in bulk. Figure 10 shows a sequence of micrographs of a specimen heated in the microscope at a temperature between 300 and 400°c, after a preliminary anneal in bulk for 15 min at 390°c (the region is one of maximum loop density after this pre-anneal). Between figs. 10 (*a*) and 10 (*b*) some of the loops had become much narrower, but part of this process may be due to slip rather than climb. (The background of small spots in fig. 10 (*a*) is due to surface contamination.) On comparing figs. 10 (*b*) to 10 (*f*) the loops labelled A are observed to shrink, the decrease in length being rather more rapid than the decrease in width. Some loops are also seen to pinch off (B), after which the shrinkage seems particularly rapid.

Fig. 8

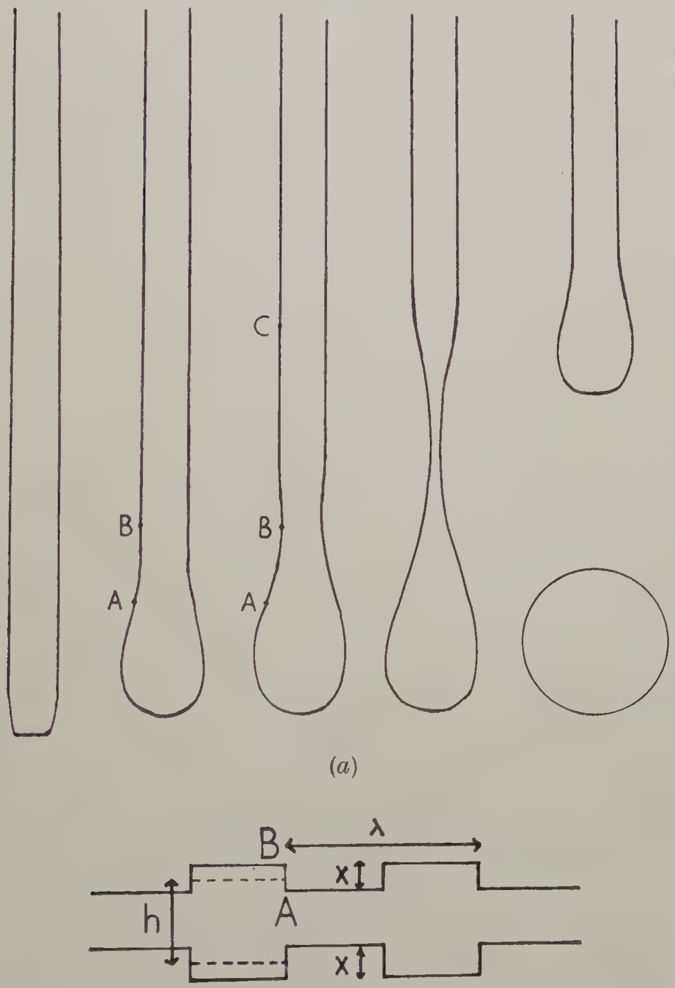

(*a*)

(*b*)

(*a*) Schematic diagram showing successive stages in the ‘ pinching ’ process.
(*b*) Model used for calculation.

### 4.2. *Discussion of Annealing Experiments*

The process of annealing of prismatic dislocation loops by climb has been discussed by Silcox and Whelan (1960), following the theory of climb due to Friedel (1956). At any particular stage of the annealing, loops smaller than a critical size shrink, while those larger than the critical size grow. The distribution of loop sizes therefore changes continuously with time in a way such that the mean loop radius increases. Eventually only very few large loops remain, but even these can anneal out at sufficiently long times if there are other dislocations or grain boundaries present to act as vacancy sinks. (The discussion in this and the following sections tacitly assumes that the loops are vacancy loops; however similar arguments would apply to interstitial loops.) The fact that small loops anneal out first is confirmed in the present experiments. Although the details of the annealing kinetics are clearly complicated, the results can be discussed approximately in terms of a simple model in which the loops anneal out independently, the vacancies disappearing at other sinks. Then the time $\tau$ for a loop of radius $r$ to anneal out at temperature $T$ is given by

$$\tau=(r^2/z\nu_a b^2\alpha)\exp(U/kT) \quad . \quad . \quad . \quad . \quad . \quad . \quad (1)$$

where $U$ is the activation energy for self diffusion, $z$ the coordination number, $\nu_a$ an atomic frequency of vibration, $\mathbf{b}$ the Burgers vector, $k$ the Boltzmann constant, and $\alpha$ a parameter depending on the line tension of the loop; $\alpha$ is given approximately by

$$\alpha\sim Gb^3\log(r/b_0)/4\pi(1-\nu)kT \quad . \quad . \quad . \quad . \quad . \quad . \quad . \quad (2)$$

for a radius $r$ of the order of $100b$ ($G$ is the shear modulus, $\nu$ Poisson's ratio and $b_0$ the core radius).

Using eqn. (1) and putting in suitable values for the various parameters, the time taken for loops of a given size to anneal out at a given temperature can be calculated. Alternatively, by comparing the observed temperatures for Cu and Ni at which loops anneal out in a few minutes, with that observed previously for Al by Silcox and Whelan (1960) and Vandervoort and Washburn (1960) for loops of similar size, the ratios of activation energies can be deduced immediately. Assuming $\tau$, $r$, $z$, $\nu_a$, $b$ and $\alpha$ to be the same for all these metals

$$U_1/T_1=U_2/T_2. \quad . \quad . \quad . \quad . \quad . \quad . \quad . \quad . \quad . \quad (3)$$

This assumption is justified for $\tau$, $r$, $z$, $b$ and $\alpha$, none of which differs from the values in Al by more than a factor 2; $\nu_a$ however is uncertain by at least a factor 10, so that the relative values of $U$ obtained in this way are uncertain by about 10%. Table 2 gives the temperatures at which about 90% of the loops anneal out in 10–15 min in Al, Cu and Ni and the values of activation energy calculated from these, using (3) and assuming the value $U=1{\cdot}35$ ev for Al.

The agreement between the values of activation energy of self-diffusion determined in this way with those obtained by other methods is excellent (for review see e.g. Cottrell 1957, Turnbull and Hoffman 1959) and leaves little doubt that the process of annealing is as described by Silcox and Whelan.

It should be noted that the smaller loops will anneal out in the same time at a considerably lower temperature. Reference to table 2 shows that loops of diameter 100 Å anneal at temperatures 25–50°K lower for Al, Cu and Ni than the temperature corresponding to the larger loops. Smaller loops will anneal at even lower temperatures, but a more elaborate theory is necessary for estimates to be made. In fact, observations on specimens annealed in bulk suggest that the overall density of loops begins to decrease already at about 300°C for Cu and 400°C for Ni (see fig. 6). Thus very small loops would anneal out at these temperatures, and although no direct observations from heating stage experiments are available on this point, this suggestion is consistent with the data from the bulk annealing experiments which indicate that the smaller loops anneal out first (see § 4.1).

Table 2 also gives for comparison the temperatures at which loops of similar sizes are expected to anneal out in Au and Ag, the generally accepted values of the activation energy of self-diffusion being used in these calculations.

Table 2. Data on loop annealing in face-centred cubic metals

| Metal | Average diameter of loop (Å) | $T_{\mathrm{obs}}$ (°K) | $E$ (ev) | $E$ from other data (ev) | $T_{\mathrm{calc}}$ (100 Å) (°K) |
|---|---|---|---|---|---|
| Al | 300 | 430 | 1·35 | 1·35 | 400 |
| Cu | 300 | 660 | 2·1 | 2·05 | 620 |
| Ni | 300 | 820 | 2·6 | 2·7 | 770 |

| Metal | $E$ (ev) assumed | $T_{\mathrm{calc}}$ (300 Å) (°K) | $T_{\mathrm{calc}}$ (100 Å) (°K) |
|---|---|---|---|
| Ag | 1·9 | 610 | 570 |
| Au | 1·8 | 580 | 540 |

$T_{\mathrm{obs}}$ is the temperature at which about 90% of loops anneal out in Cu and Ni in 10–15 min. For Al this temperature is estimated from the annealing data available at 473°K (see Silcox and Whelan 1960). $T_{\mathrm{calc}}$ is the calculated temperature at which loops of diameter 300 Å and 100 Å are expected to anneal out in the same time.

### 4.3. *Annealing of Elongated Loops*

Long loops can anneal out in two ways. Firstly, if diffusion along the dislocation lines (i.e. 'pipe diffusion') is easy, the loop can change its shape to a configuration of lower energy. Thus Price (1960) and

Washburn *et al.* (1960) showed that it is energetically favourable for a long loop to break up into a series of circular loops of equal total area, provided the following condition is satisfied:

$$d/\log(d/b_0) \geqslant 2h/\{\log(h/b_0)+\tfrac{1}{2}\} \quad . \quad . \quad . \quad . \quad . \quad . \quad (4)$$

where $d$ is the diameter of the circular loops, $h$ the width of the long loop, and $b_0$ the core radius. The mechanism by which the loop changes its shape may be considered in a manner similar to Friedel's theory of climb. At any time every jog on the loop emits vacancies which can travel along the dislocation pipe, and absorbs vacancies if there is a local supersaturation. The rate of emission at a jog is controlled by an activation energy ${}_{\mathrm{p}}U_{\mathrm{f}}+{}_{\mathrm{p}}U_{\mathrm{m}}-F_{\mathrm{c}}b^2$ where ${}_{\mathrm{p}}U_{\mathrm{f}}$ and ${}_{\mathrm{p}}U_{\mathrm{m}}$ are the activation energies of formation and movement of a vacancy along the dislocation, $F_{\mathrm{c}}$ is the force on the jog due to line tension or to the attraction of the dislocation of opposite sign on the other side of the loop. However, during the change of shape of the loop, jogs must be created. Some of these, where the loop increases in diameter, may be formed by condensation of vacancies on the dislocation; others, where the loop becomes narrower, must be formed with the aid of thermal activation. The rate controlling process may therefore be the formation of jogs rather than their movement along the dislocation.

The details of the process of change of shape of the loop are complicated, and have been observed directly in Zn by Price (1961). Thus he finds that the loops pinch off first from the ends. We may obtain an approximate picture of the physical process as follows. We shall assume for simplicity that the plane of the loop is normal to the Burgers vector.

The loop will begin to change its shape at the ends where the line tension at the corners is a maximum. The radius of curvature at the end of the loops must at some point have a value equal to or less than $h/2$. Now the force due to the line tension is given by

$${}_{\mathrm{T}}F_{\mathrm{c}}=Gb^2\log(R/b_0)/4\pi(1-\nu)R \quad . \quad . \quad . \quad . \quad . \quad . \quad . \quad (5)$$

where $R$ is the local radius of curvature, while the force on the straight dislocation making up the dipole is

$${}_{\mathrm{S}}F_{\mathrm{c}}=Gb^2/2\pi(1-\nu)h \quad . \quad . \quad . \quad . \quad . \quad . \quad . \quad . \quad (6)$$

since $R \leqslant h/2$, it is clear that ${}_{\mathrm{T}}F_{\mathrm{c}} > {}_{\mathrm{S}}F_{\mathrm{c}}$, hence vacancies are emitted more rapidly at the end, forming a shape with a larger radius of curvature. The flux of vacancies from the curved to the straight part of the loop will stop when $\log(R/b_0)/2R \sim 1/h$ which means that for the usual dimensions observed, the diameter is of the order of $4h$. Price's observations suggest that in practice $d$ is of the order of $3h$.

However, a dipole with a curved loop with $d > h$ at the end cannot be in equilibrium, for the rate of emission of vacancies from jogs near the point of inflexion A in the dislocation is expected to be smaller than at the straight parts of the loop. Hence vacancies will flow from the straight parts of the loop to the bulge. The flow of vacancies from the nearest straight part (B) may create a slight dip at B (see fig. 8 (*a*)); this will develop into a pinch, for the flow of vacancies from points such as C will always ensure that the radius of curvature at the pinch is sufficiently large so that the increase in ${}_{\mathrm{S}}F_{\mathrm{c}}$ due to the decrease in $h$ is greater than the negative line tension term ${}_{\mathrm{T}}F_{\mathrm{c}}$. Thus, once the pinch is initiated it will continue to grow till the loop is completely pinched off. A similar process will now begin at C. This mechanism explains roughly the sequence of events observed by Price (1961). The time ($\tau_{\mathrm{p}}'$) taken for a pinch to occur can be estimated approximately as follows†. We shall assume that pipe diffusion is the rate controlling process. Consider the simplified model of a vacancy loop shown in fig. 8 (*b*). The equilibrium concentration of vacancies at jogs in the pipe will be higher at A ($c_1$) than at B ($c_2$), since the force of attraction on the dislocation due to the dislocation on the other side of the loop is larger the narrower the loop. Vacancies will therefore flow along the concentration gradient from A to B causing the pinch to occur. The rate of flow of vacancies is approximately

$$dn/dt \sim \{f\nu_{\mathrm{a}}b(c_1-c_2)/x\}\exp(-{}_{\mathrm{p}}U_{\mathrm{m}}/kT) \quad . \quad . \quad . \quad . \quad . \quad (7)$$

where $x$ is the distance indicated in fig. 8 (*b*), and $f$ is of the order of the number of atoms per cross section of pipe.

Now $dx/dt \sim (8b^2/\lambda)dn/dt$, where $\lambda$ is the distance between neighbouring pinches, and, assuming saturation conditions at the jogs, the concentrations are given by terms of the form $c=\exp(-{}_{\mathrm{p}}U_{\mathrm{f}}+F_{\mathrm{c}}b^2)/kT$, where ${}_1F_{\mathrm{c}}=Gb^2/2\pi(1-\nu)(h-x)$, for $c_1$, and ${}_2F_{\mathrm{c}}=Gb^2/2\pi(1-\nu)(h+x)$, for $c_2$. Hence, writing ${}_{\mathrm{p}}U={}_{\mathrm{p}}U_{\mathrm{f}}+{}_{\mathrm{p}}U_{\mathrm{m}}$,

$$dx/dt=(8b^3f\nu_{\mathrm{a}}/\lambda x)[\exp({}_1F_{\mathrm{c}}b^2/kT)-\exp({}_2F_{\mathrm{c}}b^2/kT)]\exp(-{}_{\mathrm{p}}U/kT). \quad (8)$$

For all but the smallest distances $x$, $F_{\mathrm{c}}b^2/kT<1$, and therefore

$$dx/dt=\{16f\nu_{\mathrm{a}}b^4\alpha'/\lambda(h^2-x^2)\}\exp(-{}_{\mathrm{p}}U/kT) \quad . \quad . \quad . \quad . \quad (9)$$

where

$$\alpha'=Gb^3/2\pi(1-\nu)kT. \quad . \quad . \quad . \quad . \quad . \quad . \quad . \quad . \quad (10)$$

Hence

$$\tau_{\mathrm{p}}'\sim\{\lambda\, h^3/24\nu_{\mathrm{a}}fb^4\alpha'\}\exp({}_{\mathrm{p}}U/kT). \quad . \quad . \quad . \quad . \quad (11)$$

A similar expression is obtained for interstitial loops. Comparing this expression with that for annealing of a circular loop by self diffusion (eqn. (1)), it is clear that for pinching the factor in front of the exponential exceeds that for annealing by self-diffusion by $\sim(h/b)^2$. Hence, since $h/b\sim100$, and since for Cu and Ni some loops of this width are observed to pinch at a rate comparable to that of shrinking of circular loops, ${}_{\mathrm{p}}U\sim1{\cdot}5$ ev for Cu and $\sim2{\cdot}0$ ev for Ni. These estimates should be regarded as approximate, but nevertheless, it seems that if pipe diffusion is the rate-determining process, the activation energy for pipe diffusion, ${}_{\mathrm{p}}U$, is considerably less than that for self-diffusion in these metals.

---

† A more detailed treatment of this problem has been developed independently by Groves and Kelly; to them and to Silcox and Whelan we are indebted for a useful discussion on this problem.

On the other hand, the annealing may be controlled by the rate of jog formation. The activation energy for this process will be ${}_{\mathrm{p}}U+U_{\mathrm{j}}-F_{\mathrm{c}}b^2$, since a jog (of energy $U_{\mathrm{j}}$) must be formed and a vacancy emitted and moved in the same process of activation. The rate will also depend on the number of sites at which jogs can be formed. It is thought that it will be easier to create new jogs at corner sites such as A rather than along the straight parts of the loop, particularly if the dislocation is extended. Assuming that jogs are formed only at A

$$dx/dt \sim 2b\nu_{\mathrm{a}}[\exp-({}_{\mathrm{p}}U+U_{\mathrm{j}}-{}_{1}F_{\mathrm{c}}b^2)/kT - \exp-({}_{\mathrm{p}}U+U_{\mathrm{j}}-{}_{2}F_{\mathrm{c}}b^2)/kT]. \quad . \quad . \quad . \quad (12)$$

Expanding the exponentials in the usual way, we find

$$\tau_{\mathrm{j}} \sim \{h^2[\log h/b-\tfrac{1}{2}]/4\nu_{\mathrm{a}}\alpha' b^2\}\exp-({}_{\mathrm{p}}U+U_{\mathrm{j}})/kT. \quad . \quad . \quad . \quad (13)$$

Now $U_{\mathrm{p}}$ is expected to be smaller the larger the Burgers vector, and the narrower the dislocation width. Both these factors lead to an opening-up of the core. Activation energies for jog formation are expected to be larger for wider dislocations. The fact that in Ni loops are observed to ' pinch-off ' more frequently than in Cu is attributed to the larger dislocation widths for Cu than for Ni. The fact that the pinching effect is relatively difficult for both Cu and Ni is again attributed to the extension of the dislocation and the small Burgers vectors. However, in the case of Zn studied by Price (1960) the conditions are favourable for the pinching effect since the pyramidal Burgers vector is very large and the dislocation is probably not dissociated (Seeger 1957). In fatigued Al the loops tend to be much rounder than in Ni or Cu (Segall and Partridge 1959, Wilson and Forsyth 1959) suggesting again that the loops can change their shape more easily in this metal, which is to be expected since the dislocation is rather narrow and has a larger Burgers vector. There is however another effect which will tend to round off the loops in Al. During fatigue vacancies are created and these can migrate rapidly at room temperature in this metal, causing any elongated loops to become rounded. In Ni these vacancies cannot migrate at room temperature, and annealing at higher temperature will lead in the first instance to the formation of small clusters since there will then be a very high degree of supersaturation of vacancies. In Cu the situation is not clear since there is no agreement about the temperature at which vacancies are mobile in this metal.

The second process by which long loops may anneal out is directly by self-diffusion. The ends of the loop will tend to become curved, but the radius of curvature will always be less than $h/2$ locally. Hence vacancies will be emitted preferentially at the curved ends and the loop shrinks by becoming shorter. This is in agreement with the heating stage observations in Cu (fig. 10, § 4.1). The rate of advance of the end of the dislocation will be

$$\tfrac{1}{2}\,dL/dt = -(\alpha z\nu_{\mathrm{a}}b^2/2R)\exp(-U/kT) \quad . \quad . \quad . \quad . \quad (14)$$

where $L$ is the loop length and $R$ is the radius of curvature at the end (see Silcox and Whelan 1960). Hence the annealing time will be

$$\tau \sim (hL/2\alpha z \nu_a b^2) \exp (U/kT) \quad . \quad . \quad . \quad . \quad . \quad . \quad . \quad (15)$$

where $2R$ has been put equal to $h$. Thus the annealing time exceeds that of a loop of radius $h$ by a factor $L/2h$. We have neglected here the rather faster annealing rate at the end of the life time of the loop, when its length is of the same order as the radius. In this calculation it has been assumed that the concentration of jogs along the curved part of the dislocation is constant and of the order $\frac{1}{2}$. On the other hand, the annealing may be controlled by the activation energy for jog formation, in which case

$$\tau_j \sim (L/2\alpha z \nu_a b) \exp (U+U_j)/kT. \quad . \quad . \quad . \quad . \quad (16)$$

The experiments for Cu and Ni are consistent with the view that the loops anneal out with the activation energy of self diffusion. This suggests that formation of jogs at the curved ends is not a controlling factor and that (15) applies. Nevertheless the results could also be explained in terms of eqn. (16), the increase in activation energy due to $U_j$ compensating the decrease in the term in front of the exponential.

## § 5. Discussion

### 5.1. *Fatigue-hardened State*

The dislocation distribution in fatigued Cu, Ni and Au differs from that in these metals deformed unidirectionally in that in the former most of the dislocations are in the form of loops, and that no cell structure is formed. There is relatively little plastic curvature in the grains. This at once explains the observations (Gough and Wood 1936, Barrett 1937) that there may be little x-ray asterism after fatigue.

The observed distribution of loops also explains at once the characteristic annealing behaviour of a fatigued metal. Figure 11 shows data by Clarebrough *et al.* (1957) on the annealing of stored energy after fatigue and unidirectional deformation in Cu and Ni. For impure Ni there is an annealing peak around 530°c, for specimens deformed in tension and fatigue. Comparison with the electron microscope observation, and reference to fig. 6 and table 2 leaves little doubt that this peak corresponds to the annealing of dislocation loops by climb, with an activation energy of self-diffusion. Of course very joggy dislocations will also straighten out in this temperature range by a similar process; this has also been observed on the micrographs (see § 4.1). In the specimens deformed in tension there is also a recrystallization peak B at higher temperatures, presumably because of the low mobility of grain boundaries in impure material. This peak occurs at a lower temperature in the purer material; under suitable conditions this temperature can be lower than that corresponding to loop annealing (Clarebrough *et al.* 1960).

Fig. 11

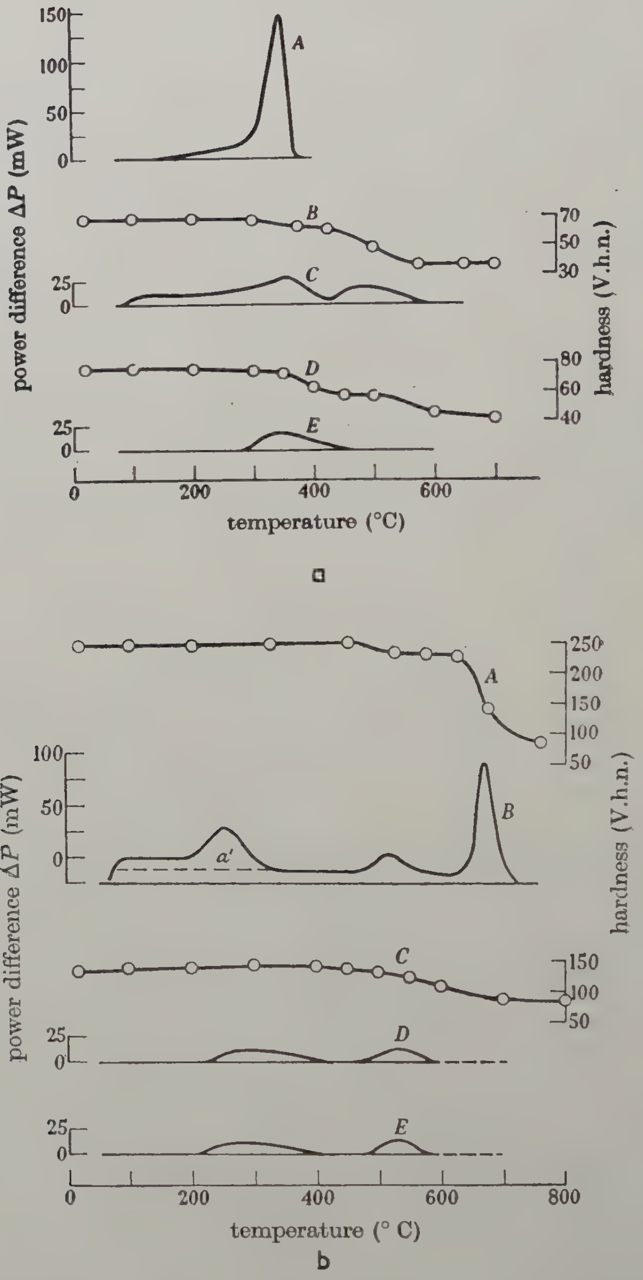

(*a*) Power difference ($\Delta P$) and hardness (V.h.n.) for specimens of copper deformed by compression (curve A), fatigue at a high stress (curves B and C) and fatigue at a low stress (curves D and E) and heated at 6°c/min, from Clarebrough *et al.* (1957). (*Courtesy Royal Society.*)

(*b*) Power difference ($\Delta P$) and hardness (V.h.n.) for specimens of impure nickel (99·6%) deformed by torsion (curves A and B) and by fatigue (curves C, D and E), from Clarebrough *et al.* (1957). (*Courtesy Royal Society.*)

The fatigued specimens show no recrystallization peak (Clarebrough *et al.* 1957); most of the energy in the form of loops anneals out by climb leaving a crystal with only few dislocations. Thus there remains little driving force for recrystallization.

More than half the stored energy is already released at a lower temperature, between 200°C and 400°C in the fatigued specimen. No change in the electron micrographs could be detected in this temperature range. Although a change in density of dislocation loops of perhaps 25% might escape detection, the release in energy on fig. 11 would represent a rather larger change in dislocation loop density. The evidence suggests therefore that this release of energy is associated with sub-microscopic defects such as single vacancies or very small clusters of vacancies or interstitials.

In the case of Cu fatigued at a low stress, all the energy is released in a peak around 350°C. Reference to fig. 6 and table 2 shows that this corresponds again to the annealing of the dislocation loops, the low temperature end of the peak corresponding to rather small loops, probably less than about 10 Burgers vectors in diameter.

The stored energy per unit volume of the circular loops of mean diameter $d$, is approximately equal to

$$[\rho G b^2/4\pi(1-\nu)][\log(d/b_0)+1]$$

where $\rho$ is the dislocation density. The stored energy per unit volume of pairs of parallel edge dislocations of length large compared with their mean separation $h$, is approximately equal to

$$[\rho G b^2/4\pi(1-\nu)][\log(h/b_0)+\tfrac{3}{2}].$$

In both these expressions the contribution due to the core energy has been included as a term equal to $\rho G b^2/4\pi(1-\nu)$. For the copper we take $b_0$, the core radius, equal to $b/2$, $h$ and $d$ are of the order of $50b$ and the total dislocation line length in loops is of the order of $3\times10^{10}$ cm$^{-2}$. This gives a total stored energy arising from all the visible loops of about 0·015 calories g$^{-1}$. This is of the same order as the value of 0·03 calories g$^{-1}$ obtained by Clarebrough *et al.* (1957) for polycrystalline copper fatigued at low stress, although there may be an additional contribution from the submicroscopic defects which anneal out below about 320°C.

The energy release curve for a specimen fatigued at a high stress shows in addition a recrystallization peak and at lower temperatures a broad peak which we interpret again in terms of a process of annealing of submicroscopic defects, i.e. single vacancies or very small clusters of vacancies or interstitials. The recrystallization peak in the specimens fatigued at high stress is probably due to the fact that at high stress, plastic curvature is introduced during the fatigue test, providing the necessary driving force for recrystallization. It may be that it is more difficult to avoid a superimposed unidirectional stress in local areas during a high stress fatigue test.

### 5.2. *Fatigue Hardening*

Although according to the surface markings, slip is confined to striations after the first few per cent of the fatigue life, the distribution of loops inside the metal does not show any variation which could be correlated with these striations and the matrix. Broom and Ham (1959) have shown that in Cu single crystals the matrix is harder than the striations; the difference in yield stress is about 20%, so that the difference in dislocation distribution may well be too slight to be observed. We suggest therefore that there is only a small difference in structure between striations and matrix in Cu, Ni and Au.

One of the striking differences between fatigue-hardened and work-hardened metals is the larger temperature dependence of the flow stress in the former (Broom and Ham 1957, 1959). The electron microscope observations indicate that the hardening in a fatigued metal is mainly due to the loops, as suggested by Broom and Ham (1959) and this is confirmed by the work of Clarebrough *et al.* (1957) which shows that the hardness anneals in the same temperature range as the energy release associated with the loops (see fig. 11, § 5.1).

The precise mechanism by which loops cause hardening is not clear. According to the mechanism of formation of the loops (see § 5.3) most of the loops are expected to have the same Burgers vector as the moving dislocations. Hence the applied stress necessary to overcome the elastic stress of the dislocations will be of the order

$$\tau = Gb\sqrt{\rho}/2\pi \qquad (17)$$

where $\rho$ is the dislocation density. Substituting for $\rho$ the value $10^{11}$ cm$^{-2}$ found in typical dense areas of dislocations in Cu, $\tau$ is found to be of the order of 5 kg mm$^{-2}$, i.e. of the same order as the experimental values of flow stress of fatigue hardened Cu with a similar life (Broom and Ham 1959). With such a distribution of dislocations, jogs are not formed if the moving dislocations simply intersect the loops.

There is also the possibility that the loops combine with the dislocations, forming large jogs which are difficult to move. There is little doubt that such a process occurs in practice, since observations of specimens which have been extended after fatigue show that the density of loops is reduced considerably. Figure 12 shows the dislocation distribution in a specimen of Cu pulled 10% in tension after fatigue for $10^6$ cycles, an estimated 50% of its fatigue life. The density of loops is now much reduced and the distribution appears to be intermediate between that of a fatigued and that of a unidirectionally deformed specimen. A similar result for quenched specimens of Al has been reported by Vandervoort and Washburn (1960). The stress required to move the joggy dislocations is not known at present, and this mechanism will not be considered further.

In the first of these models, if the loops are large, the flow stress is essentially temperature independent, after correction for the shear modulus. The temperature dependent part of the flow stress of a fatigue-hardened metal is thus likely to be due to interaction with sub-microscopic defects, such as very small loops or clusters. If the defects are in the form of circular loops the average maximum interaction energy for a dislocation intersecting a loop of radius $r$ is of the order of $Gb^2r/4$ (Kroupa, unpublished). The average of this interaction energy over the effective radius of interaction (of the order of $2r$) of the loop, is about $Gb^2r/8$. The temperature dependent part of the flow stress must be due to interaction energies not exceeding a few electron volts. Although such small interactions can occur at large distances from the loops observable on the micrographs, the spacing between these does not seem to be much greater than their diameter, so that the large temperature dependence is more likely to be due to non-observable loops only a few Burgers vectors in diameter. In this range of sizes the defect may not be in the form of a loop but resemble a cavity.

It is instructive to compare fatigue hardening with quench and irradiation hardening. Quench hardening in Al has a temperature dependence similar to that of cold-worked Al (Tanner 1960), and this is consistent with the fact that in quenched Al the loops are relatively large, several 100 Å in diameter (Hirsch *et al.* 1958). On the other hand, irradiation hardening has a large temperature dependence (Makin and Minter 1960, Blewitt *et al.* 1961) and there is now some direct evidence that this is associated with sub-microscopic defects (Makin *et al.* 1962) as suggested by Seeger (1958). The temperature dependence of fatigue hardening appears to be similar to that of irradiation hardening, and sub-microscopic defects and loops may therefore be present in similar proportions in these two states of hardening.

It should be emphasized, however, that the temperature dependent part of the flow stress is not due to single or di-vacancies, for the hardness measurements of Clarebrough *et al.* (1957), show that this does not anneal out in the temperature range in which these are mobile (see fig. 11). It is known, of course, that quench hardening occurs only after ageing (Maddin and Cottrell 1955, Kimura *et al.* 1959), and also that irradiation hardening does not anneal out until the temperature range typical of loop annealing is reached (Silcox and Hirsch 1959 b, Makin and Minter 1960). The defects causing the hardening must therefore be small enough to be overcome with the aid of thermal activation, and large enough to be immobile up to temperatures at which self diffusion becomes important; i.e. they are probably of the order of 10 Burgers vectors in diameter. Irradiation hardening is thought to be due mainly to defects of this size (Seeger 1958, Makin *et al.* 1962). These defects would be expected to coarsen at temperatures somewhat below those calculated in table 2 for defects of 100 Å diameter; thus, after annealing at such temperatures the flow stress would be expected to become less temperature dependent. Although no data are available on this point for fatigue hardened Cu, such an effect has been observed after irradiation hardening (Makin and Minter 1960).

### 5.3. *Mechanism of Loop Formation*

The observation that elongated loops tend to be parallel to the ⟨211⟩ direction, normal to the Burgers vector suggests that these loops originate from sessile jogs in screw dislocations as illustrated in fig. 13. The advancing screw dislocation leaves behind a dipole which can be terminated by cross slip to form a closed prismatic loop. This will tend to lie along the direction normal to the Burgers vector in order to keep the length of loop as short as possible. This mechanism has also been observed independently in Zn (Price 1960) and in MgO (Washburn *et al.* 1960), and was suggested by Johnston and Gilman (1960) to account for their observations in LiF.

Fig. 13

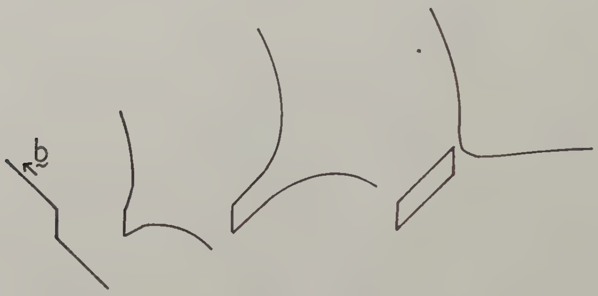

Mechanism by which a screw dislocation with a long jog can form a loop.

The long jogs may be formed by cross slip initiated at forest dislocations during an intersection process, or at impurity obstacles, or by interaction between the dislocations and loops formed previously. Long jogs formed by cross slip are not necessarily sessile (Hirsch, unpublished) and the sessile behaviour remains to be explained. One possibility is that the jog changes into a sessile configuration by combining with vacancies (i.e. climb) during glide along the screw. Other jogs may be held up by elastic interaction with loops formed previously, or by interaction with impurities.

In crystals orientated for double slip the loops tend to be small and more equiaxed. This may be the result of interaction between the secondary slip system and the loops, but the details are not understood. Thus, while it is quite possible for loops to interact with dislocations with the same Burgers vector, forming large jogs, and leaving smaller loops behind, it is not clear how interaction with dislocations of different Burgers vectors could lead to the same result, unless the loop changes its Burgers vector in the presence of the large stress from the intersecting dislocation.

There is no reason why the sessile jog mechanism for loop formation should not also occur in unidirectional deformation. In fact, Price (1960) and Washburn *et al.* (1960) have observed it in Zn, and MgO respectively. Loops are often observed in unidirectionally deformed Cu and Cu alloys (Howie 1960), Ag, Ni (Bailey 1959) and other face-centred cubic metals. However, the density of loops is generally much smaller than in fatigue. This is presumably due to the continuous sweeping up of loops by successive fresh dislocations containing few jogs. Vandervoort and Washburn (1960) have reported that loops in quenched Al are eliminated after a few per cent tensile deformation, and we have found that the same process occurs after fatigue (see § 5.2). Loops are eliminated probably partly by combining with the moving dislocations, and partly by being swept by prismatic glide into local areas (' cell boundaries ') where they could combine with each other and other dislocations to form complex networks. In the fatigue case, however, only a few heavily jogged dislocations may be moving to and fro, continuously forming new loops and annihilating others. There exists presumably some steady state density of dislocation loops for each fatigue stress. Any prismatic glide of the loops may be expected to be in the nature of a to and fro motion.

### 5.4. *Comparison with Other Metals*

The distribution of dislocations in Al fatigued at low stress is similar to that in Cu, Ni or Au, in that some regions contain predominantly dislocation loops (Segall and Partridge 1959, Wilson and Forsyth 1959), but differs from these in that there are more regions which consist of rather irregular arrangements of joggy dislocations. Polygonization does not occur in any of these metals after fatigue at low stresses. Furthermore no correlation between dislocation distribution and striations has been observed in any of these metals. The absence of elongated loops in Al is attributed to the high mobility of vacancies and the probable ease of pipe diffusion in this metal (see § 4.3).

While the dislocation distribution in stainless steel fatigued at high stress is rather similar to that in Cu, Ni or Au, it is rather different after fatigue at low stress (Hirsch *et al.* 1959). In the latter case the striations are clearly marked and correlate with the dislocation distribution inside the metal. There is thus an analogy here between fatigue and unidirectional deformation. In both cases the surface slip lines do not correlate with the distribution of dislocations in the interior in the case of Cu, Ni, Au and Al, but they do in the low stacking-fault energy alloys such as stainless steel, at least at low and moderate stresses. This difference may be due to the difficulty of cross slip in the low stacking-fault energy alloys, or perhaps due to the high jog energy which prevents forest dislocations from multiplying once slip has occurred on the primary system. In either case the difference is due to the difference in dislocation width.

It seems that of the metals tested, only in stainless steel is it possible to obtain experimentally observable fatigue lives at a stress below that necessary for cross slip (or easy jog formation) at room temperature.

In stainless steel tested at high stress and in Cu, Ni, Au and Al, slip spreads over the whole specimen in the first $10^4$ cycles forming dislocation loops everywhere. Fine surface slip occurs over the whole specimen at this stage in the fatigue life of Cu single crystals (Broom and Ham 1959). Striations then occur in local regions which are presumably softer merely by accident. In the low stress stainless steel specimens on the other hand, striations must be formed from the beginning and loops are not formed in the matrix. This indicates that slip can continue more easily on the same planes in stainless steel; a similar situation is found in unidirectionally deformed $\alpha$-brass, where appreciable slip continues to occur on the same slip planes (Wilsdorf and Fourie 1956) whereas this is not the case in Cu (Seeger *et al.* 1957). This relative ease of slip on the same planes may be due to a smaller density of forest dislocations or simply to the difficulty of cross slip.

The main effect of the difference in stacking-fault energy seems therefore to be on the distribution of slip, as found for unidirectional deformation. Just as in the case of unidirectional deformation, the dislocation ribbon width determines the stress at which certain processes, for example cross slip, can take place. Thus, even in stainless steel the dislocation distribution is similar to that in the other metals provided the fatigue test is carried out at a sufficiently high stress.

The stacking-fault energy also seems to affect the shape of the loops, as discussed in § 4.3.

### 5.5. *Conclusions*

The observation that fatigue-hardened Cu, Ni and Au contain a high density of dislocation loops at once explains many of their properties. Thus, the absence of x-ray asterism and polygonization, the annealing behaviour, the absence of recrystallization in low-stress fatigue specimens, the high flow stress and its temperature dependence can all be understood in terms of this distribution of defects. The details of the process of formation of the dense clusters of loops are still obscure. Furthermore, the observations in this paper do not lead directly to a clarification of the process of fatigue failure itself. The questions still remain as to how dislocations moving to and fro through this distribution of loops actually form a fatigue crack, and how this propagates.

## ACKNOWLEDGMENTS

Our thanks are due to Professor N. F. Mott, F.R.S. and Dr. W. H. Taylor for their interest and encouragement. We would like to thank Mr. A. Howie for generously supplying the single crystals of copper and Dr. R. K. Ham for a number of valuable discussions. We are grateful to Dr. P. B. Price for allowing us access to his unpublished work. Our thanks are also due to the Metallurgy Department, Cambridge University and to the British Welding Research Association for the provision of testing facilities, to Mr. G. Rickards for his careful attention to the microscope and to Mr. J. Bell for help with the photographic work. One of us (R. L. S.) is indebted to the Commonwealth Scientific and Industrial Research Organization, Australia, and another (P. G. P.) to the Admiralty for financial support.

## REFERENCES

BAILEY, J. E., 1959, Ph.D. Thesis, University of Cambridge.

BARRETT, C. S., 1937, *Trans. Amer. Soc. Met.*, **25,** 1115.

BLEWITT, T. H., COLTMAN, R. R., JAMISON, R. E., and REDMAN, J. K., 1961, *J. nucl. Materials* (in the press).

BROOM, T., and HAM, R. K., 1957, *Proc. roy. Soc.* A, **242,** 166; 1959, *Ibid.*, **251,** 186.

CLAREBROUGH, L. M., HARGREAVES, M. E., WEST, G. W., and HEAD, A. K., 1957, *Proc. roy. Soc.* A, **242,** 160.

CLAREBROUGH, L. M., HARGREAVES, M. E., LORETTO, M. H., and WEST, G. W., 1960, *Acta Met.*, **8,** 797.

COTTRELL, A. H., 1957, Institute of Metals Monograph & Report Series, No. 23, p. 1.

FRIEDEL, J., 1956, *Les Dislocations* (Paris: Gauthier-Villars).

GOUGH, H. J., and WOOD, W. A., 1936, *Proc. roy. Soc.* A, **154,** 510.

HIRSCH, P. B., 1958, *Report on Symposium on Internal Stress and Fatigue in Metals* (Detroit: General Motors Labs.), p. 139.

HIRSCH, P. B., PARTRIDGE, P. G., and SEGALL, R. L., 1959, *Phil. Mag.*, **4,** 721.

HIRSCH, P. B., SILCOX, J., SMALLMAN, R. E., and WESTMACOTT, K. H., 1958, *Phil. Mag.*, **3,** 897.

HOWIE, A., 1960, Ph.D. Thesis, University of Cambridge.

JOHNSTON, W. G., and GILMAN, J. J., 1960, *J. appl. Phys.*, **31,** 632.

KIMURA, H., MADDIN, R., and KUHLMANN-WILSDORF, D., 1959, *Acta Met.*, **7,** 154.

MADDIN, R., and COTTRELL, A. H., 1955, *Phil. Mag.*, **46,** 735.

MAKIN, M. J., and MINTER, F. J., 1960, *Acta Met.*, **8,** 691.

MAKIN, M. J., WHAPHAM, A. D., and MINTER, F. J., 1962, *Phil. Mag.* (in the press).

PRICE, P. B., 1960, *Phil. Mag.*, **5,** 873; 1961, *Ibid.*, **6,** 449.

SEEGER, A., 1957, *Report of Lake Placid Conference on Dislocations and Mechanical Properties of Crystals* (New York: Wiley), p. 243; 1958, *Proc. 2nd U.N. Intern. Conf. of Peaceful Uses of Atomic Energy, Geneva*, **6,** 250.

SEEGER, A., DIEHL, J., MADER, S., and REBSTOCK, H., 1957, *Phil. Mag.*, **2,** 323.

SEGALL, R. L., and PARTRIDGE, P. G., 1959, *Phil. Mag.*, **4,** 912.

SILCOX, J., and HIRSCH, P. B., 1959 a, *Phil. Mag.*, **4,** 72; 1959 b, *Ibid.*, **4,** 1356.

SILCOX, J., and WHELAN, M. J., 1960, *Phil. Mag.*, **5,** 1.

TANNER, L. E., 1960, *Acta Met.*, **8,** 730.

THOMAS, K., and HALE, K. F., 1959, *Phil. Mag.*, **4,** 531.

THOMPSON, N., WADSWORTH, N. J., and LOUAT, N., 1956, *Phil. Mag.*, **1,** 113.

TOMLINSON, H. M., 1958, *Phil. Mag.*, **3,** 867.

TURNBULL, D., and HOFFMAN, R. E., 1959, *Acta Met.*, **7,** 407.

VANDERVOORT, R., and WASHBURN, J., 1960, *Phil. Mag.*, **5,** 24.

WASHBURN, J., GROVES, G. N., KELLY, A., and WILLIAMSON, G. K., 1960, *Phil. Mag.*, **5,** 991.

WHELAN, M. J., 1960, *Fourth International Conference on Electron Microscopy* (Berlin: Springer-Verlag), p. 96.

WILSDORF, H., and FOURIE, J. T., 1956, *Acta Met.*, **4,** 271.

WILSON, R. N., and FORSYTH, P. J. E., 1959, *J. Inst. Met.*, **87,** 336.

# A Surface Effect Associated with Dislocation Ribbons

By R. Gevers, S. Amelinckx and P. Delavignette
Solid State Physics Department,
Centre d'Etude de l'Energie Nucléaire—MOL (Belgium)

[Received April 19, 1961]

## Abstract

A new surface effect associated with extended dislocations, in materials with small stacking-fault energy, and which consists in a widening of the ribbons at the surface, is discussed from a theoretical point of view and illustrated with observations in graphite and molybdenum sulphide. The effect leads to a method for estimating surface energies. The surface energy of graphite as deduced from the widening effect is in fair agreement with the value found by other methods.

## § 1. Introduction

In the course of an electron microscopic study of dislocations in molybdenum sulphide and graphite (Amelinckx and Delavignette, 1961), both layer structures with a small stacking-fault energy, a striking surface effect was found. In a number of cases it was found that dislocation ribbons widen or close when emerging in a cleavage step, in the manner shown schematically in fig. 2. This paper is concerned with a possible explanation of this effect. If the interpretation is correct it leads to a method for estimating surface energies of solids, a quantity which is difficult to measure.

## § 2. Geometrical Considerations

A dislocation having a Burgers vector with a component normal to a free surface produces an exposed ledge when intersecting this surface. Such ledges result, e.g., on cleaving crystals containing dislocations (Amelinckx and Votava 1954). The exposed ledges wind up into spirals when the crystal grows (Frank 1949) or evaporates (Amelinckx and Votava 1954). Glide movement of dislocations changes the length of the exposed ledge, i.e. increases the surface area and hence changes the energy associated with the surface. Since movement over the unit distance changes the surface area by $h$ ($h$=step height) a force of magnitude $h\sigma$ acts parallel to the surface on the endpoint of the dislocation ($\sigma$=specific surface energy) (Nabarro 1952). On a *clean* surface this force is in such a sense that it tends to decrease the step length. Adsorption, oxydation and other surface phenomena may however change the behaviour and may even make it energetically more favourable to increase the step length. In such circumstances the surface energy is effectively negative (Frank 1953).

Consider now the surface topography where a set of dissociated dislocation ribbons meets a clean surface as in fig. 1†. The horizontal plane in fig. 1 is a pronounced cleavage plane, e.g. the *c*-plane in graphite, and a secondary cleavage plane forms the macrostep. Cleavage is supposed to proceed in the sense indicated by the arrows. From geometrical considerations it follows that the different situations pictured in fig. 1 may result, depending on the exact manner in which cleavage took place, and on the orientation of the Burgers vector with respect to the steps.

Fig. 1

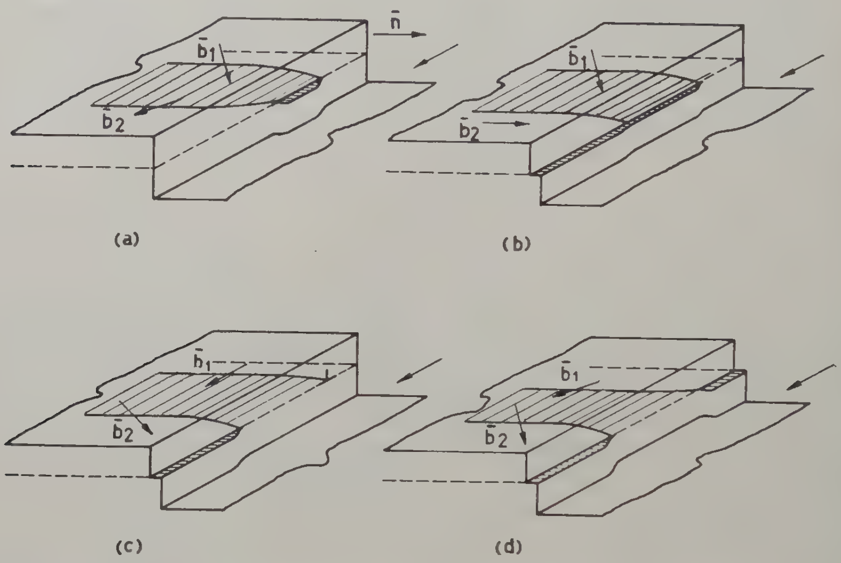

Surface topography for dislocation ribbons emerging in a cleavage step. (*a*) The two steps are in the opposite sense. A ledge connects the two emergence points. (*b*) The two steps are in the same sense and at the same side of the ribbon. (*c*) A step is attached to only one of the dislocations. (*d*) Steps on both sides of the ribbons.

Let $\bar{n}$ be the normal to the step. In (*a*) $\bar{n} \cdot \bar{b}_1$ and $\bar{n} \cdot \bar{b}_2$ are equal in magnitude and of opposite sign; steps of opposite sense are produced, and so a ledge connects the emergence points. Due to the forces on the end-points of the dislocations, the separation of the partials will slightly decrease until the constant pull exerted by the ledges is compensated by the increase in line tension of the dislocations and the increased repulsion between partials. Since the last term increases rapidly with the decrease in distance, no large effect is to be expected. In any case the observation would be difficult since the distance between partials is generally quite small.

---

† Figures 4, 5 and 6 are shown as plates.

In the situation (*b*) $\bar{b}_1 \,.\, \bar{n} < \bar{b}_2\bar{n}$, i.e. the two ledges are of different height and they are at the same side of the ribbon. The net result is therefore that both dislocations will be pulled somewhat sideways, until the pull is compensated by the resultant of increased line tension and the other acting forces.

In situation (*c*) a ledge of height $\bar{b}_2 \,.\, \bar{n}$ is attached to only one of the partials, the other having a Burgers vector parallel to the step. In this last case a pull is exerted on one of the dislocations only. The second partial will however be deformed slightly also, due to the stacking fault that keeps the partials together. The pattern will in any case be asymmetrical.

The configurations just described can occur for an isolated ribbon; the situation pictured in (*d*) can however only occur if at least one other dislocation ribbon lying in the same glide-plane, and having a different total Burgers vector, precedes the ribbon considered. Only then can one assume the existence of an initial step. The last situation (*d*) will however, once started, repeat regularly in a sequence of similar ribbons in the same glide-plane. The two partials will now be pulled apart at the surface.

Out of the four different configurations, shown in projection in fig. 2, the last one gives the most striking feature and the only one which is easy to establish unambiguously. Below we present theoretical and experimental evidence that the effect is observable in materials with small stacking-fault energy.

## § 3. THEORETICAL ANALYSIS OF THE EFFECT

The significance of the symbols to be used is evident from fig. 3, which pictures one of the possible shapes of a ribbon close to the surface. The broken lines represent the situation in the absence of the surface effect; for the case of widening $|y| > D$ (and $\beta < 0$); $|y| < D$ (and $\beta > 0$) corresponds to narrowing.

The aim of our treatment is to obtain relations between quantities influencing the effect, such as line energy, stacking-fault energy, surface energy, and the measurable quantities $\beta_0$ and $y_0$ (the values of $\beta$ and $y$ at the surface). We will use the variational procedure. The total change in energy $E$ between the original and the considered configuration will be minimized. In order to keep the treatment simple or even possible, some effects will be approximated or neglected. It is thought that this will not alter very significantly the results. Moreover, we shall only consider the isotropic case.

The different quantities contributing to the effect are:

(*a*) The line energy of the dislocations.

We shall take for $\epsilon$, the line energy per unit length

$$\epsilon = \alpha\mu b^2(1-\nu\cos^2\phi)$$

($\mu$: shear modulus; $\bar{b}$: Burgers vector of the partial dislocation considered;

Fig. 2

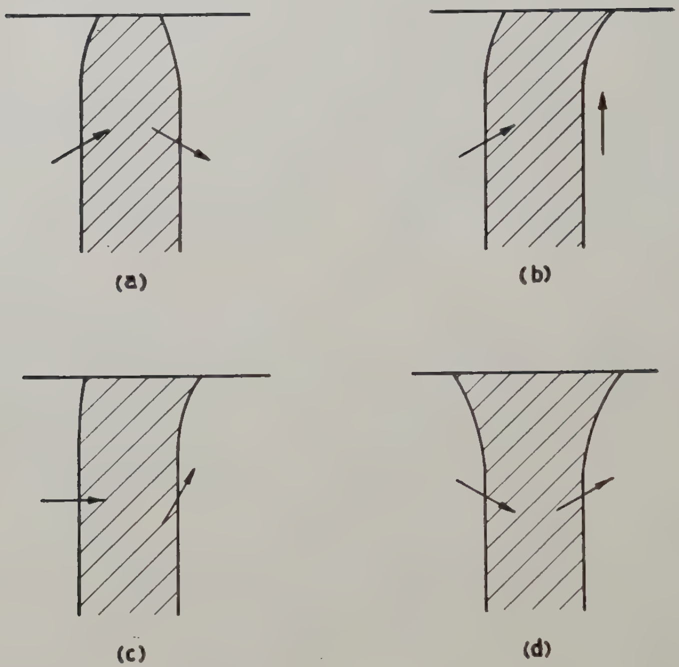

The projection on the main cleavage plane of the configuration shown in perspective in fig. 1. These are configurations as they are observed in the microscope.

$\alpha$: a numerical factor of the order 0·5–1; $\nu$: Poisson's ratio; $\phi=\psi-\beta$). (Cottrell 1958.)

(*b*) The stacking-fault energy. We will note $\gamma_s$ for the stacking-fault energy per unit area.

(*c*) The surface energy. We will call $\sigma$ the surface energy per unit area of the *c*-face.

(*d*) The interaction energy of the partials forming the ribbons. We will take the effect into account by using the approximations introduced by Siems *et al.* (1961) in his treatment of the dislocation nodes in graphite.

A force of repulsion proportional to $2D$ acts between two parallel straight dislocations in an infinite block of material. Since the dislocations forming the ribbon depart only mildly from straightness and parallelism, it seems a plausible approximate extension to accept that a law of this type still governs the repulsive effect. We propose for the difference in interaction energy between the opened (closed) and the original configuration

$$\Delta E_{\mathrm{I}}=k\frac{\mu b^2}{8\pi}\int_0^\infty \ln\frac{y_1+y_2}{2D}\,dx,$$

$y_1$ and $y_2$ referring respectively to the right and left component of the ribbon;

$$k=\frac{2-\nu-2\nu\cos 2\alpha}{1-\nu}$$

if $\alpha$ is the angle between the ribbon and the resulting Burgers vector of the extended dislocation (Read 1953).

In general it will not be possible to separate this expression into two parts, each depending only on one of the unknown functions $y$. This fact should complicate the mathematical treatment, leading to a system of two differential equations for $y_1$ and $y_2$.

There exist however important cases for which the variational problem can be kept simple, involving only one unknown function, assuming the proposed approximation is sufficiently good.

These are:

the symmetrical cases, for which $y_1 \simeq y_2 = y$ (including the Burgers and Taylor ribbons);
then

$$\Delta E_{\mathrm{I}}=k\frac{\mu b^2}{8\pi}\int_0^\infty \ln\frac{y}{D}\,dx;$$

the asymmetrical cases, for which $y_1=y$; $y_2=D$;
then

$$\Delta E_{\mathrm{I}}=k\frac{\mu b^2}{8\pi}\int_0^\infty \ln\frac{y+D}{2D}\,dx;$$

the asymmetrical cases, for which $y_1+y_2 \simeq 2D$, e.g. both components are pulled to the same side over an approximately equal distance;
then

$$\Delta E_{\mathrm{I}}=0.$$

We can summarize this by noting

$$\Delta E_{\mathrm{I}}=k\frac{\mu b^2}{8\,\pi}\int_0^\infty \ln\left[1+\delta\frac{y-D}{D}\right]dx,$$

$\delta$ having the values 1, $\frac{1}{2}$ and 0 for the three mentioned cases.

By making up the energy balance later, we will of course associate half of this amount with each partial.

We are well aware that the proposed expression for $\Delta E_{\mathrm{I}}$ suffers badly from the fact that it is only a good approximation if the mutual distance between the dislocations is small compared with their distance from free surfaces, which is obviously not so. This effect may be treated in terms of image forces. Considering these, even in a rough approximate manner, would complicate greatly the mathematical treatment. This has led us to neglect these forces. The results will be quantitatively inexact for this reason, but difficult to improve on because of the further mathematical difficulties which would be entailed. We believe that our theoretical analysis, not withstanding this neglect, will be qualitatively correct, and will yield results of the right order of magnitude.

(*e*) The interaction between successive ribbons of a sequence.

For the distance $2D$ between the two components of the ribbon, far from the surface, we have, provided the interaction with neighbouring ribbons is neglected (Read 1953):

$$2D\gamma_s = \frac{\mu b^2}{8\pi} k. \qquad \ldots \ldots \ldots \quad (1)$$

The interaction between successive ribbons will be taken into account, partly by using the following procedure. In the final results $\gamma_s$ can be expressed in function of $D$, using relation (1). For $D$ we take the observed value of the width of the ribbon. We believe that this will take care of the largest part of the interaction, the separation between successive ribbons being in general rather large with respect to the width.

Fig. 3

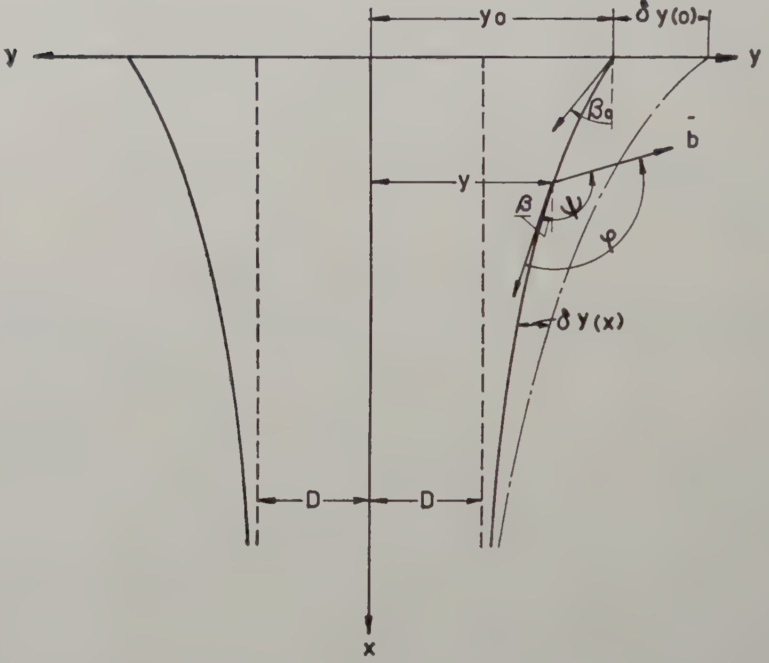

Widening of a dislocation ribbon at a cleavage step.

Taking into account all these contributions, we find for the increase in total energy per partial (we consider here the partial on the right of fig. 3):

$$\Delta E = \int_0^\infty V(y, y')\, dx \pm b \cos \psi [y(0) - D]\sigma,$$

subject to the conditions

$$y(\infty) = D, \quad y'(\infty) = 0$$

where

$$V(y, y') = \alpha\mu b^2 \left\{ \sqrt{(1+y'^2)} \left[ 1 - \nu \frac{(\cos\psi + y' \sin\psi)^2}{1+y'^2} \right] - (1-\nu\cos^2\psi) \right\} + \gamma_s(y-D) - \tfrac{1}{2}k\frac{\mu b^2}{8\pi} \ln\left(1+\delta\frac{y-D}{D}\right).$$

The plus and minus signs correspond to the two senses in which the surface forces may act.

Introducing the variation $\delta y$, with $\delta y(\infty)=0$ (see fig. 3) we obtain by standard mathematical methods

$$\delta(\Delta E) = \int_0^\infty \left( \frac{\partial V}{\partial y} - \frac{d}{dx}\frac{\partial V}{\partial y'} \right) \delta y \, dx + \frac{\partial V}{\partial y'} \delta y \Big|_0^\infty \pm \sigma b \cos\psi \, \delta y(0).$$

The condition $\delta(\Delta E)=0$ leads to:

(1) The Euler equation. Since $V$ is not depending on $x$, the Euler equation gives after one integration:

$$V - y' \frac{\partial V}{\partial y'} = \text{constant} = V(D, 0) = 0,$$

taking into account $y(\infty)=D$ and $y'(\infty)=0$.

After some calculations we find

$$\frac{1}{\sqrt{(1+y'^2)}} \left[ 1 - \nu' \frac{y'^2(\cos 2\psi + y' \sin 2\psi)}{1+y'^2} \right] = 1 - \frac{\gamma_s}{\alpha'\mu b^2}(y-D) + \tfrac{1}{2}\frac{k}{8\pi\alpha'} \ln\left(1+\delta\frac{y-D}{D}\right). \quad . \quad . \quad (2\,a)$$

$$\nu' = \nu/1-\nu\cos^2\psi, \quad \alpha' = \alpha(1-\nu\cos^2\psi). \quad . \quad . \quad (2\,b,\,c)$$

If we note that $y' = tg\,\beta$ and if we express $\gamma_s$ in function of $D$, using relation (1), we have

$$\cos\beta - \nu' \sin^2\beta \cos(2\psi-\beta) = 1 - \frac{k}{16\pi\alpha'}\,[z - \ln(1+\delta z)] \qquad (2\,d)$$

$$z = \frac{y-D}{D}. \quad . \quad . \quad . \quad . \quad . \quad . \quad (2\,e)$$

(2) The eqn. (2 *a*) is an ordinary differential equation of the first order, which is too complicated to be integrated by the standard mathematical means. However, for our purpose, we do not need to know the explicit solution. Integration of eqn. (2 *a*) would lead to a solution still depending on one arbitrary constant, which should be evaluated by expressing that $\delta(\Delta E)$ vanishes. This however leads immediately to a relation, connecting $\beta(x=0)=\beta_0$ and $\sigma$, and which has an obvious physical significance. This relation is, since $\delta y(\infty)=0$, $\delta y(0)\neq 0$:

$$\frac{\partial V}{\partial y'} \pm \sigma b \cos\psi = 0 \text{ for } x=0(y'(x=0)=y_0');$$

or after some calculations

$$\frac{y_0'}{\sqrt{(1+y_0'^2)}} - \frac{\nu''(\sin 2\psi - y_0' \cos 2\psi)}{(1+y_0'^2)\sqrt{(1+y_0'^2)}} = \pm \frac{\cos\psi}{\alpha''\mu b}\,\sigma, \qquad (3\,a)$$

$$\nu''=\frac{\nu}{1-\nu\sin^2\psi}; \quad \alpha''=\alpha(1-\nu\sin^2\psi). \qquad (3\,b, c)$$

If we put again $y_0'=tg\,\beta_0$ we obtain:

$$\sin\beta_0-\nu''\cos^2\beta_0\sin(2\psi-\beta_0)=\pm\frac{\cos\psi}{\alpha''\mu b}\sigma. \qquad (3\,d)$$

### 3.1. *Discussion of Formulae* (3)

The formula (3 *d*) enables us, if the Burgers vector is known, to calculate $\sigma$ by measuring $\beta_0$. Unfortunately the quality of the electron micrograph is not very good for a precise measurement of that angle. To this error has to be added the uncertainty due to the approximation of the analysis. However, only these approximations which would result in neglecting terms of $V(y, y')$ depending on $y'$ would alter the formulae (3). As a consequence we think that these can be trusted.

The eqn. (3 *d*) can be used for two different purposes:

if $\sigma$ is considered as unknown, to calculate its value by measuring $\beta_0$;

if $\sigma$ is considered as known, to predict the value of $\beta_0$. The eqn. (3 *d*) can in fact be considered as an equation of the sixth degree in $\sin\beta$ ($\cos\beta$) which can in principle be solved numerically by some approximation method. We will discuss the case where the surface energy can be neglected, i.e. $\sigma\simeq 0$.

In the case of a partial pure screw or pure edge, i.e. $\psi=0°$ or $90°$, $\beta_0\simeq 0$. However, for $\psi\neq 0°$ and $90°$, i.e. for a partial of mixed character, $\beta_0\neq 0$. This means that the tendency of the line to approach the Burgers orientation, will be sufficient even in the absence of forces due to surface energy. In this case ($\sigma=0$), eqn. (3 *a*) becomes:

$$y_0'^3+(1+\nu''\cos 2\psi)y_0'-\nu''\sin 2\psi=0. \qquad (4)$$

This equation has in fact a single root different from zero provided $\sin 2\psi$ differs from zero. Moreover, $y_0'<0(\beta_0<0)$ for $\sin 2\psi<0$ and $y_0'>0(\beta_0>0)$ for $\sin 2\psi>0$. In the first case, the line approaches the Burgers orientation by bending to the right, in the other case to the left.

Putting in the values $\nu$ and $\psi$ in eqn. (4)†, we obtain for an edge ribbon, i.e. $\psi=120°$ (widening) or $\psi=60°$ (narrowing): $\beta_0\simeq\pm 17°$; for a screw ribbon, i.e. $\psi=150°$ (widening) or $\psi=30°$ (narrowing): $\beta_0\simeq\pm 11°$. The observed values of $\beta_0$ are larger, this indicates clearly that the effect of the surface energy of the exposed ledge has to be considered in order to be able to explain quantitatively the shapes of the ribbons.

If we substitute these values of $\beta_0$ into eqn. (2 *d*) in which $x$ is put equal to zero, we obtain for the measure of the widening $z(x=0)=z_0$ (see eqn. (2 *e*) ) the value 1·5–1·6, for the measure of the narrowing $-z_0=0{\cdot}6$–$0{\cdot}7$ ($\alpha=0{\cdot}96$; this value shall be obtained later; $\nu=0{\cdot}26$). Here again the observed widening is more important.

---

† According to measurements made in this laboratory, and which will be published elsewhere, $\nu$ should be 0·26 in graphite.

The surface energy may act in the same or in the reverse sense of the tendency of the partial to approach the screw orientation. In the second case it would even be possible that both effects nearly annihilate each other, in such a way that the ribbons keep a nearly straight shape near the surface. This would happen for a value of $\sigma$, calculated from (3 $d$) in which $\beta_0$ is put equal to zero. This gives

$$\sigma = 2\alpha\nu\mu b \,|\sin\psi\,| \simeq \begin{cases} 110 \text{ erg/cm}^2 \text{ for } \psi = 120°,\ 60°. \\ 80 \text{ erg/cm}^2 \text{ for } \psi = 150°,\ 30°. \end{cases}$$

$$(\alpha = 0{\cdot}96;\ \nu = 0{\cdot}26;\ \mu b^2 = 4{\cdot}65 \times 10^{-6} \text{ erg/cm};\ b = 1{\cdot}42 \times 10^{-8} \text{ cm.})$$

As will be found below the probable value of $\sigma$ is about 130 erg/cm$^2$, which implies that the surface effect will always be dominant. A situation can however arise where the surface forces tend to close the ribbon, whereas the line tension tends to open it. This would result in a slight narrowing of the ribbon, as some observations suggest.

The first member of (3 $d$) not considering the sign, has a maximum value of $+1$ in the interval $(-\pi/2,\ +\pi/2)$. Thus we have

$$\sigma = \boldsymbol{\sigma} A (0 \leqslant A \leqslant 1);\ \boldsymbol{\sigma} = \frac{\alpha''\mu b}{|\cos\psi\,|}$$

This gives for

$$\psi = \phantom{00}0°,\ 180°,\quad \boldsymbol{\sigma} \simeq 310 \text{ erg/cm}^2,$$
$$\psi = 120°,\ \phantom{0}60°,\quad \boldsymbol{\sigma} \simeq 350 \text{ erg/cm}^2,$$
$$\psi = 150°,\ \phantom{0}30°,\quad \boldsymbol{\sigma} \simeq 340 \text{ erg/cm}^2.$$

For values of $\sigma$ close to this critical value, $\beta_0$ would become very nearly $\pm 90°$, i.e. the partial would become nearly parallel to the surface. It is obvious from eqn. (2 $d$) (with $x = 0$) that $z_0 = y(0) - D/D$ would become very large, 10 to 20. This situation is never observed, in agreement with the fact that the probable value of $\sigma$ is sufficiently smaller than the critical value to make $A$ sufficiently smaller than 1, to yield a value of $\beta_0$ much different from $\pm 90°$. For $\sigma$ approximately equal to $\boldsymbol{\sigma}$, some approximations of our treatment would no longer be reasonable, in particular neglecting the image forces is no longer justified. Since the observations yield a value of $\beta_0 \ll 90°$ and values of $z_0$ of at most some units, this criticism does not apply to our case.

Another feature is in fact that the left hand side of (3 $d$) is odd in $\sin\beta_0$ only if $\psi = 0°,\ 90°,\ 180°,\ 270°$ (pure screw or edge). If $\psi \neq 0°$, $90°$, $180°$ and $270°$, two values $-\beta_{0,1}$ and $\beta_{0,2}$, such that $\beta_{0,1} \neq \beta_{0,2}$, correspond to the two possible signs of the right-hand side. This fact expresses quantitatively that the surface force and the line tension help each other in one case, but counteract in the other, giving rise to different values for $\beta_0$.

### 3.2. *Discussion of Formulae* (2)

The formulae can be used in different ways:

If $\beta$ and $y$ are measured, the treatment can be checked point by point by bringing these values into the equations. Unfortunately the definition of the electron micrographs is not good enough for this purpose.

If a value of $\beta_0$ is measured, formula (2 *d*) predicts the value of $z_0$, i.e. the widening or narrowing in units $D$.

If $\beta_0$ and $z_0$ are measured, a numerical value of $\alpha$ can be computed.

It is to be noted that the right-hand side of (2 *d*) (with $x=0$), considered as a function of $z_0$, has a maximum for $z_0=0 (y_0=D)$. To a given value of $\beta_0$ correspond two values of $y_0$, one larger, and one smaller than $D$. Equation (2 *d*) has then to be interpreted in the following way: with $\beta<0$ corresponds the value $y_0>D$, with $\beta>0$ the value $y_0<D$. Notice also that the right-hand side is not symmetrical with respect to this maximum, this expresses quantitatively the fact that widening causes a loss in interaction energy, whilst narrowing, on the contrary, results in a gain of energy.

Roughly one may predict for values of $\beta_0$ of the order of the observed ones, values of $z_0$ of the order of 1 to 5, in the case of widening, of 0 to $-\frac{1}{2}$ in the case of narrowing, in agreement with the observations.

## § 4. OBSERVATIONS

The widening of ribbons at surface steps has been observed as well in molybdenum sulphide as in graphite; fig. 4 and fig. 6 refer to graphite. The configuration is presumably in equilibrium. This can be concluded from the fact that such ribbons were sometimes found to move subsequently, maintaining a wider spacing at the surface. Since the specimens were prepared by cleavage, the assumption that the surface is relatively clean is not an unreasonable one.

The same applies to molybdenum sulphide; one example of an observed sequence is shown in fig. 5. It should be pointed out here that molybdenum sulphide contains at least three kinds of dislocations which can be distinguished by differences in stacking-fault energy. One kind of dislocations is apparently undissociated; the second kind has a vanishingly small stacking-fault energy (Pashley and Presland, 1961) and the third kind has an intermediate value for the stacking-fault energy. The sequence of fig. 5 belongs to the third kind of dislocations. A detailed account on dislocations in molybdenum sulphide will be published elsewhere (Delavignette and Amelinckx, to be published).

Since numerical values for the physical constants of molybdenum sulphide are not available, a comparison of observed and calculated values of $\sigma$ is only possible for the *c*-face of graphite. The ribbon indicated by an arrow on fig. 6 is considered and measured.

We assume the ribbon to be of the edge type and that surface force and line tension both try to widen the ribbon. Putting in eqns. (2 *b*, *c*, *d*, *e*) (with $x=0$) the adequate values of the constants for graphite and the observed values for $\beta_0$ and $y_0$, i.e. $\psi=120°$, $\nu=0{\cdot}26$, $k=3{\cdot}0$; $z_0=3{\cdot}5$, $\beta_0=-30°$, gives $\alpha=0{\cdot}96$. This value is felt as well acceptable.

Substituting this value into eqns. (3 $b$, $c$ and $d$) together with the constants for graphite and the observed value of $\beta_0$, i.e. $\alpha = 0{\cdot}96$, $\nu = 0{\cdot}26$, $\psi = 120°$, $\mu b^2 = 4{\cdot}65 \times 10^{-6}$ erg/cm, $b = 1{\cdot}42 \times 10^{-8}$ cm, $\beta_0 = -30°$ we obtain a value of $\sigma = 130$ erg/cm$^2$.

The value of $\sigma$, deduced by Good *et al.* (1958) from experiments on the heat of wetting by various liquids, is 119 erg/cm$^2$ for the interface basal plane-air. The agreement is reasonable in view of the approximations used and of the errors due to difficult measurements; furthermore there is some scattering in the observed values of $z_0$ and $\beta_0$ which may, e.g. be due to adsorbed gases.

In fig. 4 it is clearly visible that one of the ribbons is almost straight at the surface. It is also evident from the difference in contrast that this ribbon has another Burgers vector; its behaviour is therefore easy to explain, referring to the different possible configurations of ledges of fig. 1. The threefold ribbons also behave differently, as one would expect, since the three dislocations have now the same Burgers vector (Amelinckx and Delavignette, in the press).

## § 5. CONCLUSIONS

We believe that the surface effect discussed in the theoretical part has really been observed in graphite and molybdenum sulphide where the circumstances are especially favourable as a consequence of the small value of the stacking-fault energy. Other, trivial, explanations have been considered. It might, e.g., be possible that a peculiar stress concentration at the step, forces locally the two partials apart. Such a stress would however be accompanied by buckling of the foil and would presumably be detected in the extinction contour pattern, which was not the case. Although the latter explanation cannot be ruled out completely, we do not think it is of application here. The fact that a widening is observed only in a fraction of the cases where ribbons emerge in a step is in accordance with the special geometrical requirements necessary to produce the effect. The effect may be used to deduce the surface energy of specific faces of a solid.

## ACKNOWLEDGMENTS

We are indebted to Mr. J. Goens, director of the CEN., Mol, for permission to publish this paper. We also wish to thank Mr. J. Nicasy for his skilful preparation of specimens and Mr. H. Beyens for careful photographic work.

## REFERENCES

AMELINCKX, S., and DELAVIGNETTE, P., 1961, *J. appl. Phys.*, **31,** 2126.

AMELINCKX, S., and VOTAVA, E., 1954, *Naturwissenschaften*, **18,** 422.

COTTRELL, A. H., 1958, *Dislocations and Plastic Flow in Crystals* (Oxford : Clarendon Press), p. 51.

DELAVIGNETTE, P., and AMELINCKX, S., 1961, *Proc. of the AIME Symposium on "Direct Observations of Dislocations in Crystals"*, St. Louis (in the press).

Frank, F. C., 1949, *Disc. Faraday Soc.*, No. 5, 48 ; 1953, *Phil. Mag.*, **44**, 854.

Good, R. I., Girifalco, L., and Kraus, G., 1958, *J. Phys. Chim.*, **62**, 1418.

Nabarro, F. R. N., 1952, *Advanc. Phys.*, **1**, 269.

Pashley, D. W., and Presland, A. E. B., 1961, *Proc. of the European Regional Conf. on Electron Microscopy* (Delft 1960), p. 417.

Read, W. T., 1953, *Dislocations in Crystals* (New York: McGraw-Hill Book Co.), p. 131.

Siems, R., Delavignette, P., and Amelinckx, S., 1961, *Z. Phys.*, **165** (in the press).

## CORRESPONDENCE

### Interstitial Dislocation Loops in Magnesium Oxide

By G. W. Groves and A. Kelly
Department of Metallurgy, University of Cambridge

[Received August 14, 1961]

Long thin prismatic loops of edge dislocation have recently been observed in plastically deformed crystals of many materials examined in the electron microscope (Price 1960, Washburn *et al.* 1960, Howie 1960, Seagall 1960). The formation of these loops has not yet been explained. It is of importance in deciding between various proposed mechanisms for their formation to know whether the loops are predominantly of vacancy or interstitial type, or whether interstitial and vacancy loops occur equally frequently.

Slip bands in cold-worked magnesium oxide contain many elongated loops (Washburn *et al.*). The two sides of the loop are usually too close together for contrast experiments to be carried out, but on annealing in the temperature range 1300–1400°c for ~1 hour a few large circular loops are formed (figs. 1–4†). The total area of dislocation loop in the specimen does not alter greatly when this occurs. The loops are then convenient for contrast experiments; they are found to lie on $\{110\}$ planes at 45° to the $\{100\}$ specimen plane, with a $\langle\bar{1}10\rangle$ Burgers vector. We have determined the sense of the Burgers vector (i.e. whether the loops are interstitial or vacancy type) in some cases by observing how the electron microscope image changes as the specimen is tilted. The method is as follows.

In figs. 1–3 the reflections responsible for the images are B and C, since for A the reciprocal lattice vector and the Burgers vector of the loop are orthogonal. The Kikuchi lines associated with the reflections B and C show the position of the reciprocal lattice points for B and C with respect to the reflecting sphere (fig. 5). Thus in fig. 1, B lies below the reflecting sphere while C lies above it, and a small rotation of the reciprocal lattice down into the paper on the B–C side of (0, 0, 0) would enhance reflection C and diminish reflection B.

Figure 6 shows the four possible configurations for the loop, together with the lattice rotations produced. Remembering that the dislocation image occurs on that side of the dislocation where Bragg reflection is enhanced (Hirsch *et al.* 1960) it is seen from figs. 2 and 3 that only

---

† Figures 1–4 are shown as plates.

Fig. 5

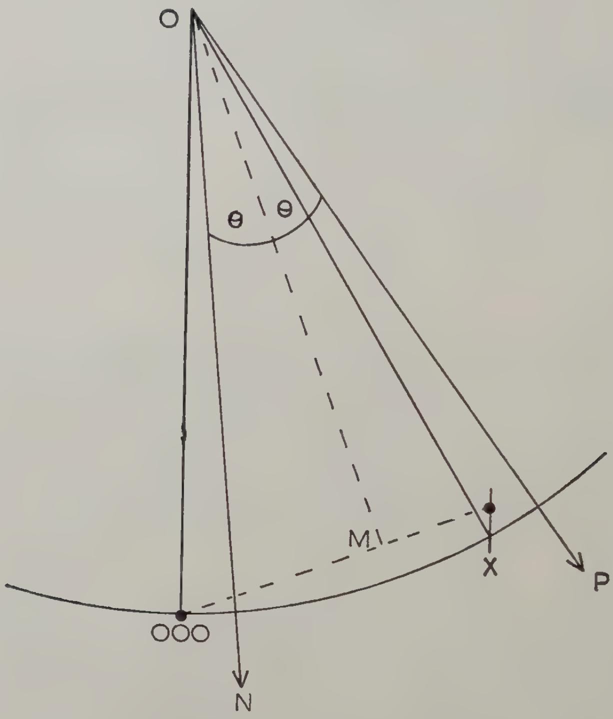

Reciprocal lattice and reflecting sphere construction, showing formation of Kikuchi lines. OX represents the diffracted beam. The background intensity is increased in direction OP, reduced in direction ON due to reflection in the plane OM at Bragg angle $\theta$.

Fig. 6

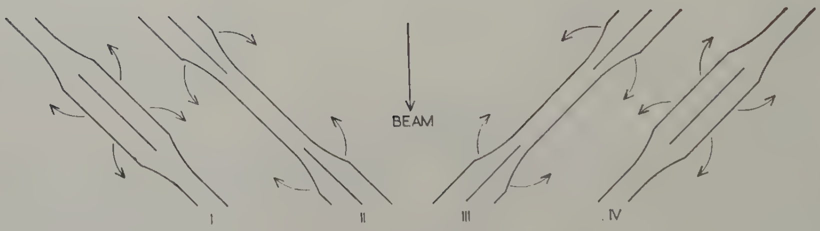

Possible configurations for the loop shown in figs. 1–4, with lattice rotations marked by arrows.

configurations (i) and (iii) are possible. To distinguish between these two possibilities the specimen is mounted on a wedge-shaped holder which when inverted holds the specimen at an angle to the beam of about 45°, the axis of tilt being made to lie approximately in the plane of the loop (fig. 7). Figure 4 shows the tilted view which eliminates configuration (iii). The loop is therefore of interstitial type.

Fig. 7

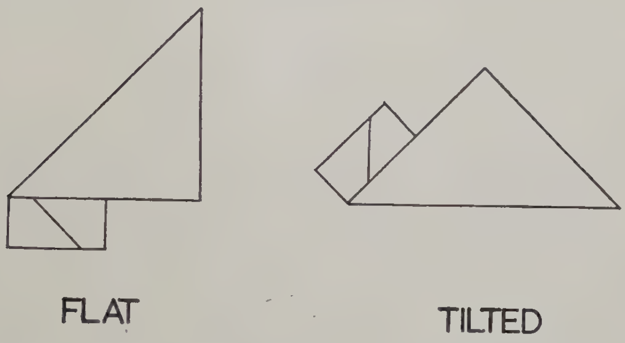

Specimen holder, showing how specimen is tilted when holder is inverted.

The same result has been obtained for six other loops from three different specimens, which were deformed by bending back and forth for 100 cycles to a maximum strain ± 0·1 %, and then annealed in the temperature range 1300–1400°C. During deformation slip occurred only on two orthogonal systems. It is concluded that most or all of the loops produced by this deformation and anneal are of interstitial type. A natural explanation is that there is an excess of interstitial point defects or loops in the cold-worked state produced by the intersection of orthogonal screw dislocations which are driven towards one another by the applied stress (Cottrell 1957).

## REFERENCES

COTTRELL, A. H., 1957, *Dislocations and Mechanical Properties of Crystals* (New York : Wiley), p. 509.
HIRSCH, P. B., HOWIE, A., and WHELAN, M. J., 1960, *Phil. Trans.* A, **252,** 499.
HOWIE, A., 1960, Ph.D. Thesis, Cambridge.
PRICE, P. B., 1960, *Phil. Mag.*, **5,** 873.
SEAGALL, R. L., 1960, Ph.D. Thesis, Cambridge.
WASHBURN, J., GROVES, G. W., KELLY, A., and WILLIAMSON, G. K., 1960, *Phil. Mag.*, **5,** 991.

# On the Temperature Dependence of Critical Resolved Shear Stress of an Al–4% Cu Alloy

By K. MATSUURA and S. KODA
The Research Institute for Iron, Steel and Other Metals, Tohoku University, Sendai, Japan

[Received July 7, 1961]

THE increase of hardening during ageing in an aluminium–4% copper alloy may be associated with the kind of decomposition products, that is with the presence of G–P(1), G–P(2), $\theta'$ or $\theta$ phases, as well as with the size and distribution of these phases in the matrix (Silcock *et al.* 1954). The alloy containing G–P(1) and G–P(2) zones can harden by two mechanisms. One of these is due to the increase of internal strain which offers an effective resistance to the movement of dislocations. This is the mechanism of age-hardening originally proposed by Mott and Nabarro (1940). The other is due to the increase of surface energy of G–P zones after they have been cut through by moving dislocations. This was proposed by Kelly and Fine (1957) and named chemical hardening. In the alloy containing $\theta'$ and $\theta$ precipitates internal strain is not important, but the critical shear stress is determined by the difficulty with which dislocations by-pass between the precipitates or cut through them. In the present investigation the temperature dependence of critical resolved shear stress was examined in order to separate the hardening mechanisms associated with the different products of decomposition.

Table 1. Ageing treatments and decomposition products

| Ageing treatments | Just after air-cooling | 12 hr–1 day at 130°c | 11–20 days at 130°c | 2 days at 240°c |
|---|---|---|---|---|
| Decomposition products | Super-saturated solid solution | G–P(1) zone | G–P(2) zone +a little $\theta'$ | $\theta'$ phase |

The specimens were air-cooled after solution-treatment at 530°c, and then subjected to the various ageing treatments indicated in table 1. The table also shows the kinds of decomposition product present after these treatments as inferred from the changes in hardness estimated on the basis of the x-ray data of Silcock *et al.* (1954).

Four or five single crystals of the same orientation were prepared for each stage of ageing. These were tested in tension in the temperature range from −195°C to room temperature. The results are shown in the figure.

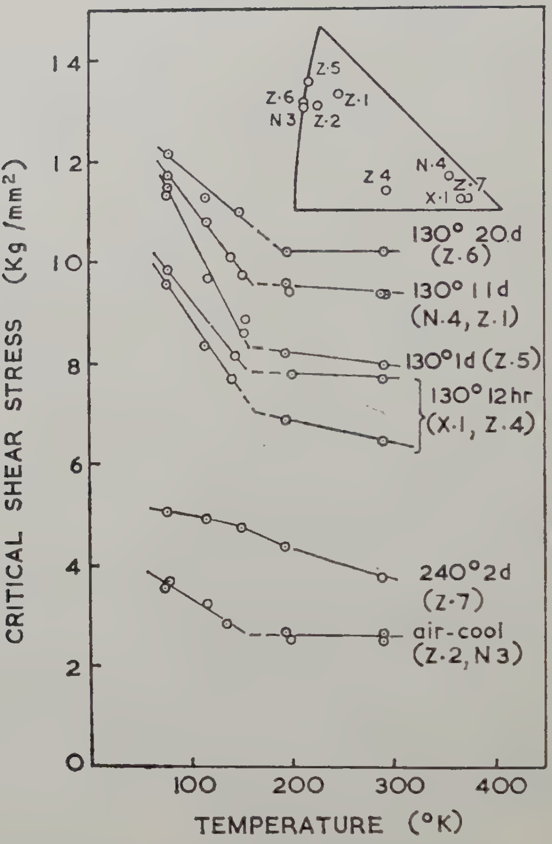

Temperature dependence of critical resolved shear stress.

The temperature dependence is greatest when G–P(1) zones are present, and the critical shear stress increases markedly below 160°K. This tendency is less in the state of ageing producing the $\theta'$ phase.

The temperature dependence of the critical shear stress in each stage of ageing except that of the $\theta'$ phase can be formally expressed by Seeger's equation (Seeger 1954, 1957), giving the critical shear stress

$$\tau = \tau_0 + \tau(T) \quad . \quad . \quad . \quad . \quad . \quad . \quad . \quad . \quad (1)$$

where $\tau(T) = (U_0 - \alpha kT)/V$ for $T \leqslant U_0/\alpha k$ or $\tau(T) = 0$ for $T > U_0/\alpha k$.

$U_0$ is an activation energy, $V$ an activation volume and $\alpha$ is a numerical constant having a value of about 25. The values of $U_0$ and $V$ obtained from the figure by this kind of analysis are shown in table 2 as $U_{0e}$ and $V_e$.

Kelly and Chiou (1958) found that the critical shear stress for the alloy containing G–P(1) zones increased markedly at low temperatures, while the temperature dependence was small in the alloy containing G–P(2) zones. They ascribed the increase of critical shear stress at low temperature to the chemical hardening. Therefore it seems desirable to examine the temperature dependence of chemical hardening following Seeger's treatment.

In this case two kinds of activation process may be considered:

(i) A process in which a dislocation completely cuts through a G–P zone. Then

$$V=Ll\mathbf{b}, \qquad (2)$$

$$U_0=\Delta E l d f/2\mathbf{b}^2, \qquad (3)$$

where $L$ is the distance between G–P zones, $l$ and $d$ are respectively length and width of the cross section of a G–P zone intersected by the slip plane, $f$ is the fraction of copper atoms in a G–P zone, $\Delta E$ is the difference in energy for a copper atom in a G–P zone and one in the matrix, and $\mathbf{b}$ is the Burgers vector of the dislocation.

(ii) The other is a process in which a dislocation cuts into the edge of a G–P zone by only one Burgers vector. Then

$$V=L\mathbf{b}^2, \qquad (4)$$

$$U_0=\Delta E d f/2\mathbf{b}. \qquad (5)$$

Putting into each equation the values:

$\Delta E=0{\cdot}08$ ev (following Suzuki 1949), or $0{\cdot}24$ ev (according to Beton and Rollason 1957),
$l=100$ Å,
$L=150$ Å, and
$fd/\mathbf{b}\simeq 1$ for G–P(1) zones, and
$\Delta E=0{\cdot}31$ ev (Beton and Rollason 1957),
$l=300$ Å,
$L=350$ Å, and
$fd/\mathbf{b}=3$ for G–P(2) zones,

the values of $U_0$ and $V$ may be calculated for the two cases. The results of these calculations are shown in table 2, where subscripts 1 and 2 are used respectively for the two kinds of processes (i) and (ii).

It can be seen from the table that the calculated values for the case (ii) are in agreement with the experimental values, at least in order of magnitude, while those for case (i) differ widely. Therefore it may be concluded that the elementary process by which a dislocation cuts a G–P zone is that described as case (ii).

However, the calculated value for $\tau(T)_{T=0}$, i.e. $U_0/V$, is smaller by a factor of 2 or 3 than the experimental value in the stage of ageing where G–P(1) zones are predominant. The difference may be ascribed to an uncertainty in the value of $\Delta E$, which is taken from the reversion heats, and that of $V$, which is affected by the preferential nucleation of G–P zones on dislocations. It may also be due to the effect of other forms of solute hardening such as the atmosphere locking of dislocations proposed by Cottrell, which are ignored in the analysis given here.

Table 2. Experimental and calculated values of $U_0$ and $V$

| | 12 hr at 130°c G–P(1) zone | 1 day at 130°c G–P(1) zone | 11 days at 130°c G–P(2) zone | 20 days at 130°c G–P(2) + a little $\theta'$ |
|---|---|---|---|---|
| $U_{0e}$ ev | 0·35 | 0·35 | 0·35 | 0·42 |
| $V_e$ cm$^3$ | $1{\cdot}5\times10^{-21}$ | $1{\cdot}0\times10^{-21}$ | $1{\cdot}5\times10^{-21}$ | $2{\cdot}1\times10^{-21}$ |
| $U_{01}$ ev | 1·4∼4·3 | | 52 | |
| $U_{02}$ ev | 0·04∼0·12 | | 0·46 | |
| $V_1$ cm$^3$ | $4{\cdot}2\times10^{-20}$ | | $2{\cdot}9\times10^{-19}$ | |
| $V_2$ cm$^3$ | $1{\cdot}2\times10^{-21}$ | | $2{\cdot}7\times10^{-21}$ | |

The slight temperature dependence of critical resolved shear stress found for the $\theta'$ phase is to be expected because of the large activation energy required for a dislocation to cut through this phase by any process.

## REFERENCES

BETON, R. H., and ROLLASON, E. C., 1957, *J. Inst. Met.*, **86,** 85.
KELLY, A., and CHIOU, C., 1958, *Acta Met.*, **6,** 565.
KELLY, A., and FINE, M. E., 1957, *Acta Met.*, **5,** 365.
MOTT, N. F., and NABARRO, F. R. N., 1940, *Proc. phys. Soc., Lond.*, **52,** 86.
SEEGER, A., 1954, *Z. Naturforsch.*, A, **9,** 870; 1957, *Dislocations and Mechanical Properties of Crystals* (John Wiley and Sons), p. 243.
SILCOCK, J. M., HEAL, T. J., and HARDY, H. K., 1954, *J. Inst. Met.*, **82,** 239.
SUZUKI, T., 1949, *Sci. Rep. Res. Insts Tohoku Univ.*, A, **1,** 183.

# OBITUARY

## Professor A. M. Tyndall

Professor Tyndall, who was from 1948 to 1961 a member of the Editorial Board of the *Philosophical Magazine*, died at his home at Bristol on October 29, 1961. He will be remembered for his work for the University of Bristol and particularly for the Department of Physics there, which he built from the smallest beginnings. As editor of the *Philosophical Magazine* I was most fortunate in being able to secure his help, since his retirement, with the task of refereeing and editing papers, in which he was active up till the week of his death. He will be greatly missed by all connected with the Magazine and with the firm of Taylor & Francis.

N. F. M.

# BOOK NOTICES

*Special Relativity.* By W. Rindler. (Edinburgh and London: Oliver & Boyd, 1960.) [Pp. 186.] Price 10*s.* 6*d.*

*The Birth of a New Physics.* By I. Bernard Cohen. The Science Study Series. (London: Heinemann, 1961.) [Pp. 200.] Price 5*s.*

1960 *Nuclear Data Tables*, Part 3. By J. B. Marion. (Washington: National Academy of Sciences; National Research Council, 1960.) For sale by the Superintendent of Documents, U.S. Government Printing Office, Washington 25, D.C. [Pp. 181.] Price $1.25.

*Introduction to Astronomy.* By C. Payne-Gaposchkin. University Paperback edition. (London: Methuen & Co., 1961.) [Pp. 508.] Price 16*s.*

*Mathematics of Engineering Systems.* By D. F. Lawden. University Paperback edition. (London: Methuen & Co., 1961.) [Pp. 404.] Price 12*s.* 6*d.*

*Advances in Electronics and Electron Physics*, Vol. XIII. Edited by L. Marton. (New York and London: Academic Press, 1960.) [Pp. 454.] Price $13.50.

*The Special Theory of Relativity.* By Herbert Dingle. (London: Methuen & Co., 1961.) [Pp. 94.] Price 8*s.* 6*d.*

*Reactors of the World.* Second Series. (London: Temple Press, 1961.) Published in association with *Nuclear Engineering.* 13 cutaway drawings reprinted from *Nuclear Engineering.* Price 17*s.* 6*d.*

*An Introduction to the Laplace Transformation.* By J. C. Jaeger. (London: Methuen & Co., 1961.) [Pp. 156.] Price 10*s.* 6*d.*

*Scientific Russian:* A Textbook for Classes and Self-Study. Second Edition. By James W. Perry. (New York: Interscience Publishers, 1961.) [Pp. 565.] Price £3 12*s.* 0*d.*

*Numerical Methods of Curve Fitting.* By P. G. Guest. (Cambridge: University Press, 1961.) [Pp. 422.] Price £4 0*s*, 0*d.*

*Physics and Archaeology.* By M. J. AITKEN. (New York: Interscience Publishers, 1961.) [Pp. 181.] Price £2 3*s*. 0*d*.

*Tables Relating to Radiation Emerging from a Planetary Atmosphere with Rayleigh Scattering.* By KINSELL L. COULSON, JITENDRA V. DAVE and ZDENEK SEKERA. (California University Press, 1960.) London agents ; Cambridge University Press. [Pp. 548.] £5 16*s*. 0*d*.

*Proceedings of the* 1960 *Annual International Conference on High Energy Physics at Rochester*, August 25–September 1, 1960. Edited by E. C. G. SUDARSHAN, J. H. TINLOT and A. C. MELISSINOS. (New York and London ; Interscience Publishers, Inc., 1960.) [Pp. 890.] $13.50.

*Annual Review of Nuclear Science*, Vol. 10. Edited by E. SEGRÈ. Assistant editors ; G. Friedlander and W. E. Meyerhof. (California ; Annual Reviews, Inc., 1960.) [Pp. 617.] $7.50.

*Space Trajectories :* A symposium sponsored by the American Astronautical Society, The Advanced Research Projects Agency, and Radiation Incorporated. By T. C. HELVEY (Chairman of the Symposium). Edited by the Technical Staff of Radiation Incorporated. (New York and London ; Academic Press, 1960.) [Pp. 298.] £4 6*s*. 0*d*.

*A Dictionary of Named Effects and Laws.* By D. W. G. BALLENTYNE and L. E. Q. WALKER. (Chapman and Hall, 1961.) [Pp. 234.] 30*s*.

*Discourse on Bodies in Water.* By GALILEO GALILEI. Translation by Thomas Salusbury. Introduction and Notes by Stillman Drake. (Urbana ; University of Illinois Press, 1960.) [Pp. 89.] $5.00.

*Lectures on Differential and Integral Equations.* By KÔSAKU YOSIDA. Series *Pure and Applied Mathematics*, Vol. X (New York ; Interscience Publishers, 1960.) [Pp. 220.] £2 13*s*. 0*d*.

*Some Ionospheric Results obtained during the International Geophysical Year.* Proceedings of a symposium organized by the URSI/AGI Committee, Brussels, 1959. Edited by W. J. G. BEYNON. (Amsterdam ; Elsevier Publishing Company, 1961.) [Pp. 399.] £3 12*s*. 0*d*.

---

[*The Editors do not hold themselves responsible for the views expressed by their correspondents.*]

Fig. 1

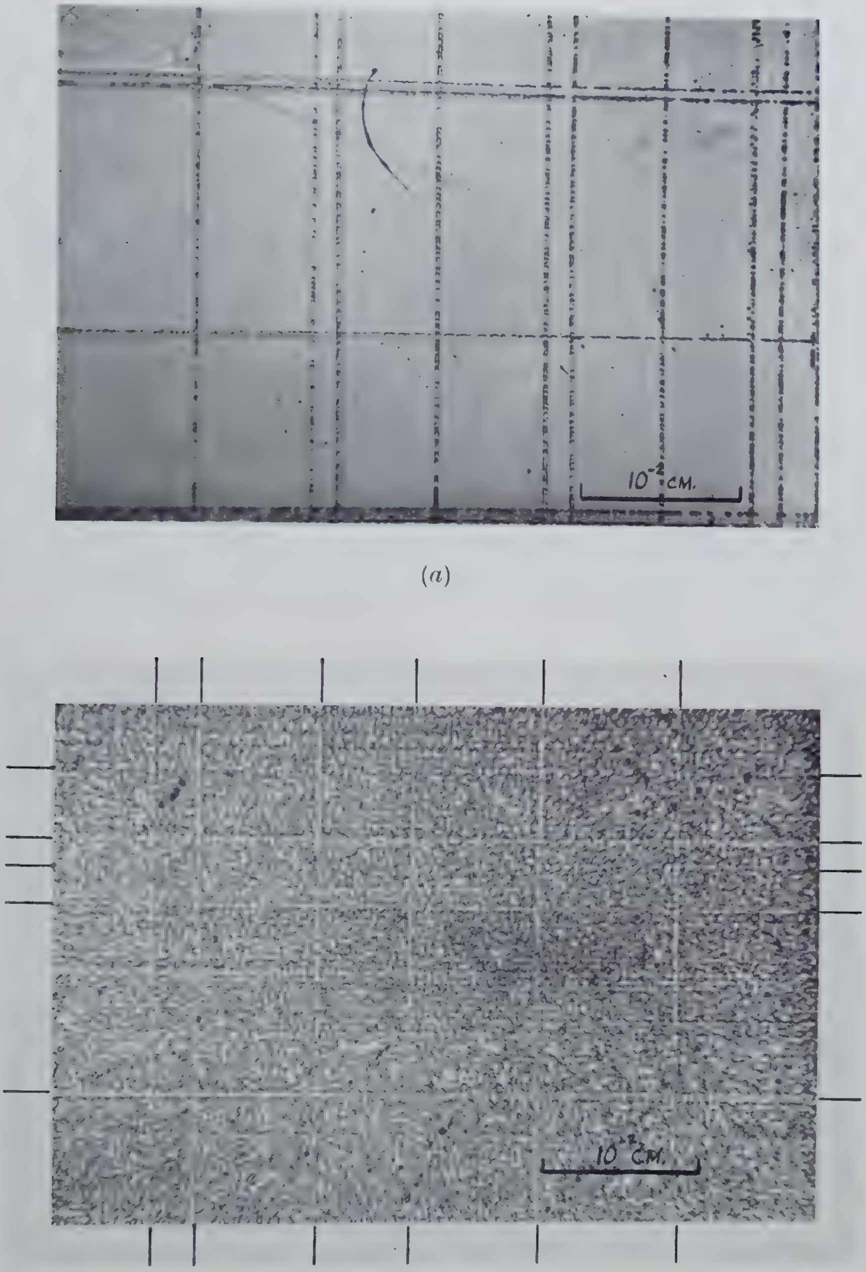

(b)

(*a*) Slip on $\{110\}_{45}$ planes in a polished crystal. $S=-0{\cdot}6$. (*b*) Slip on $\{110\}_{45}$ planes in a polished crystal. $S=+16$. N.B. The sides of all photographs are cut parallel to $\langle 100\rangle$.

Fig. 2

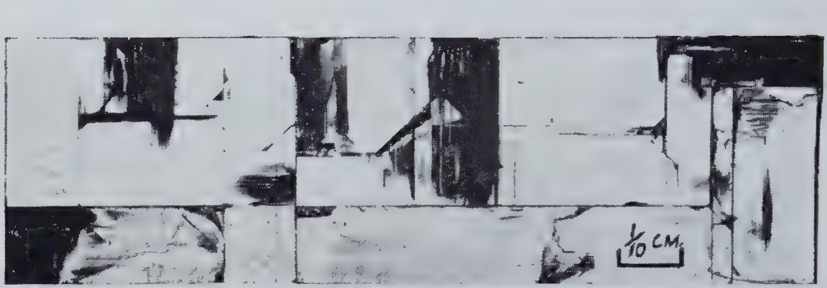

Crack pattern in an as-cleaved and quenched crystal $S=0{\cdot}8$.

Fig. 4

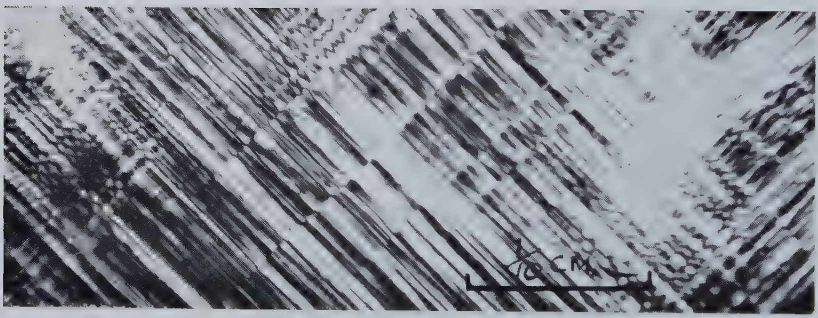

(*a*)

Fig. 4 (*continued*)

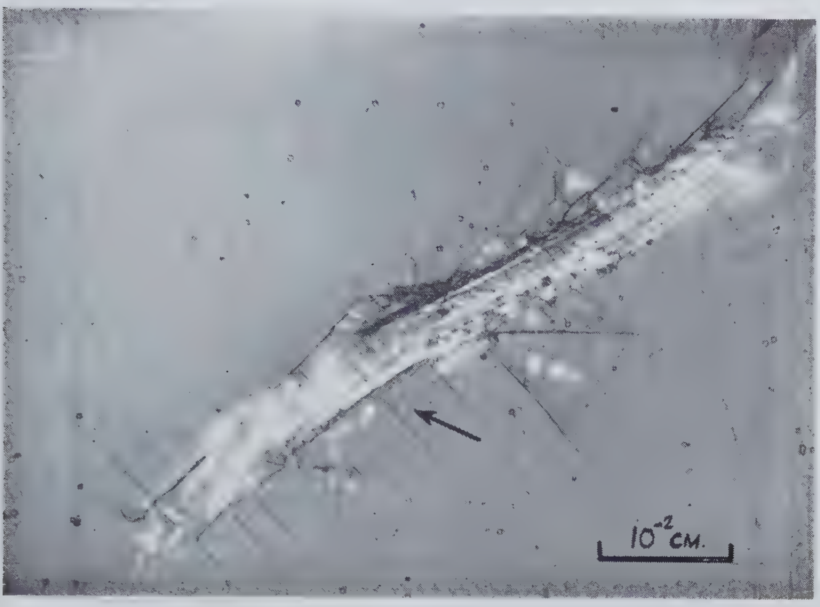

(*b*)

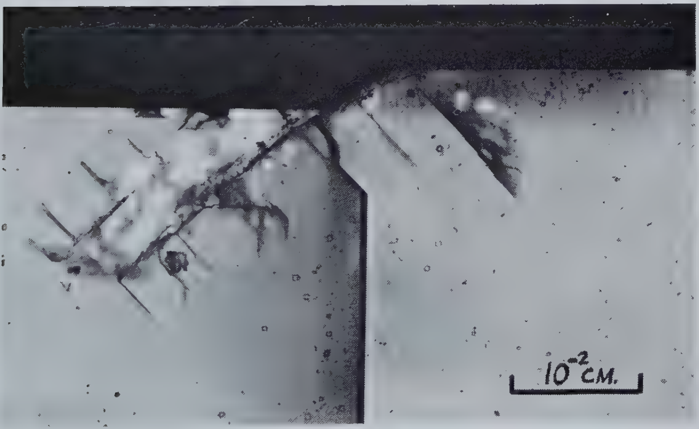

(*c*)

(*a*) Birefringence in a heavily shocked crystal $S=15{\cdot}5$. (*b*) Light scratch made on surface of crystal shown in (*a*). (*c*) One side of scratch after fracture showing crack origin.

Fig. 6

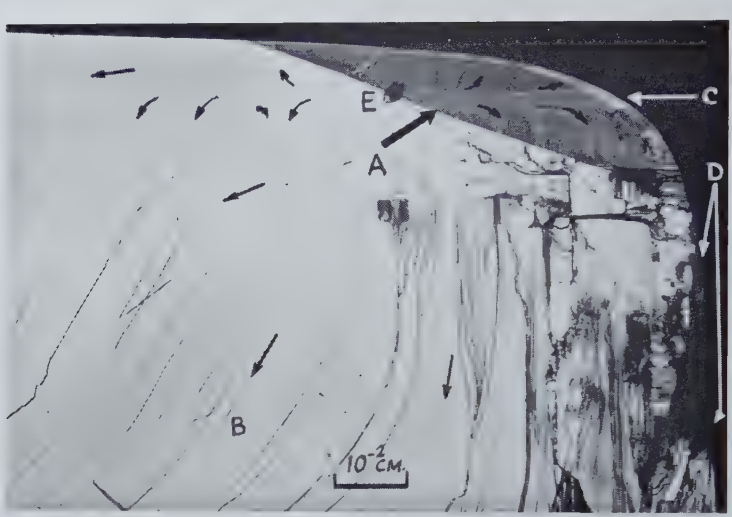

Part of the fracture face of a bi-crystal containing the crack origin which is at the intercrystalline boundary (arrowed A). Unlettered arrows indicate crack propagation directions. E marks the crack origin (the defect on the boundary at E is a speck of dust and should be disregarded).

Fig. 7

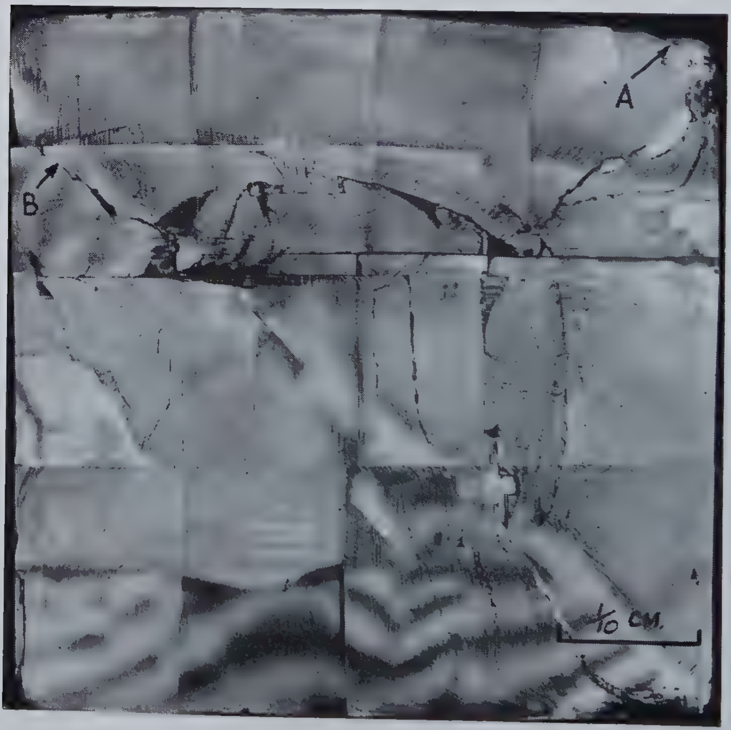

(*a*)

Fig. 7 (*continued*)

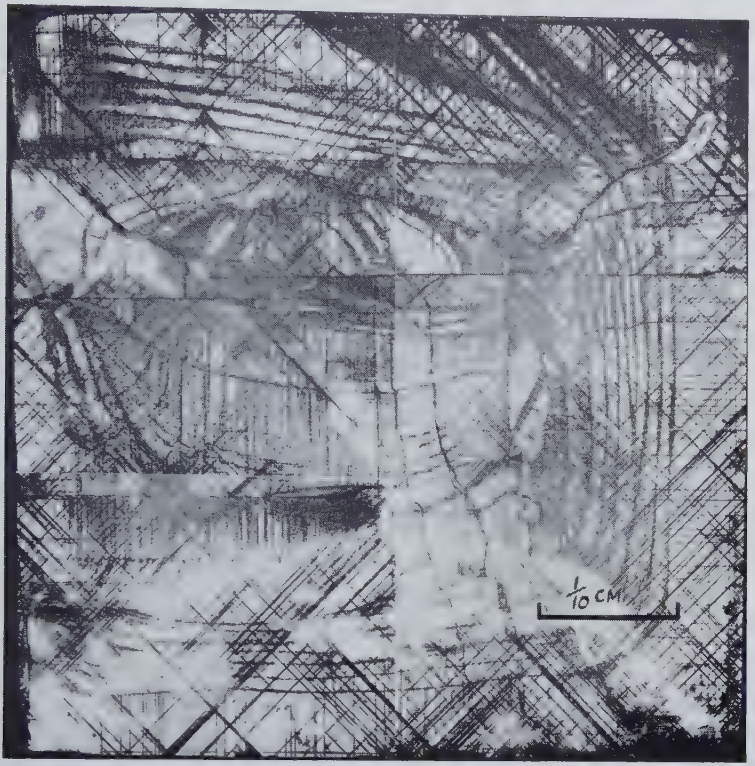

(*b*)

(*a*) Whole of a crack plane separating a crystal into two. The boundary of fig. 6 is arrowed. (*b*) Same view as 7 (*a*) but etched.

Fig. 8

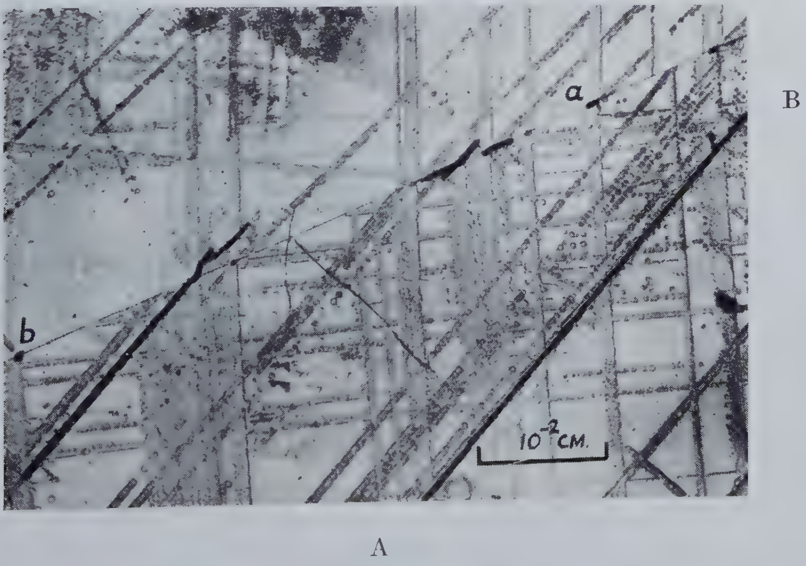

Cracks occurring at an intercrystalline boundary and caused by thermal shock $S=4{\cdot}5$.

Fig. 9

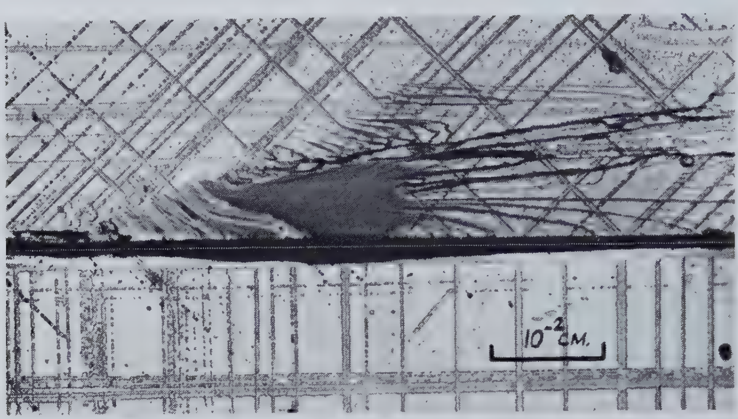
Crack face

Side face

Typical detail of type arrowed D in fig. 6. Photographs of adjacent faces are laid out side by side. This structure occurs where a moving crack front meets an edge.

Fig. 10

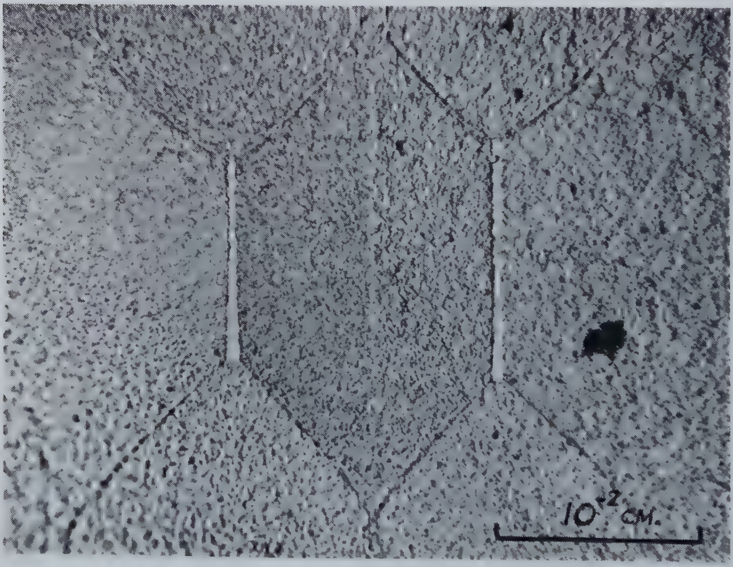

Etched surface of a repeatedly shocked crystal. 1250 shocks at $S=0{\cdot}95$/cycle. Note the unslipped blocks, and ‘ traces ’ extending from the corners of the blocks.

Fig. 11

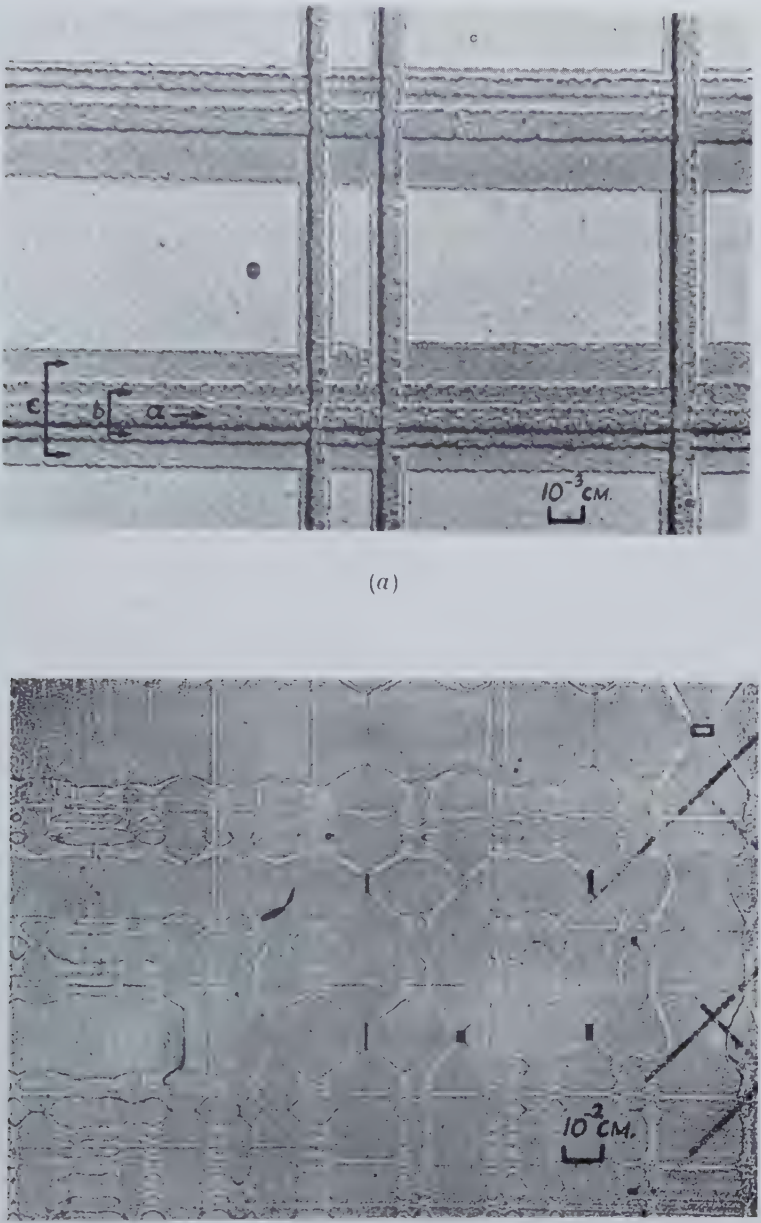

(a)

(b)

(a) Polished crystal which has been etched after 1, 10 and $\simeq 50$ shocks at $S = 1{\cdot}0$. Arrows: *a*, band width caused by 1 shock, *b*, band width caused by 10 shocks, *c*, band width caused by 50 shocks. (b) Patterns left by the blocks and traces in a repeatedly shocked crystal.

Fig. 1

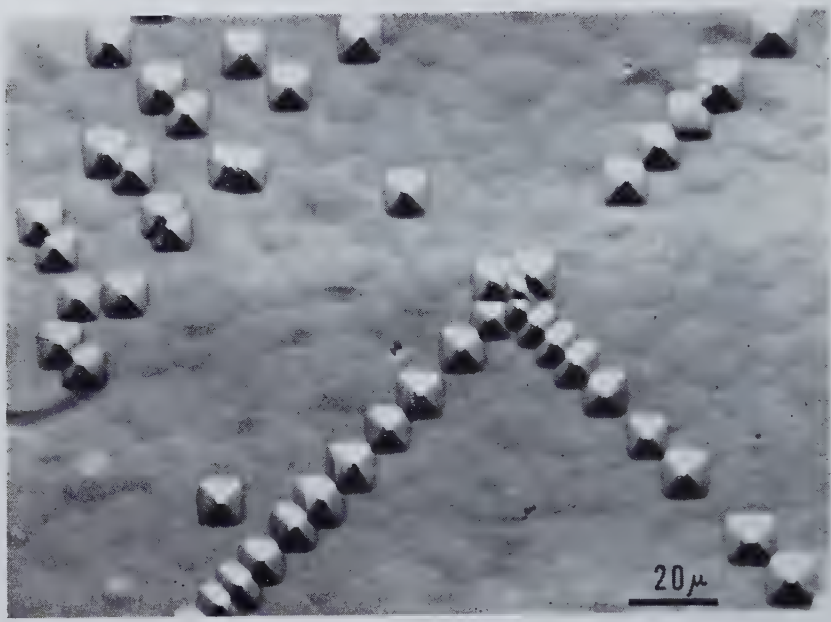

Etch pits produced in $10^{-4}$ N. caprylic acid.

Fig. 2

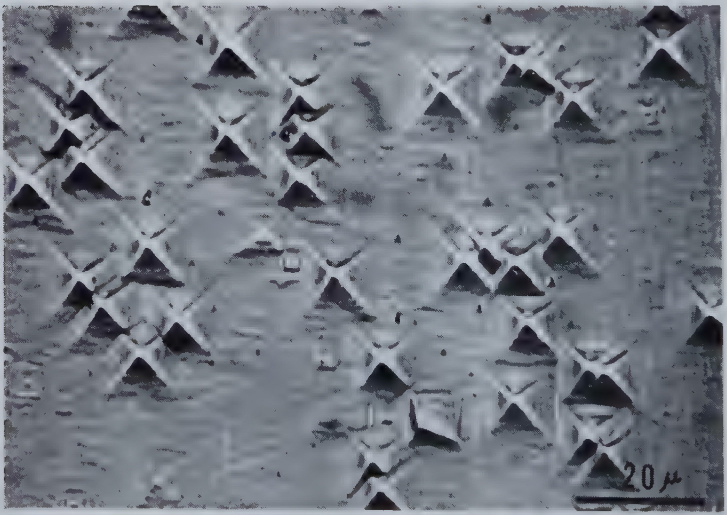

Etch pits produced in $1{\cdot}2 \times 10^{-3}$ N pentadecafluoro-octanoic acid.

Fig. 3

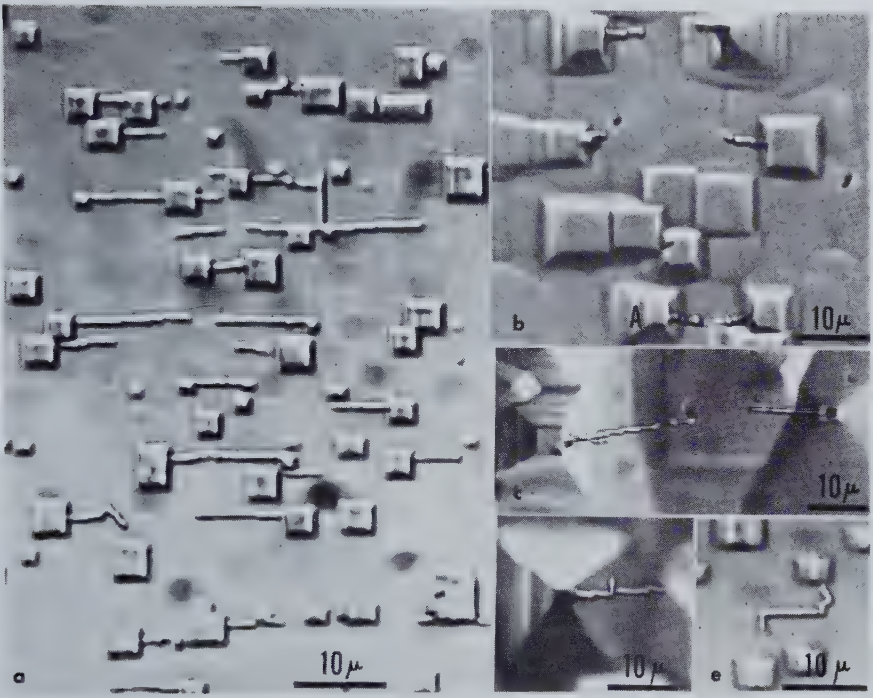

Tracks of cross-gliding screw dislocations revealed by stearic acid and myristic acid etchants.

Fig. 1

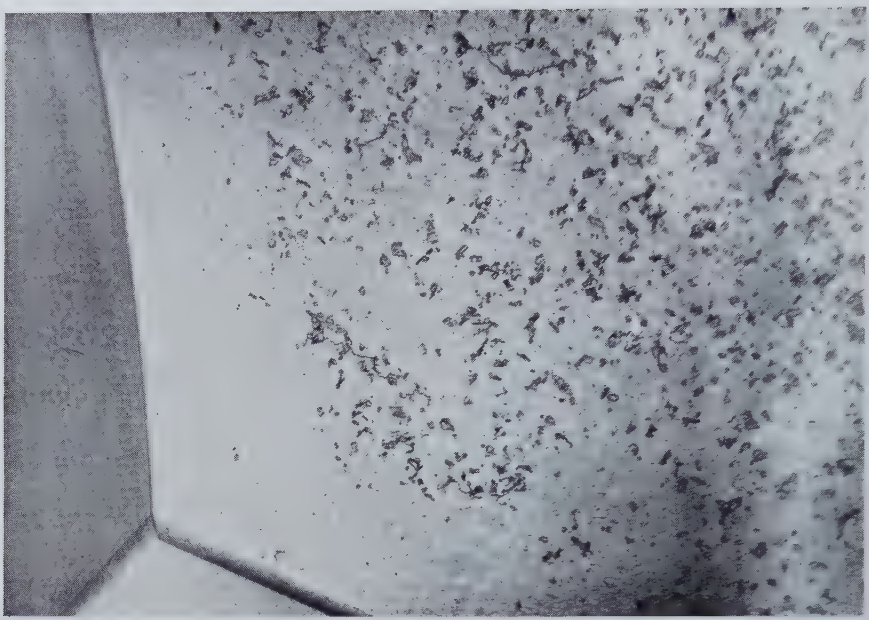

Thin film from copper through which $2{\cdot}8\times10^{17}$ alpha-particles $\mathrm{cm}^{-2}$ have passed, and then annealed for 1 hour at 325°c. The vertical grain boundary has moved to the right during the anneal and swept the small dots lying in its path showing that the dots did not form during observation. ×19 000.

Fig. 2

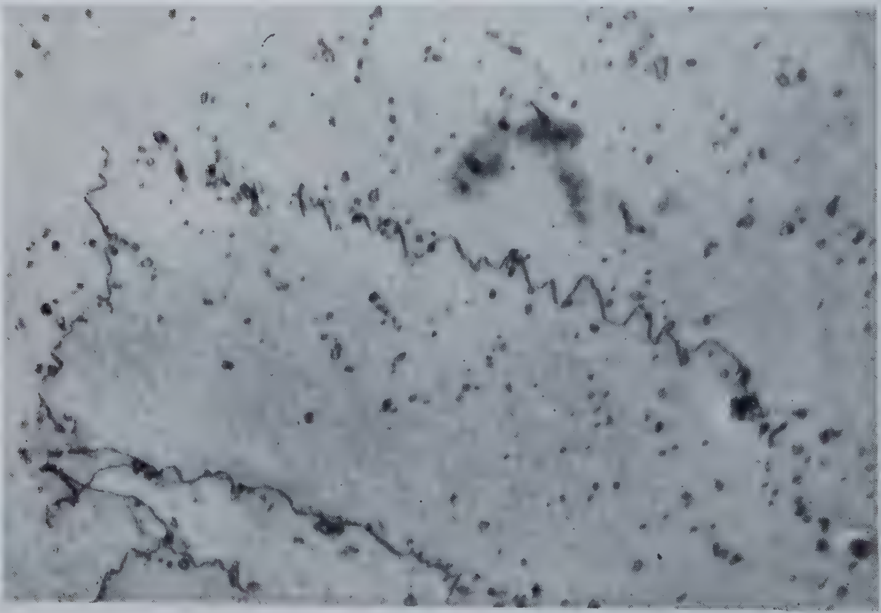

Distorted dislocation lines in copper after bombardment with alpha-particles. Some of the lines appear as irregular helices. ×45 000.

Fig. 2

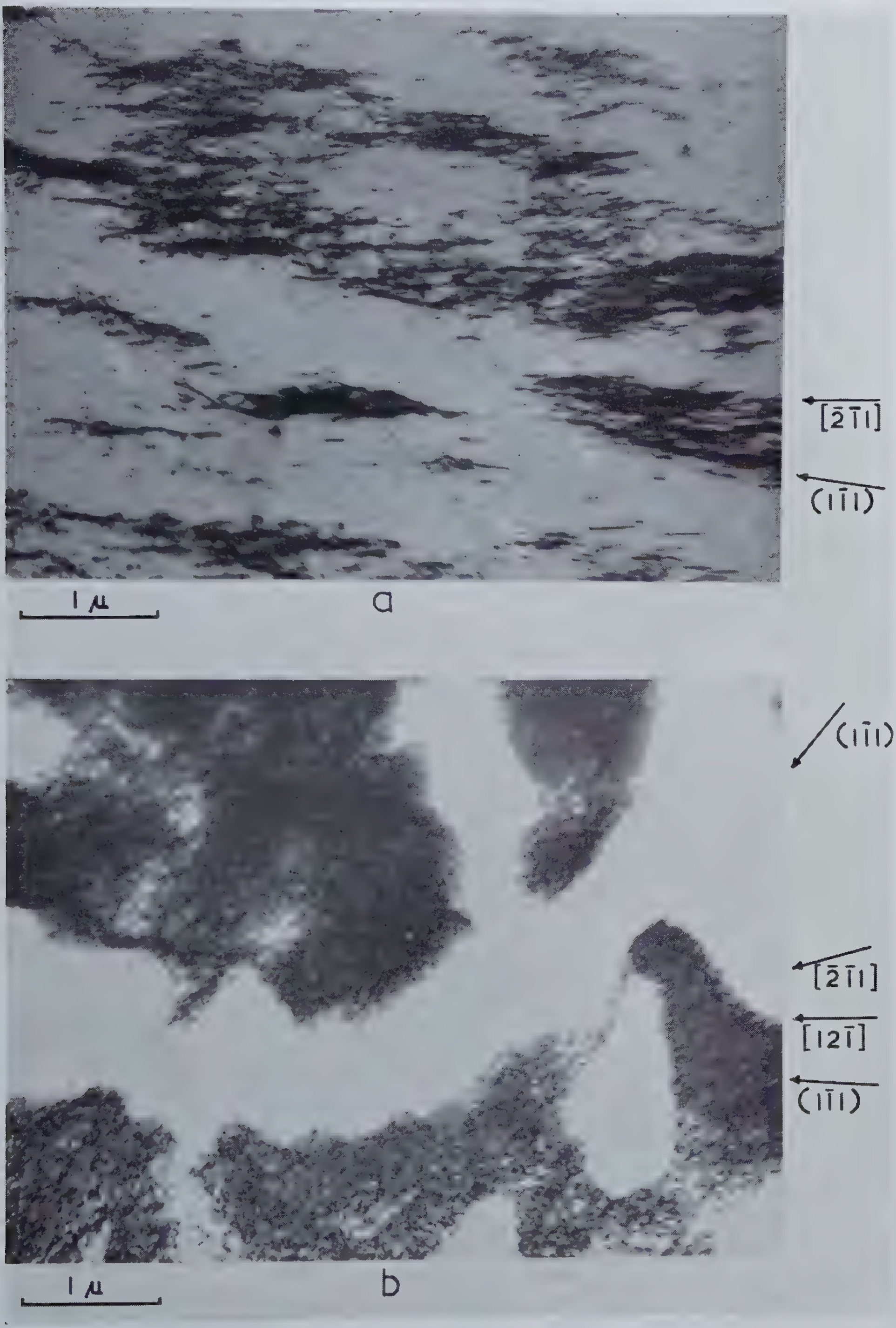

Dislocation arrangements in copper single crystals fatigued for $5 \times 10^4$ cycles. The arrows indicate the trace of the active slip plane, and the projection in the foil plane of the ⟨211⟩ direction in the slip plane and normal to the Burgers vector. (*a*) Crystal 3, oriented for single slip. ×20 000. (*b*) Crystal 4, oriented for double slip. ×20 000.

Fig. 3

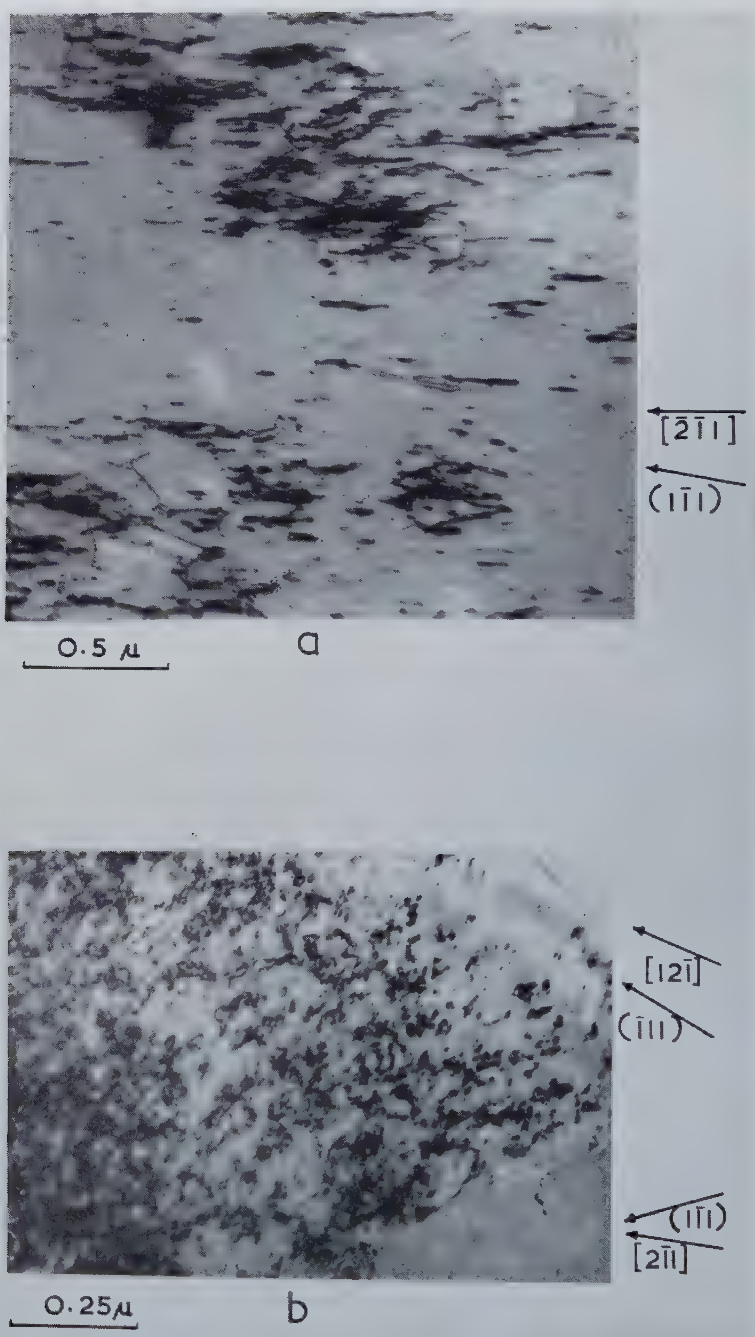

High magnification picture of areas similar to those shown in fig. 2, the dislocations can be resolved as dislocation loops. (*a*) Crystal 3, oriented for single slip. ×40 000. (*b*) Crystal 4, oriented for double slip. ×70 000.

Fig. 4

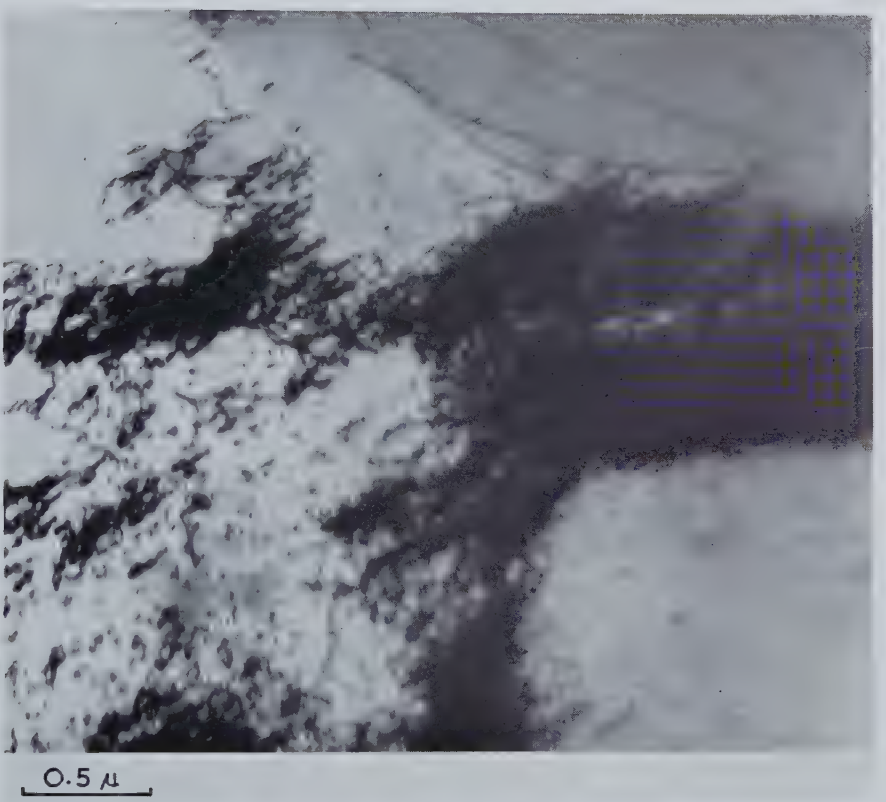

Typical region of nickel polycrystal after $10^6$ cycles of fatigue, an estimated 50% of the fatigue life. ×35 000.

Fig. 5

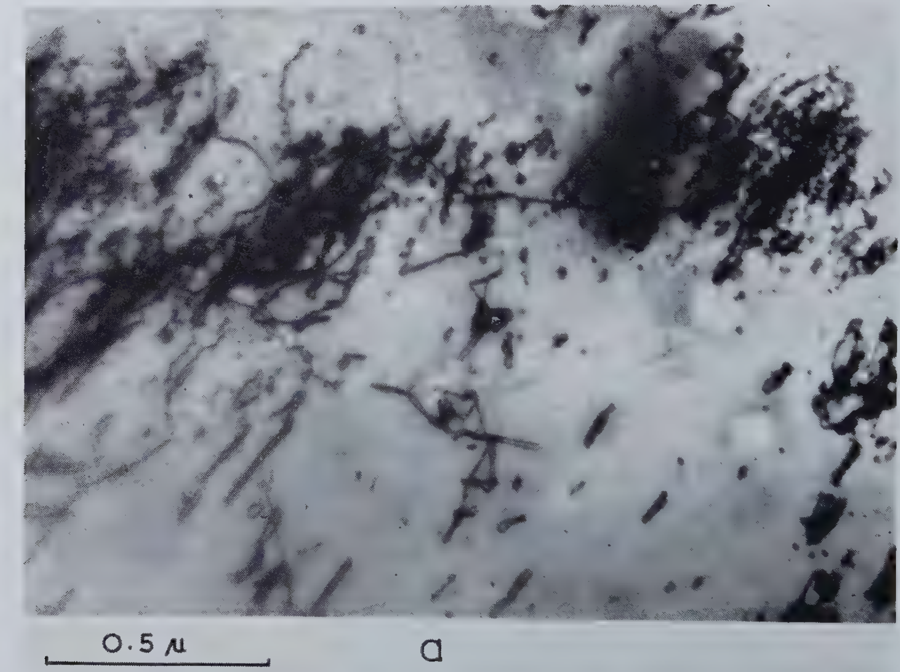

(*a*) Nickel polycrystal showing elongated dislocation loops after fatigue. ×60 000.

(*b*) Narrow elongated dislocation loops in polycrystalline copper, fatigued for $1{\cdot}6 \times 10^6$ cycles. ×35 000.

(*c*) Fatigued polycrystalline copper after $1{\cdot}6 \times 10^6$ cycles, showing numerous small dislocation loops and smaller black dots, too small to resolve as loops. ×30 000.

(*d*) Dislocation loops in fatigued polycrystalline gold after $10^6$ cycles, aged at 250°c for one hour after fatigue. ×90 000.

(*e*) Elongated dislocation loops in stainless steel, failed in $5 \times 10^4$ cycles. ×35 000.

Fig. 5 (*continued*)

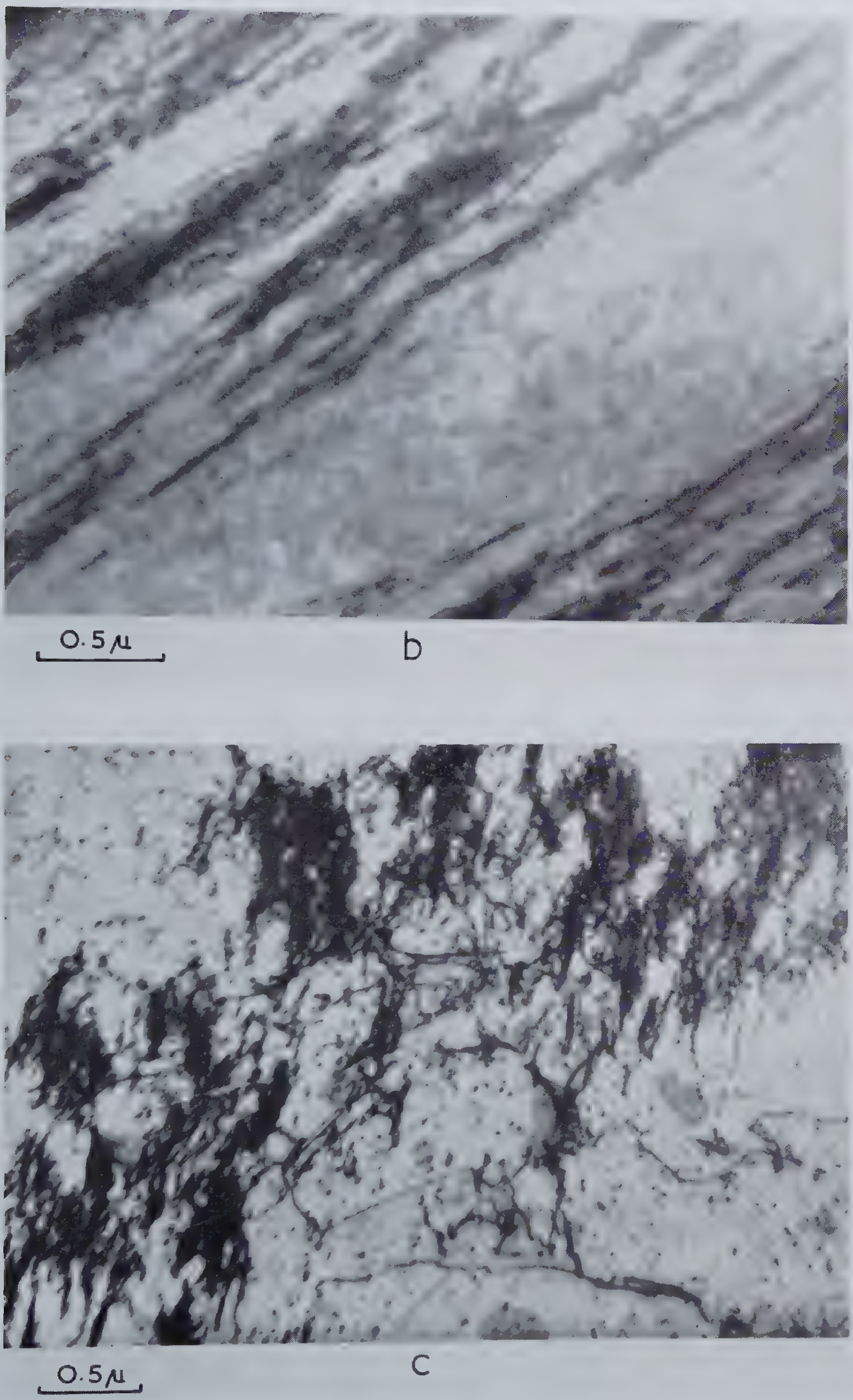

Fig. 5 (*continued*)

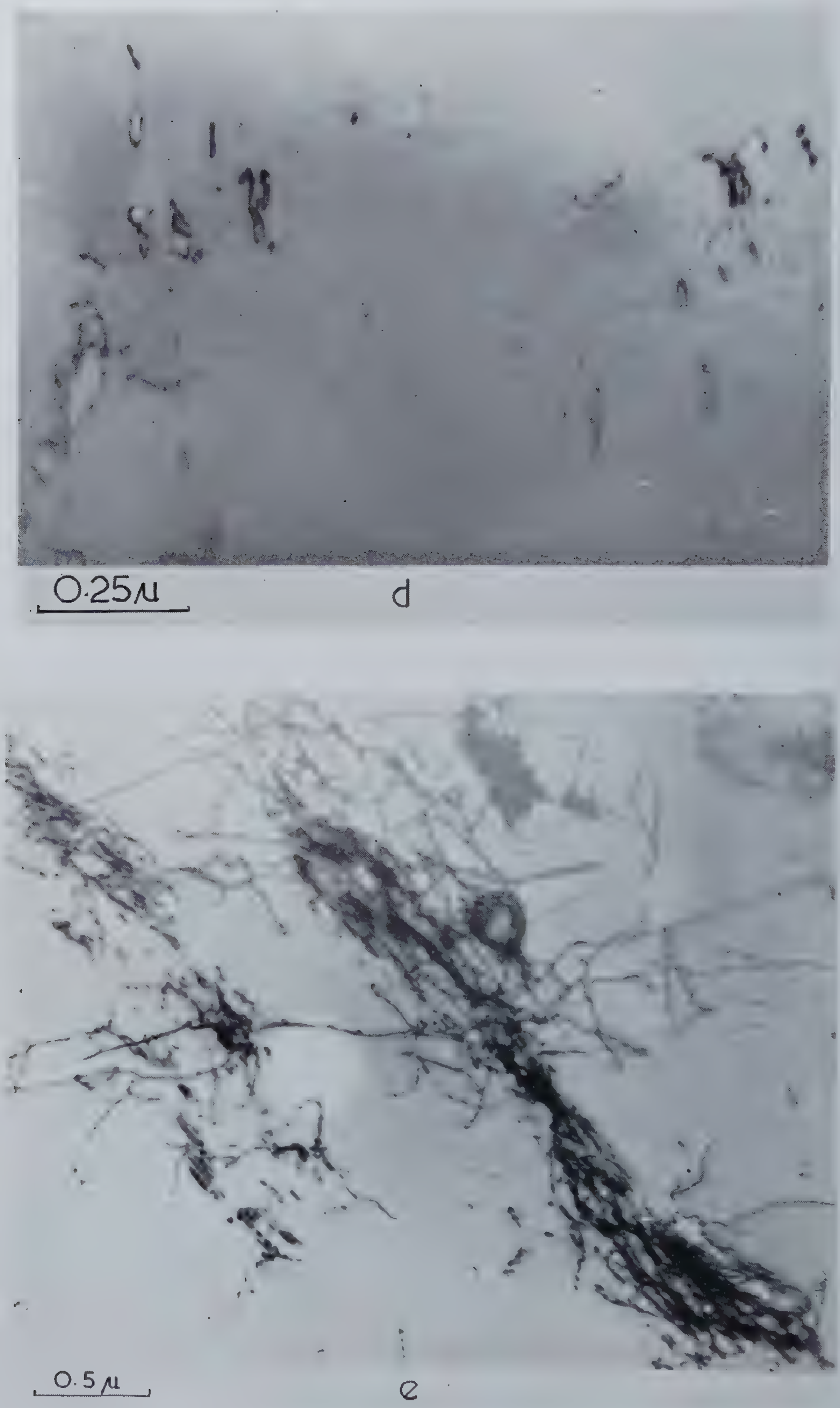

Fig. 7

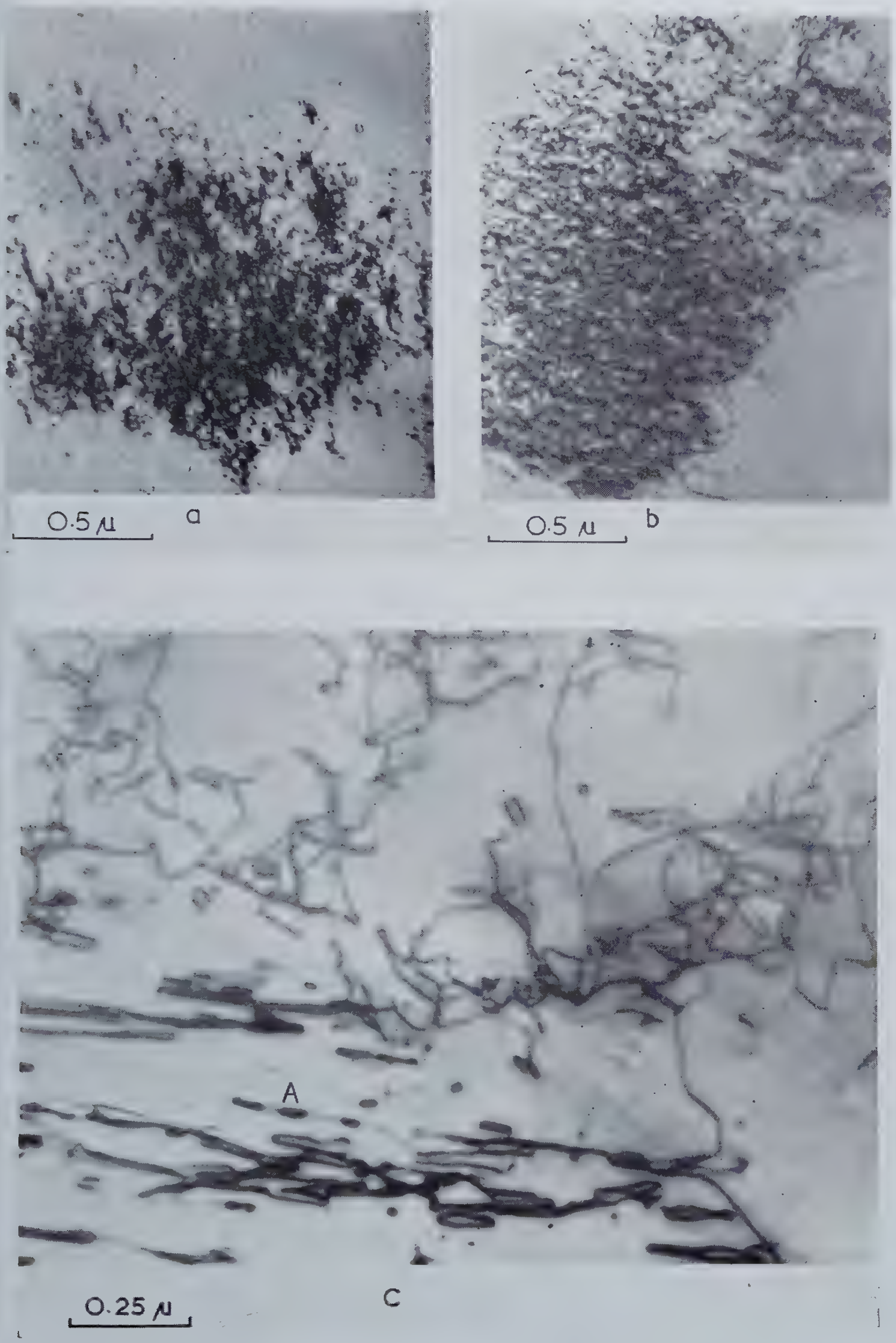

Dislocation distribution in polycrystalline nickel after $1\cdot6\times10^6$ cycles of fatigue and subsequent annealing in bulk.

(*a*) Annealed 15 min at 350°c. ×40 000.
(*b*) Annealed 15 min at 450°c. ×40 000.
(*c*) Annealed 15 min at 500°c. Note the 'pinching' effect at A. ×70 000.

Fig. 9

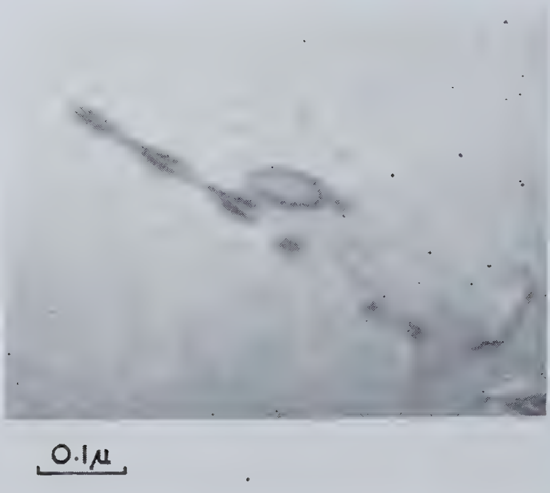

Clear example of ‘pinching’ in nickel. annealed for 15 min at 500°c after fatigue. ×120 000.

Fig. 12

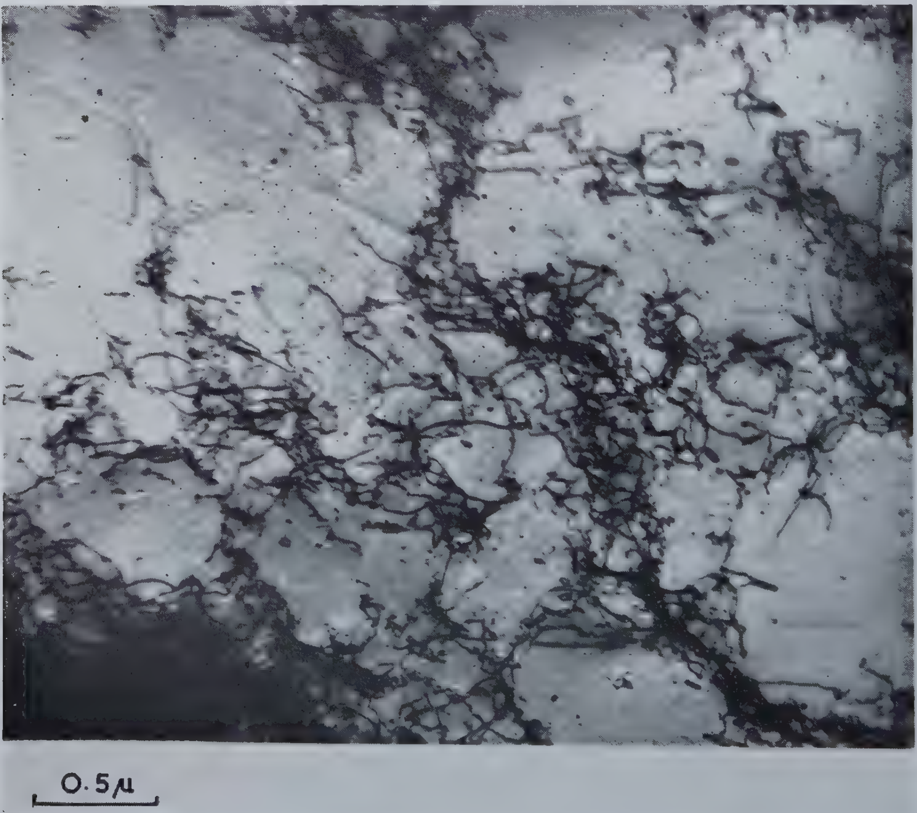

Dislocation distribution in copper specimen pulled 10% in tension after $10^6$ cycles of fatigue. ×35 000.

Fig. 10

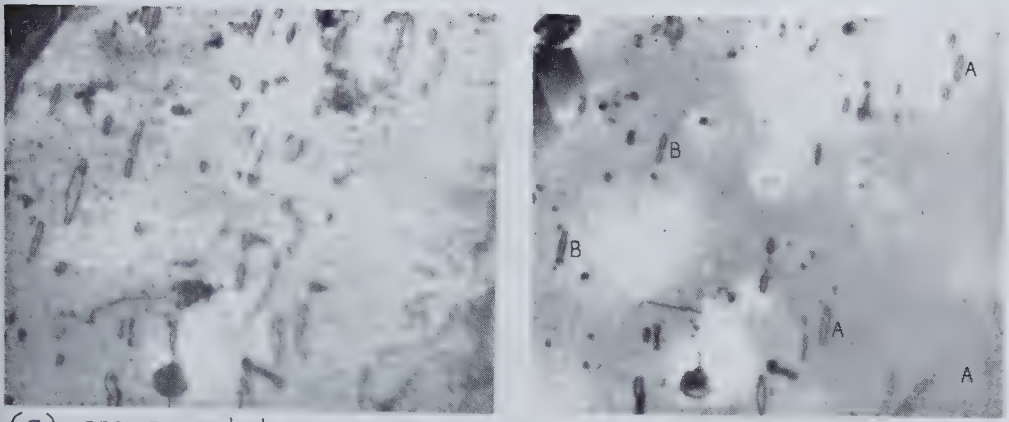

(a) pre-annealed (b) 1 m.

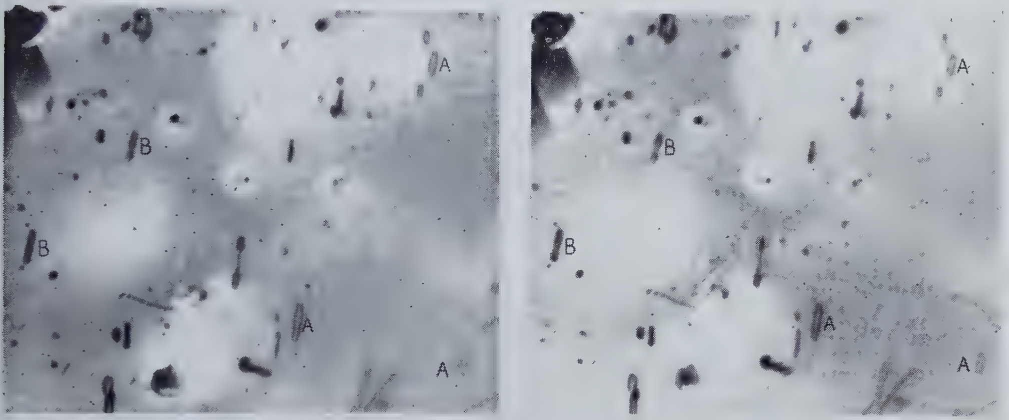

(c) 2 m. (d) 3 m.

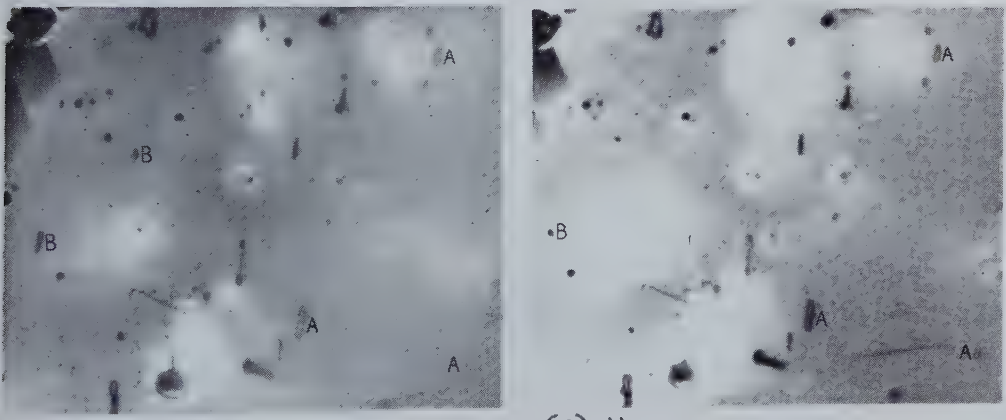

(e) 7 m. (f) 11 m.

0·5 μ

Sequence of micrographs of the same area of a fatigued copper specimen examined on the microscope heating stage after pre-annealing in bulk. Figure 10 (*a*) is as pre-annealed, the background of small dots is due to surface contamination. The loops at A shrink from the ends, those at B decrease in size more rapidly by pinching, followed by shrinking. The annealing times (in minutes) are approximate. × 28 000.

(*a*) As pre-annealed. (*b*) 1 min. (*c*) 2 min. (*d*) 3 min. (*e*) 7 min. (*f*) 11 min.

Fig. 4

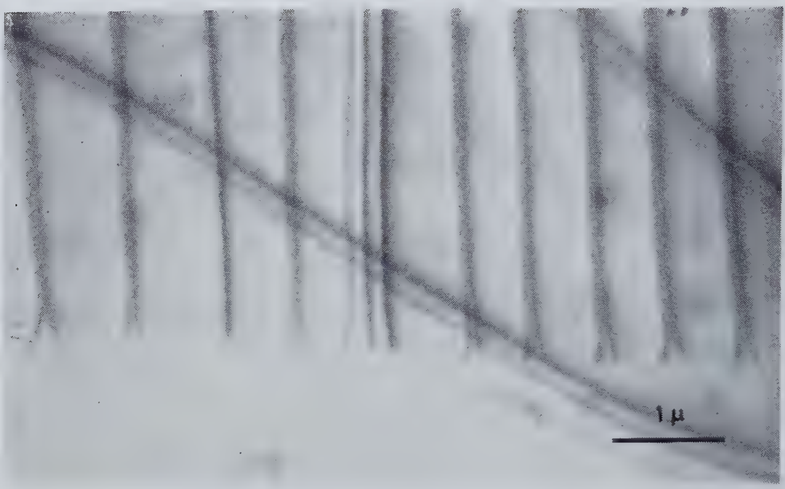

Electron micrograph of a sequence of dislocation ribbons in graphite emerging in a cleavage step, showing in particular a threefold ribbon.

Fig. 5

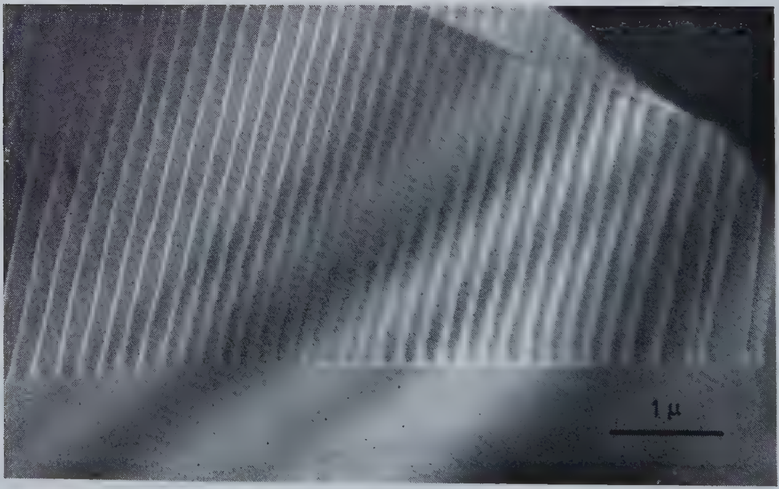

Electron micrograph of a sequence of dislocation ribbons in molybdenum sulphide emerging in a cleavage step.

Fig. 6

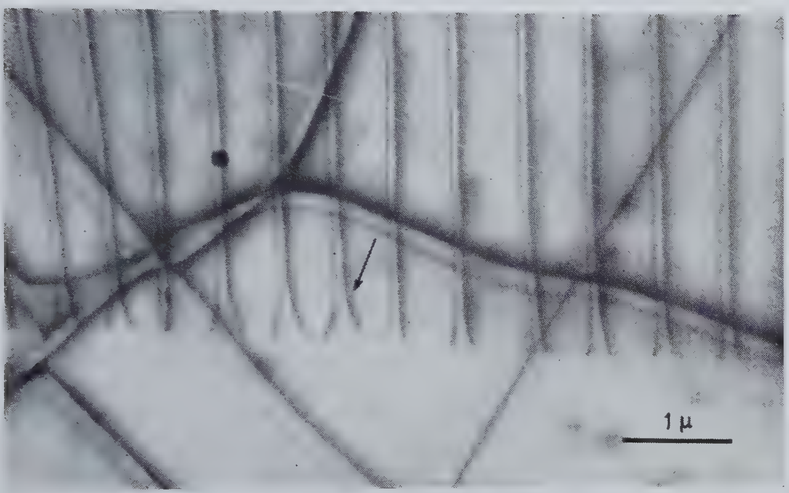

Electron micrograph of a sequence of dislocation ribbons in graphite emerging in a cleavage step. The ribbon indicated by an arrow is measured.

Fig. 1

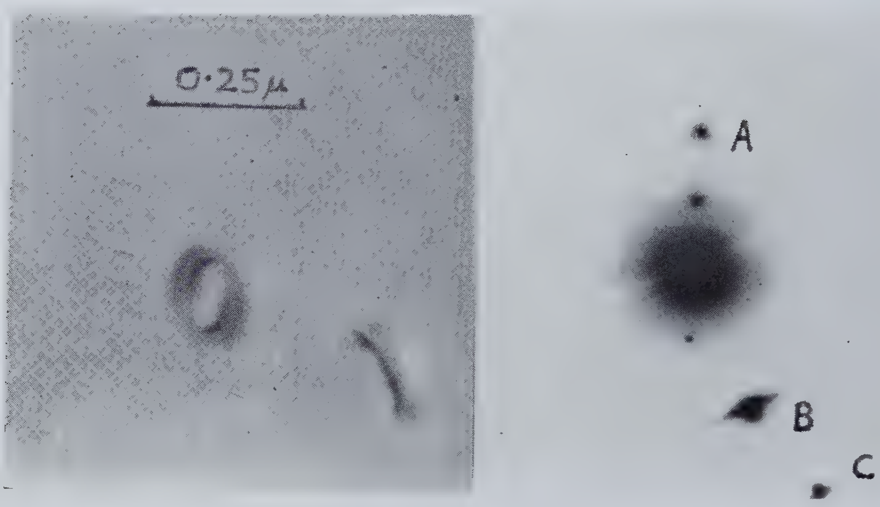

Fig. 2

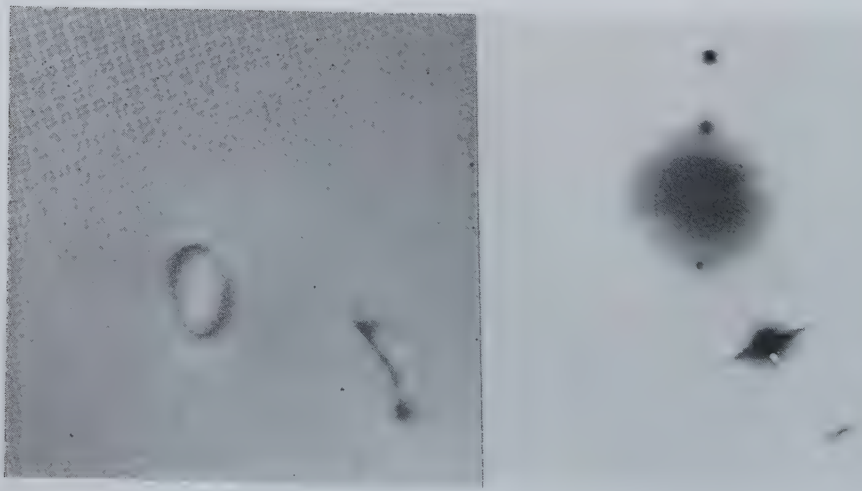

Fig. 3

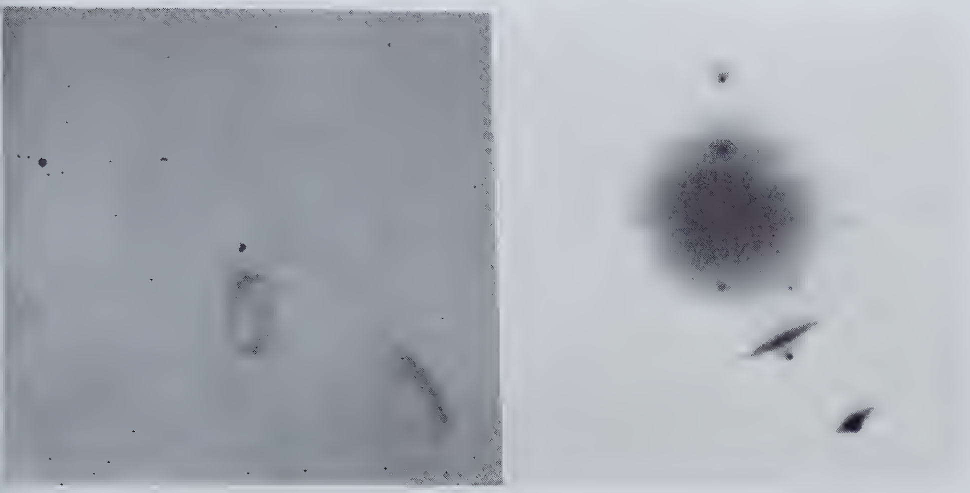

Fig. 4

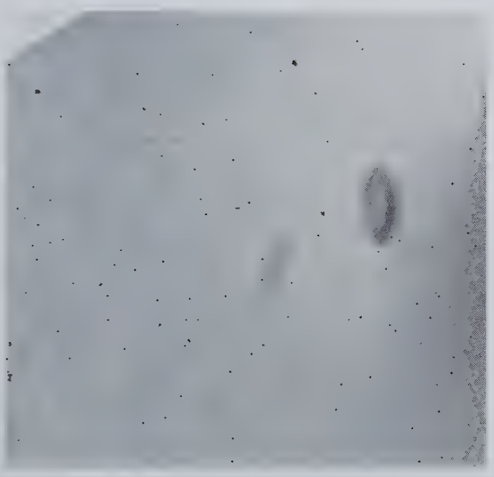

Figs. 1–4

Electron micrographs of a dislocation loop in magnesium oxide and selected area diffraction patterns. In figs. 2 and 3 the specimen is tilted slightly with respect to fig. 1; in fig. 4 the specimen has been tilted through a large angle by inverting the specimen holder.

# SUBJECT INDEX

PAGE
Alkali metals, thermoelectric power 1463
Alpha particles from $^{16}$N 163
Aluminium:
    annealing of dislocation loops 971
    cooperative movement of dislocations 453
    deformation stacking faults 491
    fatigue stressing and diffusion of zinc 979
    flow stress at high temperatures 735
    plastic deformation 37
    thermal expansion at low temperatures 277
Aluminium alloys, vacancy trapping 929
Aluminium-copper alloy
    critical shear stress 1531
    observation of precipitation 1103
    precipitation hardening 1119
Annealing kinetics of irradiated copper 839
Anti-nucleation processes in ferromagnetics 1057
Antiphase boundaries
    in $AuCu_3$ superlattice 1385
    in $Fe_3Al$ superlattice 811
Argon, refractive index of solid 939

Beta decay of $^{16}$N 171
Beta ray spectra 987
Boltzmann and anti-Boltzmann equations 1407
Brass, alpha, creep and stress relaxation 259
Book notices 472, 1312, 1535
Book reviews 175, 317, 469, 599, 711, 951, 1071, 1195, 1309, 1421

Carboniferous sills, magnetic properties 689
Cascades initiated by nuclear interaction 657
Chromium, magnetic properties 0°–350°c 155
Chromium, magnetomechanical damping 825
Copper:
    dislocation loops, hardening, after irradiation 465
    flow stress at high temperatures 735
    Hall constant and Fermi surface 1045
    helium precipitation 189
    interfacial energy of twin boundaries 937
    stacking faults 1069
    sub-surface cross-slip 315
    whiskers 1297
Copper–aluminium alloy, stacking faults 598
Copper–aluminium alloys, segregation of solute atoms 823
Copper (silver, gold), theory of solid solutions 55
Correlation function of plasma in magnetic field 61
Correlation in electron gas 371
Corrosion and fatigue limit for iron–0·5% carbon 397

PAGE

- Cosmic radiation:
  - alpha particle component . . . 517
  - high energy gamma rays . . . 89, 113
  - hydrogen nuclei . . . 965
  - intensity underground . . . 1271
  - solar diurnal variation . . . 573
- Covellite and growth of ice crystals . . . 1073
- Creep of metals at very low temperatures . . . 1301
- Creep of uranium and irradiation growth . . . 503
- Critical temperatures of binary alloys . . . 907
- Cross-slip and fatigue at low temperatures . . . 1479
- Cross-slip in fatigued copper . . . 315
- Crystal habit in long-chain compounds . . . 329, 345

- Debye temperature of silver . . . 863
- Deformation twinning in face-centred cubic metals . . . 379
- de Haas–van Alphen effect in zinc . . . 445
- Dehydration nuclei on gypsum . . . 441
- Demagnetization of igneous rocks . . . 225
- Deuteron stripping reactions . . . 1371
- Diamond:
  - etching with gases . . . 429
  - infra-red absorption . . . 1163
  - relative hardnesses . . . 701
  - trigons on octahedron surfaces . . . 1089
- Diffusion (self), theory . . . 473
- Diffusion, zinc in aluminium, and fatigue stressing . . . 979
- Dimer problem . . . 1061
- Dislocations:
  - in crystals grown from melt . . . 1227
    - free surface . . . 1147
    - ionic crystals . . . 997
    - thin films . . . 1183, 1193
    - visco-elastic materials . . . 953
    - aluminium . . . 453
    - gold–cobalt alloys . . . 531
    - lead iodide . . . 587
    - lithium fluoride . . . 1475
    - $Ni_3Mn$ . . . 871
    - silver bromide . . . 271
  - and epitaxy . . . 1419
    - fatigue . . . 49, 1493
    - impurity precipitation . . . 403
    - misfit between crystals . . . 1347
  - jogs, and elastic energies . . . 1267
  - loops,
    - conservative climb . . . 243
    - in aluminium . . . 971
      - antimony telluride . . . 601
      - graphite . . . 313
      - irradiated copper . . . 465
      - magnesium oxide . . . 1527
      - zinc . . . 449
  - moving, and debris produced . . . 217
  - moving, and forces acting . . . 1261
  - nodes, and stacking-fault energies . . . 1215
  - ribbons, at surfaces . . . 1515

PAGE

Disordered systems, electronic structure 617

Elastic energies of dislocation jogs 1267
Elastic modulus, internal friction, in sodium chloride 1115
Electrical properties of liquid metals, theory 1013
Electrical resistivity of:
  iron–aluminium alloys 1093
  iron–chromium alloys 857
  stacking faults and lattice vacancies in gold 1351
Electrical resistivity and stored energy 807
Electron microscope, damage to metal films 1003
Electron theory of interaction between point defects 1285
Electronic structure:
  disordered systems 617
  zeta phases 669
Epitaxial dislocations 1419
Etch figures on alum 791
Etch pits and dehydration nuclei on gypsum 441
Etchants for lithium fluoride 1475
Etching of diamond with gases 429
Etching (thermal) and facet growth 1313

Fatigue and cross slip 315, 1479
Fatigue and dislocation distribution 1493
Fatigue extrusion and dislocation gating mechanisms 49
Fatigue limit and corrosion of iron–0·5% carbon. 397
Fatigued lead, distribution of deformation. 321
Fermi surface and Hall constant 1045
Fermi surfaces of noble metals 727
Ferromagnetics, antinucleation processes 1057
Field ion microscopy and lattice defects 1035
Flow stress and stored energy 819
Flow stress
  of aluminium and copper at high temperatures 735
  of metals at low temperatures 209
Fracture
  of magnesium oxide single crystals 9, 1449
  of magnesium oxide Bi-crystals 195

Gamma rays produced by cosmic radiation 89, 113
Gating mechanisms for fatigue extrusion 49
Germanium, optical properties of liquid 509
Glide in magnesium crystals 177
Gold, electrical resistivity, stacking faults, lattice vacancies. 1351
Gold, ion bombardment 707, 1185
Gold–cobalt alloys, dislocation decoration 531
Gold–cobalt alloys, examination of precipitate 1343
Gold (copper, silver), theory of solid solutions 55
Grain boundary luminescence 25
Graphite, vacancy and interstitial loops 313
Gypsum, etch pits and dehydration nuclei. 441

Hall coefficient of liquid mercury 419
Hammer tracks from photodisintegration 311
Hardening of aluminium–copper alloy 1119
Heat conduction by liquid helium II 775, 1173

PAGE

Helium precipitation in irradiated copper . . . . . . . 189
Helium II, heat conduction . . . . . . . 775, 1173
Hydrogen nuclei of primary cosmic radiation . . . . . . 965

Ice-growth on covellite surfaces . . . . . . . . 1073
Igneous rocks, demagnetization . . . . . . . . 225
Igneous rocks, theory of magnetic properties . . . . . . 1241
Inelastic scattering and thermoelectric power . . . . . . 1201
Inertial mass, search for anisotropy . . . . . . . . 683
Infra-red absorption in diamond . . . . . . . . 1163
Interface between metal and electrolyte . . . . . . . 133
Ionic charge (effective) and lattice vibrations . . . . . . 27
Iron, precipitation and irradiation hardening . . . . . . 535
Iron, stress relaxation at low temperatures . . . . . . 847
Iron–0·5% carbon, corrosion and fatigue limit . . . . . . 397
Iron–aluminium alloys, electrical resistance . . . . . . 1093
Iron–chromium alloys, electrical resistivity . . . . . . 857

Krypton:
  refractive index of solid . . . . . . . . 937
  solubility in liquid cadmium and indium . . . . . . 943

Lattice vibrations and effective ionic charge . . . . . . 27
Lead:
  cross section for slow neutrons . . . . . . . . 485
  deformation after fatigue . . . . . . . . 321
  deformation stacking faults . . . . . . . . 491
  optical properties of liquid . . . . . . . . 509
Lead iodide:
  decomposition by electron irradiation . . . . . . . 895
  helical dislocations . . . . . . . . . 587
Ledge theory of recrystallization . . . . . . . . 795
Lithium, scattering of electrons by stacking faults . . . 1189, 1191
Lithium alloys, thermoelectricity . . . . . . . . 1431
Lithium fluoride, etchants . . . . . . . . . 1475
Loops (vacancy and interstitial) in graphite . . . . . . 313
Luminescence in grain boundary . . . . . . . . 25
Lutetium–176, half-life . . . . . . . . . 851

Magnesium, thermally-activated glide . . . . . . . 177
Magnesium oxide:
  fracture and slip distribution . . . . . . . . 9
  fracture and thermal shock . . . . . . . . 1449
  fracture of Bi-crystals . . . . . . . . . 195
  interstitial dislocation loops . . . . . . . . 1527
Magnetic properties:
  chromium . . . . . . . . . . 155
  igneous rocks (theory) . . . . . . . . . 1241
  three carboniferous sills . . . . . . . . . 689
Magnetic susceptibility in alloys
  and hydrogen solubility . . . . . . . . . 455
    oxygen solubility . . . . . . . . . 805
Magnetization, thermoremanent . . . . . . . . 713
Magnetomechanical damping in chromium . . . . . . 825

PAGE
Mercury, Hall coefficient of liquid . . . . . . . 419
Mesons ($\pi^-$) and complex nuclei . . . . . . . 833
Metallic state . . . . . . . . . . 287

Neutrons, cross section of lead . . . . . . . . 485
Niobium, soft x-ray emission spectrum . . . . . . 801
Nitrogen ($^{16}$N):
    beta decay . . . . . . . . . 171
    delayed alpha particles . . . . . . . . 163

Ordering and dislocations in $Ni_3Mn$ . . . . . . . 871
Oxygen ($^{16}$O), spin and parity . . . . . . . . 171

Paraffins, crystal habit of long chain compounds . . . . 329
Parity and spin in $^{16}$O . . . . . . . . . 171
Phonons, scattering by bound electrons . . . . . . 609
$\pi$–N scattering theory . . . . . . . . . 201
Plasma, correlation function . . . . . . . . 61
Plasmas, transport problems . . . . . . . . 71
Plastic deformation of aluminium . . . . . . . 37
Plastic strain and sub-grain structure . . . . . . 547
Plasticity and surface effects . . . . . . . . 159
Point defects:
    clusters in irradiated metals . . . . . . . 1487
    electron theory of interaction . . . . . . . 1285
Polyethylene crystals, surface detachment . . . . . . 1053
Polymers, crystal habit of long chain compounds . . . . 345
Potassium chloride, thermal expansion . . . . . . 1425
Precipitation:
    aluminium–4% copper alloy . . . . . . . 1103
    gold–cobalt alloys . . . . . . . . . 1343
Precipitation and irradiation hardening in iron . . . . . 535
Precipitation from solid solution, kinetics . . . . . . 1439

Recrystallization in metals, ledge theory . . . . . . 795
Refractivity, light scattering, crystal defects . . . . . 947
Rocksalt—*see* Sodium chloride . . . . . . . 359
Rotational bands in 1p shell . . . . . . . . 1207
Rubidium–87, half-life . . . . . . . . . 563

Seebeck coefficient of polar semiconductors . . . . . 167
Semiconductors, polar—Seebeck coefficient . . . . . 167
Silver, Debye temperature . . . . . . . . 863
Silver (copper, gold), theory of solid solutions . . . . . 55
Silver bromide, dislocation interactions . . . . . . 271
Snow crystals, growth at low supersaturations . . . . . 1363
Sodium chloride:
    debris produced by moving dislocations . . . . . 217
    elastic modulus and internal friction . . . . . . 1115
    electrical effects during deformation . . . . . . 1, 359

PAGE

- Solid solutions in copper, silver, gold (theory) 55
- Spin and (parity) in $^{16}O$ 171
- Stacking faults:
  - aluminium 491
  - copper 1069
  - lead, lead alloys 491
  - lithium 1189, 1191
- Stacking faults and electrical resistivity (gold) 1351
- Stacking fault energies, dislocation nodes 1215
- Stacking fault energy, graphite 1305
- Stored energy and flow stress 819
- Stress relaxation in alpha iron 847
- Surface effects and crystal plasticity 159

- Thermal expansion, aluminium 277
- Thermal expansion at low temperatures 815, 1425
- Thermal shock and fracture in magnesium oxide 1449
- Thermoelectricity of lithium alloys 1431
- Thermoelectric power, inelastic scattering 1201
- Thermoelectric power of alkali metals 1463
- Thermoremanent magnetization 713
- Tin, optical properties of liquid 509
- Transition metal alloys:
  - face-centred cubic solid solutions 769
  - oxygen solubility, magnetic susceptibility 805
- Transport problems in plasmas 71
- Travel time of wave between apertures 1065
- Twin boundaries in copper 937
- Twinning (deformation) in face-centred cubic metals 379

- Uranium, irradiation growth and creep 503

- Vacancies and electrical resistivity (gold) 1351
- Vacancy pairs, mobility in ionic crystals 1157
- Vacancy trapping in quenched aluminium alloys 929
- Vanadium–50, half-life 559

- Wavefunction, stability under perturbation 249
- Whiskers, copper 1297
- Work-hardening, hexagonal and cubic crystals 639

- Xenon, density and expansivity of solid 461
- X-ray emission spectra of light elements 365
- X-ray emission spectrum of niobium 801

- Zeta phases 669
- Zinc:
  - de Haas–van Alphen effect 445
  - dislocation loops 449

# INDEX OF AUTHORS (WITH TITLES)

PAGE

Abbiss, C. P., with Huzan, Eva, and Jones, G. O.: Thermal expansion of aluminium at low temperatures 277
Alburger, D. E., Pixley, R. E., Wilkinson, D. H., and Donovan, P.: Beta-decay of $^{16}$N: Conservation of spin and parity in $^{16}$O 171
Allen, J. E., Apostolakis, A. J., Lee, Y. J., Major, J. V., and Ferreira, E. Perez: The interactions of $\pi^-$-mesons with complex nuclei in the energy range (100–800) Mev. II: The interaction lengths and elastic scattering of 750 Mev $\pi^-$-mesons in G5 emulsion 833
Amelinckx, S., with Delavignette, P.: Large dislocation loops in antimony telluride 601
Amelinckx, S., with Delavignette, P., and Tournier, J.: Direct observation of dislocations due to epitaxy 1419
Amelinckx, with Gevers, R., and Delavignette, P.: A surface effect associated with dislocation ribbons 1515
Apostolakis, A. J., with Allen, J. E., Lee, Y. J., Major, J. V., and Ferreira, E. Perez: The interactions of $\pi^-$-mesons with complex nuclei in the energy range (100–800) Mev. II: The interaction lengths and elastic scattering of 750 Mev $\pi^-$-mesons in G5 emulsion 833
Appel, J.: Remark on the Seebeck coefficient of polar semiconductors 167
Armstrong, R., with Conrad, H., Wiedersich, H., and Schoeck, G.: Thermally-activated glide in magnesium crystals from 4·2° to 420°K 177

Baker, A. A., with Meleka, A. H., and Barr, W.: Evidence of sub-surface cross-slip in fatigued copper 315
Baker, C., Chou, Y. T., and Kelly, A.: The stacking-fault energy of graphite 1305
Baker, C., with Williamson, G. K.: A comparison of vacancy and interstitial loops in graphite 313
Barnes, R. S.: The behaviour of point defect clusters in irradiated metals 1487
Barnes, R. S., with Westmacott, K. H., Hull, D., and Smallman, R. E.: Vacancy trapping in quenched aluminium alloys 929
Barr, W., with Meleka, A. H., and Baker, A. A.: Evidence of sub-surface cross-slip in fatigued copper 315
Bartlett, J. T., and Mitchell, J. W.: Interactions between dislocations with Burgers vectors at 120° in crystals of silver bromide 271
Barton, J. C.: Intensity of the cosmic radiation at great depths underground 1271
Bassett, D. C.: Surface detachment from polyethylene crystals 1053
Bassett, D. C., and Keller, A.: Some new habit features in crystals of long chain compounds. Part II: Polymers 345
Bell, G. M., and Fairbairn, W. M.: The critical temperatures of binary alloys with one magnetic component 907
Bitler, W. R., with Pound, G. M., and Paxton, H. W.: Theory of the self-diffusion coefficient in cubic metals 473
Blackburn, W. S.: Effect of irradiation growth on the creep of uranium under a uniaxial load 503
Board, A. J., with Pearson, S., and Wheeler, C.: The effect of fatigue stressing on the diffusion rate of zinc in aluminium 979

PAGE

Bolling, G. F., Massalski, T. B., and McHargue, C. J. : An x-ray study of deformation stacking faults at low temperatures in lead, some lead alloys, and aluminium . . . . . . . . 491

Bowden, Piers, with Brandon, D. G. : The low energy ion bombardment of gold . . . . . . . . . . . . . 707

Bradfield, G., and Goodwin, E. T. : A note on abnormalities in the travel time of a wave between two extensive apertures . . . . . 1065

Brandon, D. G., and Bowden, Piers : The low energy ion bombardment of gold . . . . . . . . . . . . . 707

Brandon, D. G., and Wald, M. : The direct observations of lattice defects by field ion microscopy . . . . . . . . 1035

Brewer, D. F., and Edwards, D. O. : Heat conduction by liquid helium II in capillary tubes. I : Transition to supercritical conduction . 775

Brewer, D. F., and Edwards, D. O. : Heat conduction by liquid helium II in capillary tubes. II : Measurements of the pressure gradient 1173

Bright, J. E., and Ridge, M. J. : Etch pits and dehydration nuclei on crystals of gypsum . . . . . . . . . . 441

Brown, L. M., with Kroupa, F. : Elastic self- and interaction energies of dislocation jogs . . . . . . . . . . . 1267

Brown, N., with Marcinkowski, M. J. : The direct observation of antiphase boundaries in the $Fe_3Al$ superlattice . . . . . 811

Bryant, R. T., and Evans, E. W. : Observations on the oxygen solubility and magnetic susceptibility of body-centred cubic transition metal alloys . . . . . . . . . . . . . . 805

Buck, B., and Hodgson, P. E. : The analysis of (d, p) stripping reactions by the distorted wave Born approximation . . . . . 1371

Bullough, R., and Newman, R. C. : The kinetics of impurity precipitation on dislocations : Small drift theory . . . . . . 403

Burke, J. : The kinetics of precipitation from solid solutions by nucleation and diffusion controlled growth processes . . . . . . 1439

Byrne, J. G., Fine, M. E., and Kelly, A. : Precipitate hardening in an aluminium–copper alloy . . . . . . . . . . 1119

Campbell, R. B., and Muldawer, L. : Dislocation decoration by precipitation in gold–cobalt alloys . . . . . . . . 531

Chan Hong-Mo : On the Edwards–Matthews approach to $\pi$–$N$ scattering . . . . . . . . . . . . . . 201

Chou, Y. T., with Baker, C., and Kelly, A. : The stacking-fault energy of graphite . . . . . . . . . . . . . 1305

Clarebrough, L. M., Hargreaves, M. E., Head, A. K., and Loretto, M. H. : Stored energy and flow stress in deformed metals . . . . 819

Clarebrough, L. M., Hargreaves, M. E., and Loretto, M. H. : Stored energy and electrical resistivity in deformed metals . . . . 807

Clarke, F. J. P., with Miles, G. D. : Thermal shock and fracture in crystals of magnesium oxide . . . . . . . . . 1449

Clegg, A. B. : Rotational bands in the 1p-shell . . . . . . 1207

Collings, E. W., Hedgcock, F. T., and Siddiqi, A. : Magnetic properties of chromium between 0° and 350°C . . . . . . . . 155

Collins, M. F., and Dolling, G. : Total cross section of lead for slow neutrons . . . . . . . . . . . . . . 485

Conrad, H., Armstrong, R., Wiedersich, H., and Schoeck, G. : Thermally-activated glide in magnesium crystals from 4·2° to 420°K . . . 177

Corless, G. K., and March, N. H. : Electron theory of interaction between point defects in metals . . . . . . . . . . 1285

PAGE

Cornwell, J. F. : The Fermi surfaces of the noble metals . . . . 727
Cotterill, R. M. J. : An experimental determination of the electrical resistivity of stacking faults and lattice vacancies in gold . . 1351
Crisp, R. S., and Williams, S. E. : The soft x-ray emission spectra of sodium, beryllium, boron, silicon, and lithium . . . . 365
Cusack, N., and Kendall, P. : The Hall coefficient of liquid mercury . 419

Davidge, R. W., and Whitworth, R. W. : Evidence for the production of debris by moving dislocations in sodium chloride . . . 217
Davies, P. W., Greenough, A. P., and Wilshire, B. : The ledge theory of recrystallization in polycrystalline metals . . . . . 795
Dekeyser, W., with Rueda, F. : Charge effects during inhomogeneous deformation of rocksalt . . . . . . . . . 359
Dekeyser, W., with Vennik, J., and Reamut, G. : Observations on charged dislocations in ionic crystals . . . . . . . 997
Delavignette, P., and Amelinckx, S. : Large dislocation loops in antimony telluride . . . . . . . . . . 601
Delavignette, P., with Gevers, R., and Amelinckx, S. : A surface effect associated with dislocation ribbons . . . . . . . 1515
Delavignette, P., Tournier, J., and Amelinckx, S. : Direct observation of dislocations due to epitaxy . . . . . . . . . 1419
de Morton, M. E. : Magnetochemical damping in chromium . . 825
Dolling, G., with Collins, M. F. : Total cross section of lead for slow neutrons . . . . . . . . . . . . 485
Drever, R. W. P. : A search for anisotropy of inertial mass using a free precession technique . . . . . . . . . . 683
Dugdale, J. S., and Gugan, D. : Note on the scattering of electrons by stacking faults in lithium . . . . . . . . . 1189
Dugdale, J. S., and Mundy, J. N. : The pressure dependence of the thermoelectric power of the alkali metals at room temperature . 1463
Duthie, J. G., Fisher, C. M., Fowler, P. H., Kaddoura, A., Perkins, D. H., and Pinkau, K. : The study of high-energy $\gamma$-rays produced by cosmic radiation at 40 000 feet. Part I : Experimental disposition, and determination of energy and nature of electromagnetic cascades 89
Duthie, J. G., Fisher, C. M., Fowler, P. H., Kaddoura, A., Perkins, D. H., Pinkau, K., and Wolters, W. : The study of high-energy $\gamma$-rays produced by cosmic radiation at 40 000 feet. Part II : The energy spectrum of cascades and its interpretation . . . . . 113

Eatwell, A. J., and Smith, B. L. : Density and expansivity of solid xenon . . . . . . . . . . . . . 461
Edwards, D. O., with Brewer, D. F. : Heat conduction by liquid helium II in capillary tubes. I : Transition to supercritical conduction . 775
Edwards, D. O., with Brewer, D. F. : Heat conduction by liquid helium II in capillary tubes. II : Measurements of the pressure gradient . 1173
Edwards, S. F. : The charge correlation function of a plasma in a magnetic field . . . . . . . . . . . . 61
Edwards, S. F. : The electronic structure of disordered systems . . 617
Edwards, S. F., and Sanderson, J. J. : A new approach to transport problems in fully ionized plasmas . . . . . . . . 71
Elbaum, C., with Howe, S. : The relation between the plastic deformation of aluminium single crystals and polycrystals . . . . 37

PAGE

Elbaum, C., with Howe, S. : The occurrence of dislocations in crystals grown from the melt . . . 1227
Eshelby, J. D. : Dislocations in visco-elastic materials . . . 953
Evans, E. W., with Bryant, R. T. : Observations on the oxygen solubility and magnetic susceptibility of body-centred cubic transition metal alloys . . . 805
Evans, T., and Sauter, D. H. : Etching of diamond surfaces with gases 429
Everitt, C. W. F. : The magnetic properties of three carboniferous sills 689
Everitt, C. W. F. : Thermoremanent magnetization. I : Experiments on single domain grains . . . 713

Fairbairn, W. M., with Bell, G. M. : The critical temperatures of binary alloys with one magnetic component . . . 907
Feder, R., Thornton, P. H., and Cahn, R. W. : The high temperature electrical resistance of iron–aluminium alloys . . . 1093
Feltham, P. : The flow stress of metals at low temperatures . . . 209
Feltham, P. : Creep and stress relaxation in alpha-brass at low tempara-tures . . . 259
Feltham, P. : Stress relaxation in alpha-iron at low temperatures . 847
Feltham, P. : On the creep of metals at very low temperatures . . 1301
Feltham, P. : Cross-slip and fatigue in metals at low temperatures . 1479
Ferreira, E. Perez, with Allen, J. E., Apostolakis, A. J., Lee, Y. J., and Major, J. V. : The interactions of $\pi^-$-mesons with complex nuclei in the energy range (100–800) Mev. II : The interaction lengths and elastic scattering of 750 Mev $\pi^-$-mesons in G5 emulsion . . 833
Fine, M. E., with Byrne, J. G., and Kelly, A. : Precipitate hardening in an aluminium–copper alloy . . . 1119
Fisher, C. M., with Duthie, J. G., Fowler, P. H., Kaddoura, A., Perkins, D. H., and Pinkau, K. : The study of high-energy $\gamma$-rays produced by cosmic radiation at 40 000 feet. Part I : Experimental disposition, and determination of energy and nature of electromagnetic cascades . . . 89
Fisher, C. M., with Duthie, J. G., Fowler, P. H., Kaddoura, A., Perkins, D. H., Pinkau, K., and Wolters, W. : The study of high-energy $\gamma$-rays produced by cosmic radiation at 40 000 feet. Part II : The energy spectrum of cascades and its interpretation . . . 113
Fisher, Michael E., with Temperley, H. N. V. : Dimer problem in statistical mechanics—An exact result . . . 1061
Fisher, R. M., and Marcinkowski, M. J. : Direct observations of antiphase boundaries in the $AuCu_3$ superlattice . . . 1385
Forsyth, P. J. E., with Wilson, R. N. : The cooperative movement of dislocations in very pure aluminium foil . . . 453
Forty, A. J. : Helical dislocations in crystals of lead iodide . . 587
Forty, A. J. : The precipitation of lead during decomposition of lead iodide by electron irradiation . . . 895
Fourie, J. T., and Murphy, R. J. : Wide stacking faults in high purity copper crystals . . . 1069
Fowler, P. H., with Duthie, J. G., Fisher, C. M., Kaddoura, A., Perkins, D. H., and Pinkau, K. : The study of high-energy $\gamma$-rays produced by cosmic radiation at 40 000 feet. Part I : Experimental disposition, and determination of energy and nature of electromagnetic cascades . . . 89

PAGE

Fowler, P. H., with Duthie, J. G., Fisher, C. M., Kaddoura, A., Perkins, D. H., Pinkau, K., and Wolters, W. : The study of high-energy $\gamma$-rays produced by cosmic radiation at 40 000 feet. Part II : The energy spectrum of cascades and its interpretation 113

Gaunt, P., and Silcox, J. : An electron microscope examination of small cobalt particles precipitated in a gold matrix 1343
Gevers, R., Amelinckx, S., and Delavignette, P. : A surface effect associated with dislocation ribbons 1515
Gibbons, D. F. : Observation of de Haas–van Alphen type oscillation in the acoustomagnetic attenuation of zinc 445
Gillam, E., and Phillips, M. : The positive ion bombardment of evaporated single crystal gold films 1185
Gilman, J. J. : The mechanism of surface effects in crystal plasticity 159
Goland, A. N. : Radiation-enhanced helium precipitation in copper 189
Goldheim, D. L., with Westwood, A. R. C., and Opperhauser, Jr., H.: Etchants for revealing dislocations in lithium fluoride and other crystals 1475
Goodwin, E. T., with Bradfield, G. : A note on abnormalities in the travel time of a wave between two extensive apertures 1065
Greenough, A. P., with Davies, P. W., and Wilshire, B. : The ledge theory of recrystallization in polycrystalline metals 795
Groves, G. W., and Kelly, A. : Interstitial dislocation loops in magnesium oxide 1527
Guénault, A. M., and MacDonald, D. K. C. : A note on thermoelectric power and inelastic scattering 1201
Gugan, D., with Dugdale, J. S. : Note on the scattering by stacking faults in lithium 1189

Hall, G. G. : The stability of a wavefunction under a perturbation 249
Hallett, J. : The growth of ice crystals on freshly cleaved covellite surfaces 1073
Ham, R. K. : The determination of dislocation densities in thin films 1183
Ham, R. K., and Sharpe, N. G. : A systematic error in the determination of dislocation densities in thin films 1193
Hardy, J. R. : Effective ionic charge in relation to lattice vibrations 27
Hardy, J. R., and Smith, S. D. : Two-phonon infra-red lattice absorption in diamond 1163
Hargreaves, M. E., with Clarebrough, L. M., and Loretto, M. H. : Stored energy and electrical resistivity in deformed metals 807
Hargreaves, M. E., with Clarebrough, L. M., Head, A. K., and Loretto, M. H. : Stored energy and flow stress in deformed metals 819
Head, A. K., with Clarebrough, L. M., Hargreaves, M. E., and Loretto, M. H. : Stored energy and flow stress in deformed metals 819
Hedgcock, F. T., with Collings, E. W., and Siddiqi, A. : Magnetic properties of chromium between 0° and 350°c 155
Herbstein, F. H. : Reinterpretation of discordant x-ray results for the Debye temperature of silver 863
Hirsch, P. B., with Segall, R. L., and Partridge, P. G. : The dislocation distribution in face-centred cubic metals after fatigue 1493
Hirsch, P. B., and Warrington, D. H. : The flow stress of aluminium and copper at high temperatures 735
Hodgson, J. N. : The optical properties of liquid germanium, tin and lead 509

PAGE

Hodgson, P. E., with Buck, B. : The analysis of (d, p) stripping reactions by the distorted wave Born approximation . . . . . 1371
Holden, J. : The formation of sub-grain structure by alternating plastic strain . . . . . . . . . . . . . 547
Holliday, J. E. : Soft x-ray emission spectrum of niobium . . . . 801
Hoover, Robert L., with Shearin, Paul E. : Measurement of low-energy beta-ray spectra using a high-pressure proportional counter . . 987
Howe, S., and Elbaum, C. : The relation between the plastic deformation of aluminium single crystals and polycrystals . . . . . 37
Howe, S., and Elbaum, C. : The occurrence of dislocations in crystals grown from the melt . . . . . . . . . . 1227
Howie, A. : A possible explanation of the results of the preceding note regarding scattering of electrons by stacking faults in lithium . 1191
Howie, A., and Swann, P. R. : Direct measurements of stacking-fault energies from observations of dislocation nodes . . . . . 1215
Hull, D., and Mogford, I. L. : Precipitation and irradiation hardening in iron . . . . . . . . . . . . . . 535
Hull, D., with Westmacott, K. H., Barnes, R. S., and Smallman, R. E. : Vacancy trapping in quenched aluminium alloys . . . . . 929
Hume-Rothery, W. : The face-centred cubic solid solutions in transition metal alloys of the first long period . . . . . . . 769
Hume-Rothery, W., and Roaf, D. J. : On the theory of solid solutions in copper, silver and gold . . . . . . . . . . 55
Huzan, Eva, Abbiss, C. P., and Jones, G. O. : Thermal expansion of aluminium at low temperatures . . . . . . . 277

Illingworth, R.: Grain boundary luminescence in an alkali halide phosphor. . . . . . . . . . . . . . 25
Inman, M. C., and Khan, A. R.: The interfacial energy of coherent twin boundaries in copper . . . . . . . . . . . 937
Irving, E., Stott, P. M., and Ward, M. A.: Demagnetization of igneous rocks by alternating magnetic fields . . . . . . . 225

Jaśkiewicz, A.: Antinucleation processes in ferromagnetics . . . . 1057
Johnson, G. W.: The solubility of krypton in liquid cadmium and indium . . . . . . . . . . . . . . . 943
Johnston, T. L., with Stokes, R. J., and Li, C. H.: Effect of slip distribution on the fracture behaviour of magnesium oxide single crystals 9
Jones, D. W., Pessall, N., and McQuillan, A. D.: Correlation between magnetic susceptibility and hydrogen solubility in alloys of early transition elements . . . . . . . . . . . . . 455
Jones, G. O., with Huzan, Eva, and Abbiss, C. P.: Thermal expansion of aluminium at low temperatures . . . . . . . 277

Kaddoura, A., with Duthie, J. G., Fisher, C. M., Fowler, P. H., Perkins, D. H., and Pinkau, K.: The study of high-energy $\gamma$-rays produced by cosmic radiation at 40 000 feet. Part I: Experimental disposition, and determination of energy and nature of electromagnetic cascades 89
Kaddoura, A., with Duthie, J. G., Fisher, C. M., Fowler, P. H., Perkins, D. H., Pinkau, K., and Wolters, W.: The study of high-energy $\gamma$-rays produced by cosmic radiation at 40 000 feet. Part II: The energy spectrum of cascades and its interpretation. . . . . . . 113
Keller, A.: Some new habit features in crystals of long chain compounds. Part I: Paraffins . . . . . . . . . . . 329

PAGE

Keller, A., with Bassett, D. C.: Some new habit features in crystals of long chain compounds. Part II: Polymers . . . . . 345
Kelly, A., with Bakers, C., and Chou, Y. T.: The stacking-fault energy of graphite . . . . . . . . . . . 1305
Kelly, A., with Byrne, J. G., and Fine, M. E.: Precipitate hardening in an aluminium–copper alloy . . . . . . . . . 1119
Kelly, A., with Groves, G. W.: Interstitial dislocation loops in magnesium oxide . . . . . . . . . . . 1527
Kendall, P., with Cusack, N.: The Hall coefficient of liquid mercury . 419
Kennedy, A. J.: Possible dislocation gating mechanisms for fatigue extrusion . . . . . . . . . . . 49
Khan, A. R., with Inman, M. C.: The interfacial energy of coherent twin boundaries in copper . . . . . . . . . 937
King, H. W., and Massalski, T. B.: Lattice spacing relationships and the electronic structure of H.C.P. $\zeta$ phases based on silver . . . . 669
Klauder, J. R., with Kunzler, J. E.: The observation of four types of Hall constant anisotropy in copper and their role in the determination of the Fermi surface . . . . . . . . 1045
Kobayashi, T.: The growth of snow crystals at low supersaturations . 1363
Koda, S., with Matsuura, K.: On the temperature dependence of critical resolved shear stress of an Al–4% Cu alloy . . . . . . 1531
Koda, Shigeyasu, with Nakazima, Koichi: Segregation of solute atoms in copper–aluminium alloys . . . . . . . . 823
Kronmüller, H., with Seeger, A., Mader, S., and Träuble, H.: Work-hardening of hexagonal close-packed crystals and in the easy glide region of face-centred cubic crystals . . . . . . . 639
Kroupa, F., and Brown, L. M.: Elastic self- and interaction energies of dislocation jogs . . . . . . . . . . . 1267
Kroupa, F., and Price, P. B.: ‘Conservative climb’ of a dislocation loop due to its interaction with an edge dislocation . . . 243
Kroupa, F., Silcox, J., and Whelan, M. J.: On the annealing of prismatic dislocation loops in aluminium . . . . . . . . 971
Kunzler, J. E., and Klauder, J. R.: The observation of four types of Hall constant anisotropy in copper and their role in the determination of the Fermi surface . . . . . . . . 1045

Lee, Y. J., with Allen, J. E., Apostolakis, A. J., Major, J. V., and Ferreira, E. Perez: The interactions of $\pi^-$-mesons with complex nuclei in the energy range (100–800) MEV. II: The interaction lengths and elastic scattering of 750 MEV $\pi^-$-mesons in G5 emulsion 833
Li, C. H., with Stokes, R. J., and Johnston, T. L.: Effect of slip distribution on the fracture behaviour of magnesium oxide crystals . 9
Lidiard, A. B., with Tharmalingam, K.: Mobility of vacancy pairs in ionic crystals . . . . . . . . . . . 1157
Loretto, M. H., with Clarebrough, L. M., and Hargreaves, M. E.: Stored energy and electrical resistivity in deformed metals . . . 807
Loretto, M. H., with Clarebrough, L. M., Hargreaves, M. E., and Head, A. K.: Stored energy and flow stress in deformed metals . . 819

MacDonald, D. K. C.: Some remarks on the Boltzmann and anti-Boltzmann equations . . . . . . . . . . 1407
MacDonald, D. K. C., with Guénault, A. M.: A note on thermoelectric power and inelastic scattering . . . . . . . . 1201

PAGE

MacDonald, D. K. C., Pearson, W. B., and Templeton, I. M.: Thermoelectricity of lithium alloys at very low temperatures . . 1431
McHargue, C. J., with Bolling, G. F., and Massalski, T. B.: An x-ray study of deformation stacking faults at low temperatures in lead, some lead alloys, and aluminium . . . . . . . 491
McNair, A.: The half-life of vanadium-50 . . . . . . . 559
McNair, A.: The half-life of long-lived lutetium-176 . . . . 851
McNair, A., and Wilson, H. W.: The half-life of rubidium-87 . . 563
McQuillan, A. D., with Jones, D. W., and Pessall, N.: Correlation between magnetic susceptibility and hydrogen solubility in alloys of early transition elements . . . . . . . 455
Mader, S., with Seeger, A., Kronmüller, H., and Träuble, H.: Work-hardening of hexagonal close-packed crystals and in the easy glide region of face-centred cubic crystals . . . . . . 639
Major, J. V., with Allen, J. E., Apostolakis, A. J., Lee, Y. J., and Ferreira, E. Perez: The interactions of $\pi^-$-mesons with complex nuclei in the energy range (100–800) MEV. II: The interaction lengths and elastic scattering of 750 MEV $\pi^-$-mesons in G5 emulsion. 833
Makin, M. J., Whapham, A. D., and Minter, F. J.: Dislocation loops and hardening in neutron irradiated copper . . . . . . 465
March, N. H., with Corless, G. K.: Electron theory of interaction between point defects in metals . . . . . . . . . 1285
Marcinkowski, M. J., and Brown, N.: The direct observation of anti-phase boundaries in the $Fe_3Al$ superlattice . . . . . 811
Marcinkowski, M. J., with Fisher, R. M.: Direct observations of anti-phase boundaries in the $AuCu_3$ superlattice . . . . 1385
Marcinkowski, M. J., and Miller, D. S.: The effect of ordering on the strength and dislocation arrangements in the $Ni_3Mn$ superlattice . 871
Martin, D. G.: The influence of impurity atoms on the annealing kinetics of electron irradiated copper . . . . . . 839
Massalski, T. B., with Bolling, G. F., and McHargue, C. J.: An x-ray study of deformation stacking faults at low temperatures in lead, some lead alloys, and aluminium . . . . . . . 491
Massalski, T. B., with King, H. W.: Lattice spacing relationships and the electronic structure of H.C.P. $\zeta$ phases based on silver . . 669
Matsuura, K., and Koda, S.: On the temperature dependence of critical resolved shear stress of an Al–4% Cu alloy . . . . . . 1531
Meleka, A. H., Barr, W., and Baker, A. A.: Evidence of sub-surface cross-slip in fatigued copper . . . . . . . . 315
Miles, G. D., and Clarke, F. J. P.: Thermal shock and fracture in crystals of magnesium oxide . . . . . . . . . . 1449
Miller, D. S., with Marcinkowski, M. J.: The effect of ordering on the strength and dislocation arrangements in the $Ni_3Mn$ superlattice . 871
Minter, F. J., with Makin, M. J., and Whapham, A. D.: Dislocation loops and hardening in neutron irradiated copper . . . . 465
Mitchell, J. W., with Bartlett, J. T.: Interactions between dislocations with Burgers vectors at 120° in crystals of silver bromide . . 271
Mitchell, W. E. J., and Whitehouse, J. E.: The refractivity and light scattering of crystals containing defects . . . . . . 947
Mogford, I. L., with Hull, D.: Precipitation and irradiation hardening in iron . . . . . . . . . . . . . . 535
Morton, W. T., and Walker, T. G.: Hammer tracks from the photo-disintegration of light emulsion nuclei . . . . . . 311
Mott, N. F.: The transition to the metallic state . . . . . 287

PAGE
Muldawer, L., with Campbell, R. B.: Dislocation decoration by precipitation in gold–cobalt . . . 531
Mullins, W. W.: Theory of linear facet growth during thermal etching . 1313
Mundy, J. N., with Dugdale, J. S.: The pressure dependence of the thermoelectric power of the alkali metals at room temperature . 1463
Murphy, R. J., with Fourie, J. T.: Wide stacking faults in high purity copper crystals . . . 1069

Nabarro, F. R. N.: The force on a moving dislocation . . . 1261
Nakazima, Koichi, and Koda, Shigeyasu: Segregation of solute atoms in copper–aluminium alloys . . . 823
Newman, R. C., with Bullough, R.: The kinetics of impurity precipitation on dislocations: Small drift theory . . . 403

Olness, J. W., with Segel, R. E., and Sprenkel, E. L.: Delayed alpha particles from $^{16}$N . . . 163
Omar, M., and Youssef, T. H.: Etch figures on alum and the diamond pattern . . . 791
Opperhauser, Jr., H., with Westwood, A. R. C., and Goldheim, D. L.: Etchants for revealing dislocations in lithium fluoride and other crystals . . . 1475

Partridge, P. G., with Segall, R. L., and Hirsch, P. B.: The dislocation distribution in face-centred cubic metals after fatigue . . . 1493
Pashley, D. W., and Presland, A. E. B.: Ion damage to metal films inside an electron microscope . . . 1003
Paxton, H. W., with Pound, G. M., and Bitler, W. R.: Theory of the self-diffusion coefficient in cubic metals . . . 473
Pearson, S., Board, A. J., and Wheeler, C.: The effect of fatigue stressing on the diffusion rate of zinc in aluminium . . . 979
Pearson, W. B., with MacDonald, D. K. C., and Templeton, I. M.: Thermoelectricity of lithium alloys at very low temperatures . 1431
Perkins, D. H., with Duthie, J. G., Fisher, C. M., Fowler, P. H., Kaddoura, A., and Pinkau, K.: The study of high-energy $\gamma$-rays produced by cosmic radiation at 40 000 feet. Part I: Experimental disposition, and determination of energy and nature of electromagnetic cascades . . . 89
Perkins, D. H., with Duthie, J. G., Fisher, C. M., Fowler, P. H., Kaddoura, Pinkau, K., and Wolters, W.: The study of high-energy $\gamma$-rays produced by cosmic radiation at 40 000 feet. Part II: The energy spectrum of cascades and its interpretation . . . 113
Pessall, N., with Jones, D. W., and McQuillan, A. D.: Correlation between magnetic susceptibility and hydrogen solubility in alloys of early transition elements . . . 455
Phillips, M., with Gillam, E.: The positive ion bombardment of evaporated single crystal gold films . . . 1185
Pinkau, K.: The development of cascades initiated by nuclear interaction . . . 657
Pinkau, K., with Duthie, J. G., Fisher, C. M., Fowler, P. H., Kaddoura, A., and Perkins, D. H.: The study of high-energy $\gamma$-rays produced by cosmic radiation at 40 000 feet. Part I: Experimental disposition, and determination of energy and nature of electromagnetic cascades . . . 89

PAGE

Pinkau, K., with Duthie, J. G., Fisher, C. M., Fowler, P. H., Kaddoura, A., Perkins, D. H., and Wolters, W.: The study of high-energy $\gamma$-rays produced by cosmic radiation at 40 000 feet. Part II: The energy spectrum of cascades and its interpretation . . . . 113
Pixley, R. E., with Alburger, D. E., and Wilkinson, D. H.: Beta-decay of $^{16}$N: Conservation of spin and parity in $^{16}$O . . . . . 171
Pound, G. M., Bitler, W. R., and Paxton, H. W.: Theory of the self-diffusion coefficient in cubic metals . . . . . . . . 473
Powell, R. W., Tye, R. P., and Woodman, Margaret J.: Some electrical resistivity measurements on a series of iron–chromium alloys . 857
Presland, A. E. B., with Pashley, D. W.: Ion damage to metal films inside an electron microscope . . . . . . . . . 1003
Price, P. B.: On dislocation loops formed in zinc crystals during low temperature pyramidal glide . . . . . . . . . 449
Price, P. B., with Kroupa, F.: ‘ Conservative climb ’ of a dislocation loop due to its interaction with an edge dislocation . . . . . 243
Pyle, I. C.: The scattering of phonons by bound electrons in a semiconductor . . . . . . . . . . . 609

Remaut, G., and Vennik, J.: Observations on an electrical effect obtained during deformation of sodium chloride crystals . . 1
Remaut, G., with Vennik, J., and Dekeyser, W.: Observations on charged dislocations in ionic crystals . . . . . 997
Ridge, M. J., with Bright, J. E.: Etch pits and dehydration nuclei on crystals of gypsum . . . . . . . . . . . 441
Roaf, D. J., with Hume-Rothery, W.: On the theory of solid solutions in copper, silver and gold . . . . . . . . . . 55
Rueda, F., and Dekeyser, W.: Charge effects during inhomogeneous deformation of rocksalt . . . . . . . . . 359

Sanderson, J. J., with Edwards, S. F.: A new approach to transport problems in fully ionized plasmas . . . . . . . 71
Sauter, D. H., with Evans, T.: Etching of diamond surfaces with gases. 429
Schapink, F. W., and Wolters, H. B. M.: Quench softening of Cu whiskers . . . . . . . . . . . . . 1297
Schoeck, G., with Conrad, H., Armstrong, R., and Wiedersich, H.: Thermally-activated glide in magnesium crystals from 4·2° and 420°K . . . . . . . . . . . . . 177
Seeger, A., Kronmüller, H., Mader, S., and Träuble, H.: Work-hardening of hexagonal close-packed crystals and in the easy glide region of face-centred cubic crystals. . . . . . . . . . 639
Segall, R. L., Partridge, P. G., and Hirsch, P. B.: The dislocation distribution in face-centred cubic metals after fatigue . . . . 1493
Segel, R. E., Olness, J. W., and Sprenkel, E. L.: Delayed alpha particles from $^{16}$N . . . . . . . . . . . . 163
Sharpe, N. G., with Ham, R. K.: A systematic error in the determination of dislocation densities in thin films . . . . . . 1193
Shearin, Paul E., and Hoover, Robert L.: Measurement of low-energy beta-ray spectra using a high-pressure proportional counter . 987
Siddiqi, A., with Collings, E. W., and Hedgcock, F. T.: Magnetic properties of chromium between 0° and 350°C . . . . . 155
Silcox, J., with Gaunt, P.: An electron microscope examination of small cobalt particles precipitated in a gold matrix . . . . 1343

PAGE

Silcox, J., with Kroupa, F., and Whelan, M. J.: On the annealing of prismatic dislocation loops in aluminium 971
Smallman, R. E., with Westmacott, K. H., Barnes, R. S., and Hull, D.: Vacancy trapping in quenched aluminium alloys 929
Smith, B. L.: Refractive index of solid krypton and solid argon 939
Smith, B. L., with Eatwell, A. J.: Density and expansivity of solid xenon 461
Smith, S. D., with Hardy, J. R.: Two-phonon infra-red lattice absorption in diamond 1163
Snowden, K. U.: The distribution of deformation in lead fatigued *in vacuo* 321
Sprenkel, E. K., with Segel, R. E., and Olness, J. W.: Delayed alpha particles from $^{16}$N 163
Stacey, F. D.: Theory of the magnetic properties of igneous rocks in alternating fields 1241
Stevenson, G. R., and Waddington, C. J.: The alpha-particle component of the primary cosmic radiation over northern England 517
Stokes, R. J., Johnston, T. L., and Li, C. H.: Effect of slip distribution on the fracture behaviour of magnesium oxide single crystals 9
Stott, P. M., with Irving, E., and Ward, M. A.: Demagnetization of igneous rocks by alternating magnetic fields 225
Swann, P. R., with Howie, A.: Direct measurements of stacking-fault energies from observations of dislocation nodes 1215

Temperley, H. N. V., and Fisher, Michael E.: Dimer problem in statistical mechanics—An exact result 1061
Templeton, I. M., with MacDonald, D. K. C., and Pearson, W. B.: Thermoelectricity of lithium alloys at very low temperatures 1431
Tharmalingam, K., and Lidiard, A. B.: Mobility of vacancy pairs in ionic crystals 1157
Thomas, G., and Whelan, M. J.: Observations of precipitation in thin foils of aluminium $+4\%$ copper alloy 1103
Thomson, D. M.: The solar variation of cosmic rays during 1958 and 1959, at Makerere, Hermanus and Herstmonceux 573
Thornton, P. H., with Feder, R., and Cahn, R. W.: The high temperature electrical resistance of iron–aluminium alloys 1093
Tournier, J., with Delavignette, P., and Amelinckx, S.: Direct observation of dislocations due to epitaxy 1419
Träuble, H., with Seeger, A., Kronmüller, H., and Mader, S.: Work-hardening of hexagonal close-packed crystals and in the easy glide region of face-centred cubic crystals 639
Tye, R. P., with Powell, R. W., and Woodman, Margaret J.: Some electrical resistivity measurements on a series of iron–chromium alloys 857

Venables, J. A.: Deformation twinning in face-centred cubic metals 379
Vennik, J., with Remaut, G.: Observations on an electrical effect obtained during deformation of sodium chloride crystals 1
Vennik, J., Remaut, G., and Dekeyser, W.: Observations on charged dislocations in ionic crystals 997

Waddington, C. J.: Hydrogen nuclei of the primary cosmic radiation 965
Waddington, C. J., with Stevenson, G. R.: The alpha-particle component of the primary cosmic radiation over northern England 517

PAGE

Wadsworth, N. J. : The influence of atmospheric corrosion on the fatigue limit of iron–0·5% carbon . . . . . . . 397
Wald, M., with Brandon, D. G. : The direct observation of lattice defects by field ion microscopy . . . . . . . 1035
Walker, T. G., with Morton, W. T. : Hammer tracks from the photodisintegration of light emulsion nuclei . . . . . . 311
Ward, M. A., with Irving, E., and Stott, P. M. : Demagnetization of igneous rocks by alternating magnetic fields . . . . . 225
Warrington, D. H., with Hirsch, P. B. : The flow stress of aluminium and copper at high temperatures . . . . . . . 735
Watts-Tobin, R. J. : The interface between a metal and an electrolytic solution . . . . . . . . . . . . . . 133
Westmacott, K. H., Barnes, R. S., Hull, D., and Smallman, R. E. : Vacancy trapping in quenched aluminium alloys . . . . . 929
Westwood, A. R. C. : On the fracture behaviour of magnesium oxide Bi-crystals . . . . . . . . . . . 195
Westwood, A. R. C., Opperhauser, Jr., H., and Goldheim, D. L. : Etchants for revealing dislocations in lithium fluoride and other crystals . . . . . . . . . . . . . . 1475
Whapham, A. D., with Makin, M. J., and Minter, F. J. : Dislocation loops and hardening in neutron irradiated copper . . . . 465
Wheeler, C., with Pearson, S., and Board, A. J. : The effect of fatigue stressing on the diffusion rate of zinc in aluminium . . . . 979
Whelan, M. J., with Kroupa, F., and Silcox, J. : On the annealing of prismatic dislocation loops in aluminium . . . . . . 971
Whelan, M. J., with Thomas, G. : Observations of precipitation in thin foils of aluminium +4% copper alloy . . . . . . 1103
White, G. K. : Thermal expansion at low temperatures. II : Electronic component in metals . . . . . . . . . . 815
White, G. K. : Thermal expansion at low temperatures. III : Potassium chloride . . . . . . . . . . . . . . 1425
Whitehouse, J. E., with Mitchell, E. W. J. : The refractivity and light scattering of crystals containing defects . . . . . . 947
Whitworth, R. W. : Changes of elastic modulus associated with internal friction in sodium chloride . . . . . . . . . 1115
Whitworth, R. W., with Davidge, R. W. : Evidence for the production of debris by moving dislocations in sodium chloride . . . . 217
Wiedersich, H., with Conrad, H., Armstrong, R., and Schoeck, G. : Thermally-activated glide in magnesium crystals from 4·2° to 420°K . . . . . . . . . . . . . . 177
Williams, S. E., with Crisp, R. S. : The soft x-ray emission spectra of sodium, beryllium, boron, silicon, and lithium . . . . 365
Williamson, G. K., and Baker, C. : A comparison of vacancy and interstitial loops in graphite . . . . . . . . . . 313
Wilkinson, D. H., with Alburger, D. E., and Pixley, R. E. : Beta-decay of $^{16}$N : Conservation of spin and parity in $^{16}$O . . . . . 171
Wilks, Eileen M. : The relative hardness of the hard directions in diamond . . . . . . . . . . . . . . 701
Wilks, Eileen M. : Steep-sided trigons on diamonds . . . . . 1089
Wilshire, B., with Davies, P. W., and Greenough, A. P. : The ledge theory of recrystallization in polycrystalline metals . . . . 795
Wilson, H. W., with McNair, A. : The half-life of rubidium-87 . . 563
Wilson, R. N., and Forsyth, P. J. E. : The cooperative movement of dislocations in very pure aluminium foil . . . . . . 453

PAGE

Wolters, H. B. M., with Schapink, F. W.: Quench softening of Cu whiskers . . . . . . . . . . . 1297
Wolters, W., with Duthie, J. G., Fisher, C. M., Fowler, P. H., Kaddoura, A., Perkins, D. H., and Pinkau, K.: The study of high-energy $\gamma$-rays produced by cosmic radiation at 40 000 feet. Part II: The energy spectrum of cascades and its interpretation . . 113
Woodman, Margaret J., with Powell, R. W., and Tye, R. P.: Some electrical resistivity measurements on a series of iron–chromium alloys . . . . . . . . . . . 857

Yoffe, Elizabeth H.: A dislocation at a free surface . . . . 1147
Young, W. H.: A variational approach to correlation in an electron gas 371
Youssef, T. H., with Omar, M.: Etch figures on alum and the diamond pattern . . . . . . . . . . . 791

Ziman, J. M.: A theory of the electrical properties of liquid metals. I: The monovalent metals . . . . . . . 1013

END OF THE SIXTH VOLUME

*Printed by Taylor & Francis Ltd*
*Red Lion Court, Fleet Street, London, E.C.4*

U. of Haw.